SOLAR PHOTOVOLTAIC POWER GENERATING SYSTEM & GRID INTEGRATION
−Modeling, Controller Design and Optimization

A DISSERTATION

submitted in partial fulfilment of the requirements for the degree

of

DOCTOR OF PHILOSOPHY

By

Ravi Nath Tripathi

(Student Number: 14899026)

under the supervision of

Prof. Tsuyoshi Hanamoto

Graduate School of Life Science and Systems Engineering (LSSE)

Green Electronics Division

Kyushu Institute of Technology

Hibikino, Wakamatsu-ku, Kitakyushu-shi

Fukuoka-ken, Japan

2017

ABSTRACT

Solar photovoltaic power generating system is an alternative as a renewable energy source and rapidly growing market since last decade. The performance of a solar photovoltaic array PV is dependent upon the temperature and irradiance level and it is necessary to study the characteristics of photovoltaic (PV) array. The solar photovoltaic modules can be modelled on the electrical equivalent model of solar cell. The two-diode model based Solar PV simulator is proposed with partial shading capability with bypass and blocking diode effect and the parameters: reverse saturation current and resistances are computed using the circuit equations associated with the electrical models of solar cell. The mathematical computational scheme for modelling is simplified for two diode model with better accuracy. The two diode based modelling method proposed for PV simulator in MATLAB-Simulink used the computational data of the first diode equation and the computation of second diode equation is replaced by the coefficient multiplied with the data of first diode. This simulator model accuracy is analysed for the combined effect of irradiance and temperature as according to the standard PV module datasheet. Incremental conductance MPPT algorithm is utilized through dc-dc converter to track MPP and boost the dc voltage for required application.

One of the most efficient and adequate application and utilization of power generated through PV is operation in grid connected mode. The grid integration of PV system requires a power electronics interface capable of conversion from dc-ac. Voltage source inverter(VSI) used as a power electronics interface and dc voltage as an input to converter have to be regulated to the required level for the power flow from converter side to load/grid side. It may be difficult to achieve good control of dc voltage using conventional PI controller having only one-degree-of-freedom (1-DOF) due to the trade-off between overshoot (in step response) and disturbance response. 2-DOF controller is reported and implemented for dc voltage control. The PLL is used for the grid frequency synchronization and SRFT, PBT and fryze conductance theory has been discussed for reference current generation. LCL filter is comprehensively designed with passive damping to minimize the ripple generated through VSI. The controller gains of dc voltage is optimally tuned using proposed application of data driven tuning method (FRIT) programmed in MATLAB based

upon the particle swarm optimization (PSO) algorithm. The fundamental idea related to FRIT method is the extraction of input and output data, reference model setting and range of controller gains. Also, the better set point and transient response is reported considering performance parameters.

Grid integrated PV system is modelled in MATLAB-Simulink and some part of the modelling also developed in Xilinx system generator (XSG) used for DSP and FPGA design. The focus is to design a model in XSG to develop an experimental prototype of the grid connected system controlled using FPGA through VIVADO interface.

Acknowledgements

Everybody born to do some designated and assigned task. I am thankful to almighty nature for whatever task I am carrying. There are people through whom it is possible to work for PhD. First and foremost, I would like to express my deepest thanks and appreciation to my supervisor Prof. Tsuyoshi Hanamoto, for providing a research environment with freedom of thoughts and working style which always motivates me to work in my own way and enjoy the research. I can go to him anytime without a single thought of hesitation and he used to be available to provide time for discussion and teaching. I consider myself fortunate to had a chance to work under his supervision.

Next, very special thanks to my committee members, Prof. Yasunori Mitani, Prof. Naitoh Masamichi and Prof. Masaaki Tamagawa for their suggestions and particularly for their patience in reading my draft of dissertation.

I would take this opportunity to thank Prof. Shyam S. Pandey who guided me to work in Hanamoto laboratory and provided time to time suggestions in different aspects of learning and study.

I would take this opportunity to pay a warm regard to my respected master's supervisor in India Prof. Alka Singh, for providing a nice research background which genuinely helped me to carry out my research to a new level during PhD.

I am also very thankful to all my laboratory members for helping and supporting me during the period of PhD. Especially, Tsuchiya Atsushi who helped me during my first and second year stay of PhD in Japan. Nagaoka, Masutomo and Masaya for teaching and providing special helps in research and had enjoyed the time with them. In this order, Yoshino and Maehata who always makes the laboratory environment humorous, enjoyable and friendly and helped me during this study period whenever required.

I wish to give my special thanks to Gaurav Kapil and Gyanendra Nath Tripathi, as an elder brother and as a friend, who always provide and input special thoughts and ideas during my PhD.

I express warm thanks to Nishant Koganti, Mallikarjun Yelameli and Ravikant Pandey for their enjoyable friendship company. Also, being in the same lab a lot of nice research discussions with Ravikant Pandey which really helps me to widen my research area and knowledge.

In India, I would like to thank my teacher Sanjeev Sharma, who motivated to aspire for higher studies during undergraduate study and developed an interest in learning process. Also, my another teacher Sunil Thapa, who also helped to understand different learnings.

In addition, I also place on record, express my gratitude to all the staff members and students of KIT who helped me directly or indirectly during my PhD period and stay in Japan.

Last but not the least, it's a formality with a lot of sincerity to express my sense of gratitude to my parents and my elder brothers and other family members for supporting me throughout the academic career and life.

Ravi Nath Tripathi

TABLE OF CONTENTS

LIST OF FIGURES

LIST OF TABLES

CHAPTER 1

INTRODUCTION AND LITERATURE REVIEW

1.1 General

The global energy demand is one of the prime concern in developed as well as developing country. The rapid increase of the consumption with the evolving technological gadgets and instruments keeps the demand on toe. The most of the energy and power generation is dominantly depends upon the conventional source of energy. In the last decades, there is a lot of focus to reduce the dependency on the conventional sources of energy and look for the alternative sources of energy. The concern about the alternative source of energy is that it should be clean and green energy source due to environmental issues.

The energy that comes from resources which are continually replenished such as sunlight, wind, rain, tides, waves and geothermal heat are termed as renewable energy. Approximately 23.7% of global electricity production in the world is from renewable energy sources (RES). The sub-divisions of RES percentage are 16.6% from hydroelectricity, 3.7% of all energy from wind, 2% of all energy from bio-power, 1.2% from solar PV and sources as geothermal, CSP, and ocean account for another 0.4% in Fig. 1.1 (a) and (b) and are growing very rapidly (Estimated Renewable energy share of global electricity production, End 2015) [1].

1.2 Renewable Energy: Solar Energy an Alternative Source

The renewable energy sources are emerging as a key alternative to fill the energy gap with the research and advancement in power electronics devices, system and control. In the newer aspects of energy, solar energy is one of the prominent source. The advantage of solar energy is the possibility of uses in variety of forms and application. The solar energy used as solar thermal energy, solar photovoltaic system and various applications as stand-alone mode and grid connected mode. In addition, the use of solar energy as an alternative RES can significantly reduce the carbon emission, which may help to reduce the level of greenhouse gases (defined by Kyoto Protocol) [2]. The aspects of energy generation based upon considering the idea to make the individual houses, offices and societies self-sufficient in terms of uses. The global evolution of installation of annual PV capacity in Fig. 1.2 is showing cumulative growth in

percentage for Asia and other regions (including developing countries) and it point towards the trend of utilization of PV in as one of the main alternative source [3].

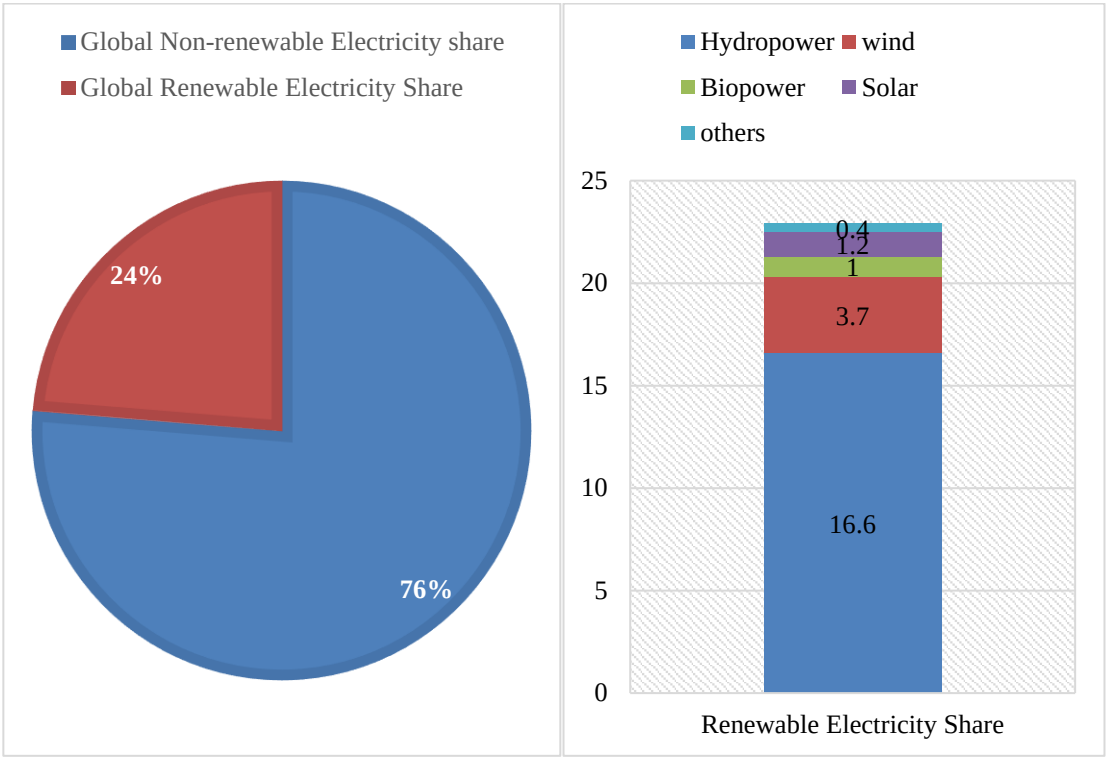

(a) (b)

Fig 1.1 Global electricity generation share in the year 2015
a) Percentage of renewable and non-renewable sources in electricity generation
b) Percentage combination of different renewable sources for generating electricity.

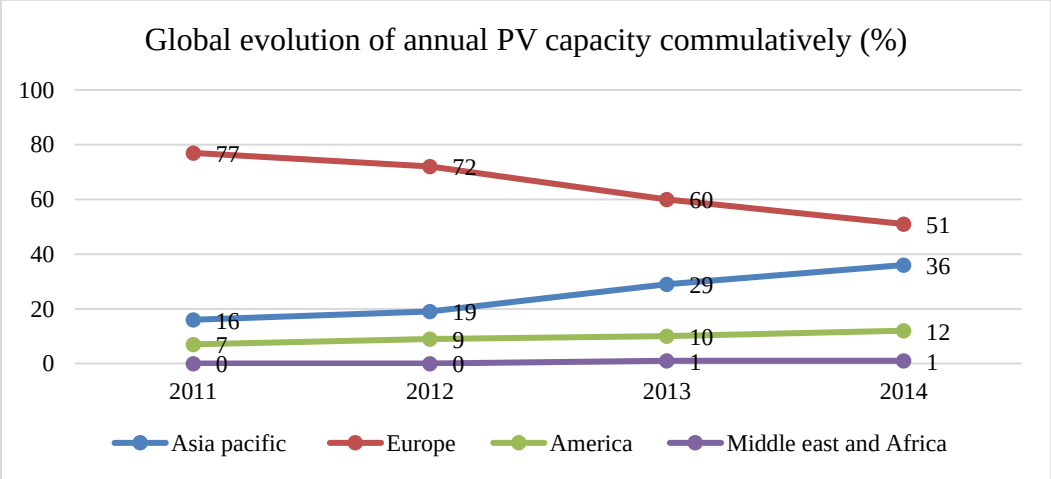

Fig 1.2 Percentage cumulative global evolution of PV capacity from the year 2011-2014.

1.3 Motivation: India, Japan and World

It is nearly impossible to meet the rise in electricity demands using conventional sources of energy, which are non-exhaustive and important to exploit the resources in a better way with the fast growing technology keeping the thought of sustainable and environmental friendly system. Considering various critical points, solar energy is exhaustive and improving year by year with advancement in scientific and technological advancement.

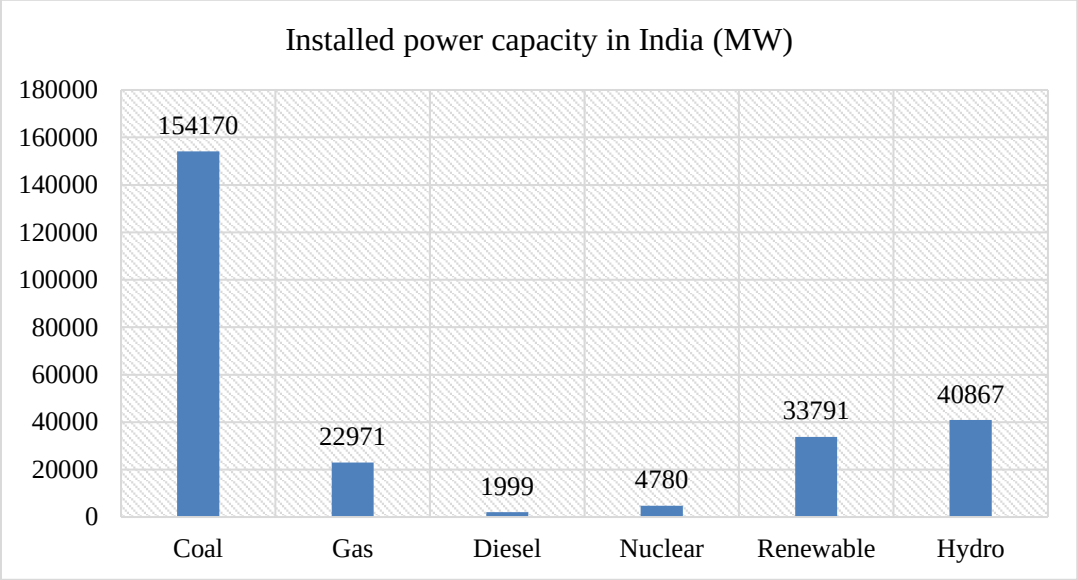

Fig 1.3 Overall installed power capacity in India using different sources of power as of December 2014.

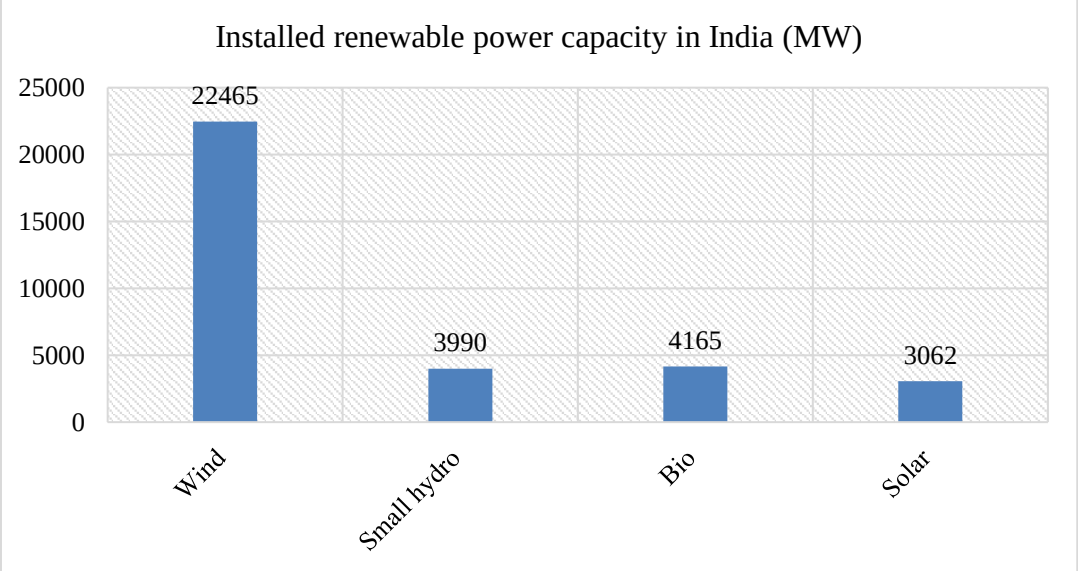

Fig 1.4 Breakup of installed renewable power capacity in India as of December 2014.

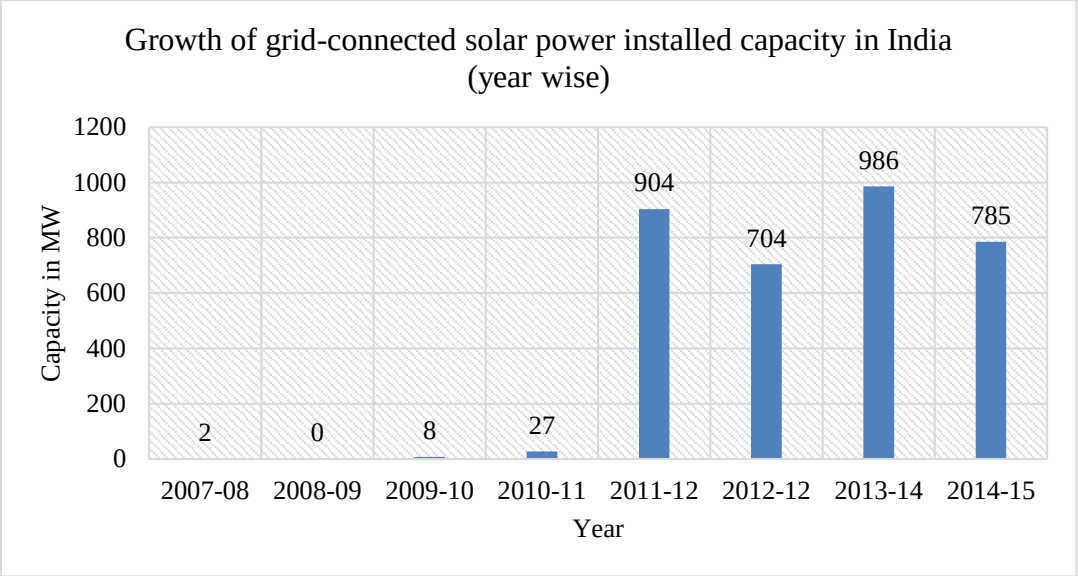

Fig 1.5 Grid-connected PV power system Installation growth in India from year 2007 to till December 2014.

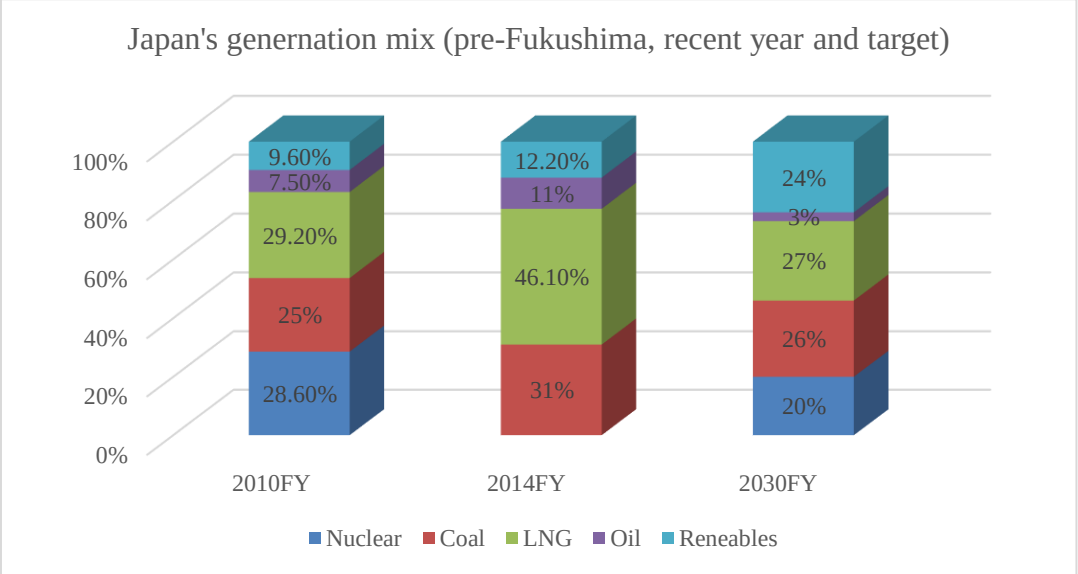

Fig 1.6 Power generation breakup of Japan for pre-Fukushima scenario (year 2010), post Fukushima scenario (year 2014) and future target (year 2030) set by government.

India is one of the developing country with rapid increase in demand of power every year and suffering from power outage due to shortage of power. The mix of installed power capacity in India is having significant contribution of renewable energy in Fig. 1.3 [4]. Several countries having a lot of potential for generation of solar energy based upon their geographical position. India is one of the potential country with good average solar isolation level in most part of the country. The solar power is having

significant contribution in overall renewable power generation Fig. 1.4 [4] with wind power as a major contributor, and it is increasing year by year. There are lot of initiatives like as roof-top solar PV, solar based water pumps and solar lights with the support subsidies have been started by the Ministry of renewable energy (MNRE), Government of India (GoI) under Jawaharlal Nehru national solar mission programme (JNNSM) to boost the solar power generation and also various plans for other types of renewable energy sources.

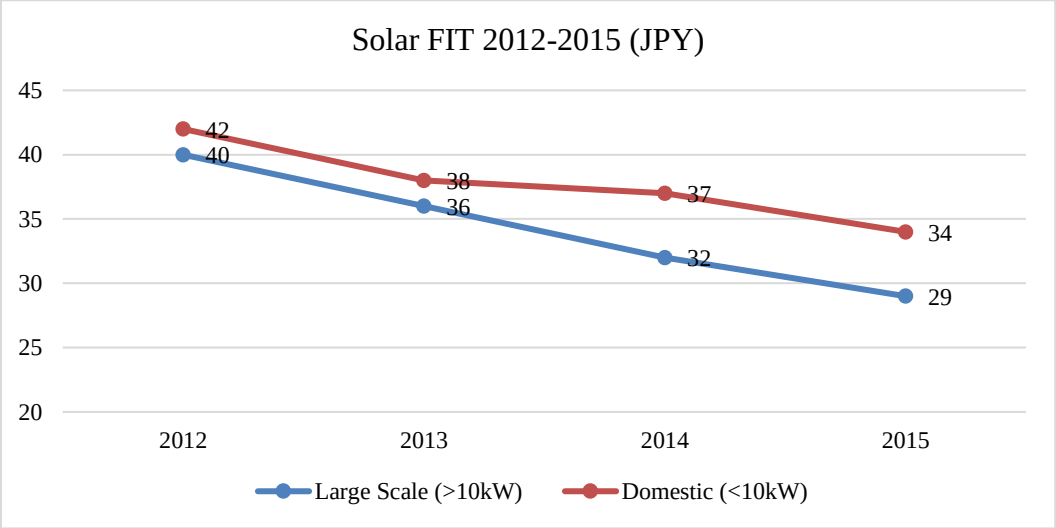

Fig 1.7 Feed-in-Tariff (FIT) rate for large scale and domestic PV system in Japanese yen (JPY) for the year 2012 to 2015

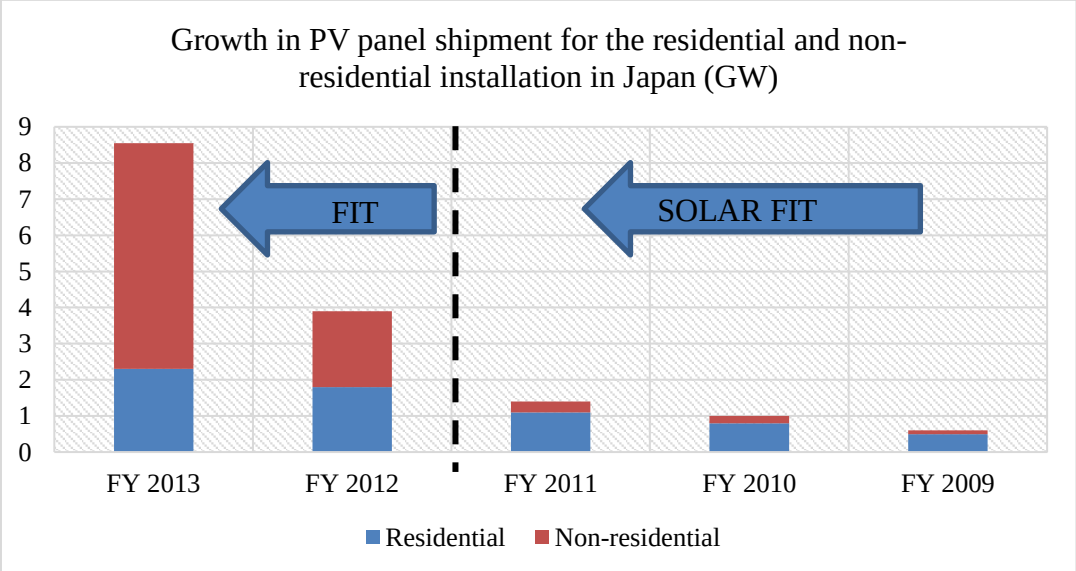

Fig 1.8 The effect of FIT scheme in the growth of PV panel shipment for residential and non-residential installation from year 2009 to 2013.

Table 1.1 Cumulative installation capacity of different renewable energy sources till the end of year 2014 and installed before 2014.

	Up to the end of 2014FY (GW)	**Installed before 2014FY (GW)**
PV (residential)	3.79	861,00
PV (non-residential)	78.84	3.1
Wind	2.29	0.33
Hydraulic	0.66	0.09
Geothermal	0.07	0.01
Biomass	2.03	0.22
Total	87.68	18.76

Table 1.2 Installation of PV power considering AC-based and DC-based capacity under different power rating for the year 2014.

	Capacity (AC-based)	**Capacity (DC-based)**
<10kW	860,58	861,00
<10kW− <50kW	3049,435	3201,91
<50kW− <500kW	980,0929	1107,50
<500kW− <1MW	1078,244	1218,42
<1MW− <2MW	1935,07	2322,08
2MW or more	662,099	827,62
Total	8565,521	9538,54

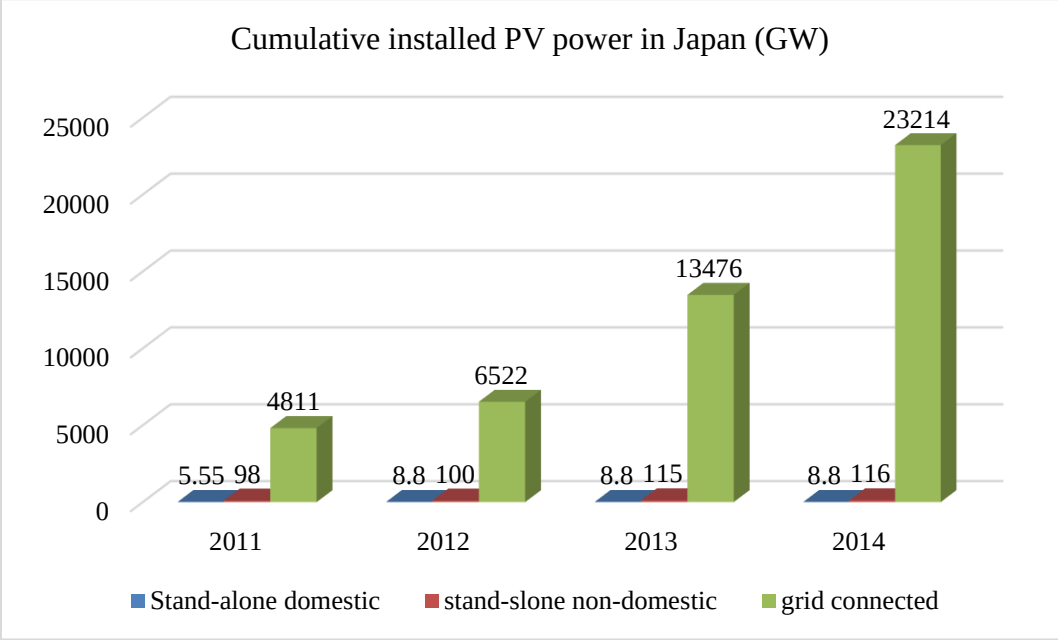

Fig 1.9 Cumulative installed PV power capacity under stand-alone (domestic and non-domestic) and grid connected mode for the year 2011 to 2014.

The power generation mix of the Japan Fig. 1.6 [5] is having LNG, nuclear power and coal as a major contributor of power source for the year 2010 (i.e. before Fukushima incident). The mix of generation source is changing significantly after the natural disaster of Tsunami causing nuclear plant related issues. In the year 2014, LNG and coal are the main contributor of power sources and ministry of economy, trade and industry (METI) Fig. 1.6 proposes future target of power generation mix.

The Feed-in-Tariff (FIT) has been introduced in the Japan in July 2012 Fig. 1.7 [6] and it was the turn-around for the PV market in Japan Fig. 1.8 [7]. In addition, the nuclear disaster in Fukushima, Japan of March 2011 has activated the governmental and people to adopt better and safe alternative source of energy, which has given a boom in the renewable energy (solar PV) generation. The evolved boom in solar PV market can be seen in the survey in which Japan was at the 5th place in 2012, reached to 2nd place in 2013 and remained at 2nd in 2014 [3]. Installed PV power capacity Table 1.1 [6] is showing rapid growth comparing to various renewable source before and after year 2014 Table 1.1. Growth in ac and dc PV capacity observed for application under different power ratings Table 1.2 [8].

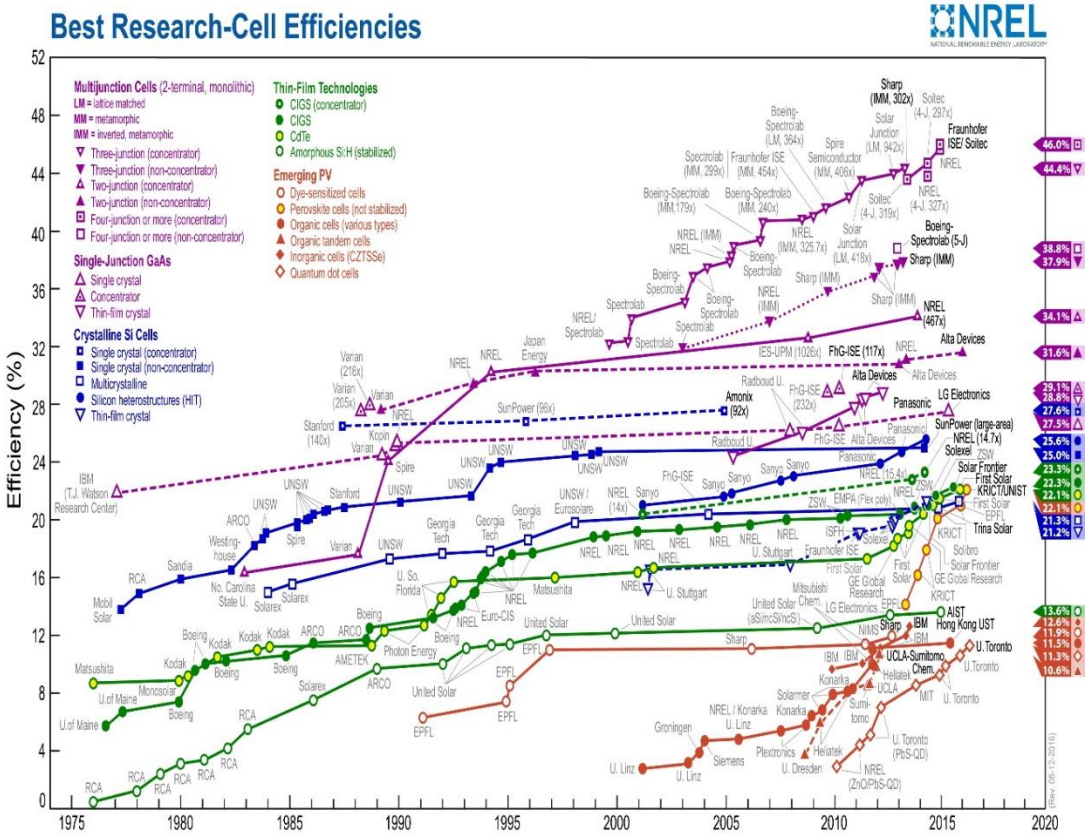

Fig 1.10 PV Cell conversion efficiency provided by national research energy laboratory (NREL).

The cumulative growth of install PV power (in Japan) is most attractive for the grid connected mode applications Fig. 1.9 [10] and showing increasing trend from year 2012 to 2014 In Japan and India, 9.7 GW and 0.7-0.8GW capacity of solar PV added in 2014 respectively raising total capacity to 23.3GW fed to the grid for Japan [1].

The cost and efficiency of solar panel, cost and efficiency of overall installed solar PV system considering other electrical arrangements are the deterrent factors for the increase in solar PV power generating system. In this decade, the cost solar PV modules have been declined so as the price per watt of overall installed solar PV power generating system is reduced [1], [3], [9].

There are a lot of research going on to improve the efficiency of solar cell considering different materials and designing solar cells for specific application. The solar cell efficiencies are as low as 0.5-6% to as high as 46% in Fig. 1.10 [10]. There are different constraint regarding the use of solar cells like as high efficiency solar cell may be economically not viable due to high production cost or may be the life time of solar cell is low there the performance deteriorates (not stable) for longer period of time. Economically feasible solar cells having 13-21% with average life span of 25 years are commercially available.

1.4 Photovoltaic (PV) Power Generating System

PV power generating system used in various modes and fundamentally categorized as stand-alone and grid-connected system, for residential (rooftop), agriculture, commercial and industrial purposes. PV cell used for very small power applications (in calculators and watches) and high power applications in module/array configuration. The PV system categorization represented in hierarchal chart in Fig. 1.11 based upon the working modes and application. The stand-alone PV system is best suitable for remote village areas where supplying electricity through electrical grid networks is not an economically feasible solution and used for specified application such as solar PV pumping in agriculture. The stand-alone system utilized with or without storage and as a hybrid system according to the requirement of application. However, the standalone system without storage is having very low utilization capability of the generated power if not been utilized now and cannot be utilized during night or low light condition. There are six basic applications of PV system is mentioned in [3] and considered as Pico PV system, off-grid domestic, off-grid non-domestic, hybrid system, grid connected centralized and grid connected decentralized system. It has mentioned that

pico-system utilized for lightening efficient LEDs using well controlled and designed charge controllers for batteries, phone charging, and providing power to small radio and other low power appliances.

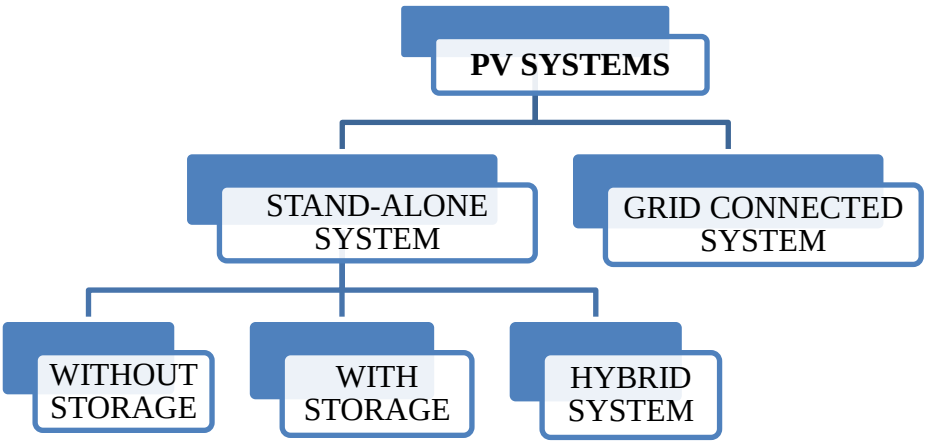

(a)

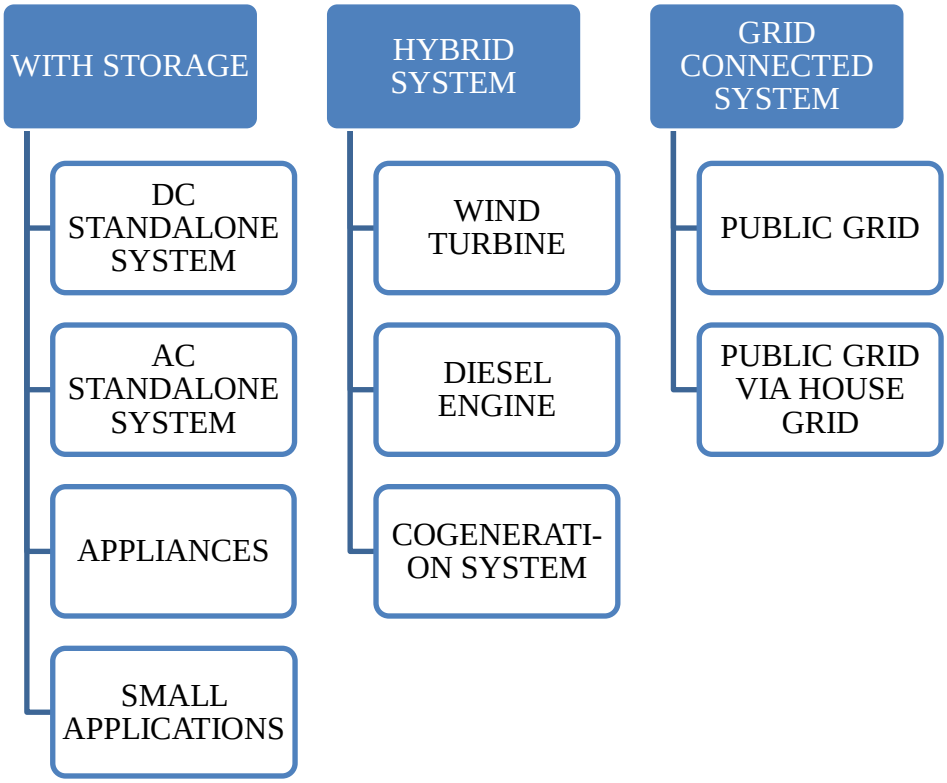

(b)

Fig 1.11 Hierarchical chart of utilization of PV system in different mode and forms:
a) General categorization of modes of PV system
b) Application based categorization considering generalized modes.

Off-grid domestic systems mentioned as enabling the remote houses and village with electricity where electrical grid connection is not available. In recent years, these systems developed like a mini grid to have better utilization of the energy as a local community independent electrical grid. The use of PV system for agriculture (PV fed water pumping system), terrestrial system (satellites for communication and others purposes) and for refrigeration is defined as off-grid non-domestic PV system installation.

Hybrid system represented in Fig. 1.11 and PV integrated with diesel engine generating electrical power as a hybrid system. The hybrid system also utilized with wind turbine and cogeneration system. The diesel generator based PV system micro-grid is expanding and utilized for feeding electricity to telecom network stations providing cost effective and reliable system. Especially much useful for small remote places in developing countries where information system (internet and mobile) is growing rapidly.

In last decade, most of the installed PV units are grid-connected system in Fig. 1.12 and 1.13 [3]. The grid-connected system employed as decentralized power generating unit i.e. connected to electrical grid via residential grid and centralized power generating unit i.e. directly connected to the electrical grid network. The increased penetration of PV power to the grid is due to inherent storage property of the electrical grid, which evacuates the overall generated power, and economic advantages as cost per watt reduced.

The power electronic interface is required for integration of PV power generating system to ac grid by converting the dc output of solar PV into ac i.e. dc-ac converter. Current source inverter (CSI) or voltage source inverter (VSI) Fig. 1.14 used as a power electronics interface for grid integration PV system [11], [12]. The advantage of CSI is reported for the number of modules connected in series is reduced which declines the effect of partial shading as number of PV modules in series governs the number of peaks in PV output [13], [14]. CSI improves the potency of the maximum power point tracking (MPPT) and voltage boost capability improves the efficiency of overall system by utilizing single stage conversion [15], [16], [17].

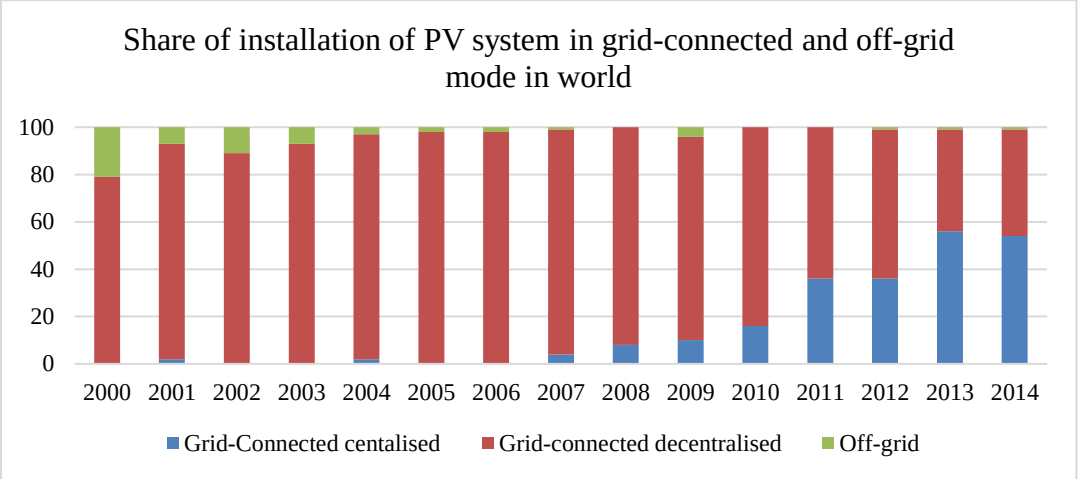

Fig 1.12 Cumulative installed PV power capacity under stand-alone (domestic and non-domestic) and grid connected mode for the year 2011 to 2014.

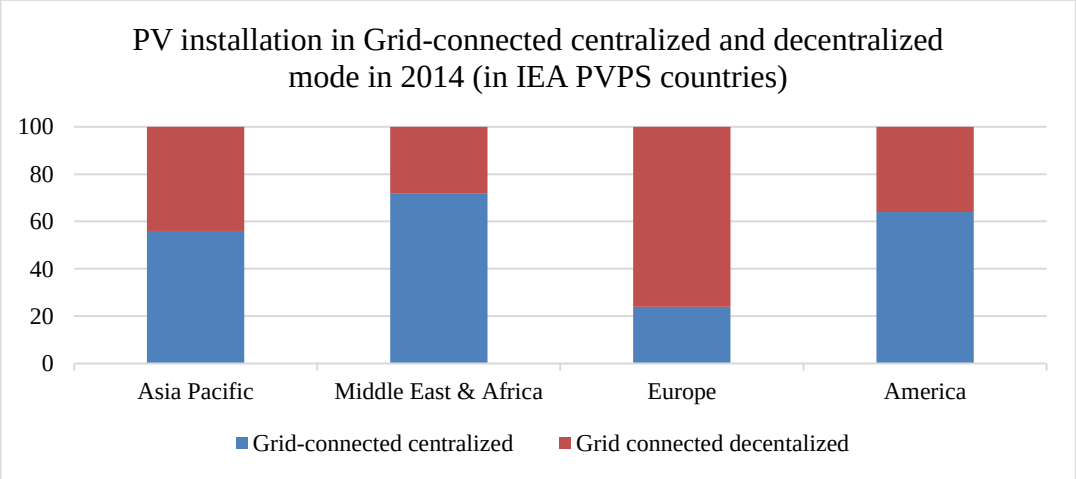

Fig 1.13 Installed PV power capacity in grid-connected mode: centralized and decentralized in IEA PVPS countries.

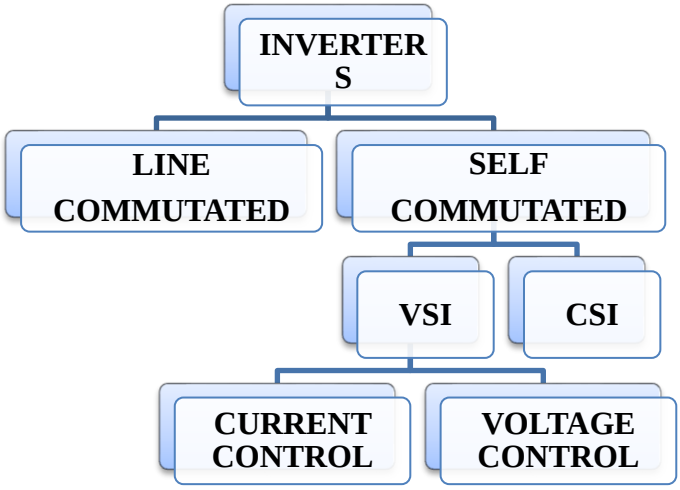

Fig 1.14 Different type of inverters based upon commutation.

CSI is not a feasible option for PV power penetration to grid at high-medium power medium voltage level due to increased switching device losses as compared to VSI under similar operating conditions (grid parameters, rating, switching frequency) [15]. Therefore, VSI is preferred for medium and high power medium voltage three-phase ac grid system. However, the disadvantages are there like as quality of output voltage and switching losses.

The classifications of grid integrated of PV system are as single stage inverters: PV inverter without dc-dc converter (with or without isolation), two stage inverters: PV inverter with dc-dc converter (with or without isolation) and multi-stage inverters: number of dc-dc converter/dc-ac inverter corresponding to PV configuration Fig. 1.15 [18] [19], [20]. MPPT, voltage and current control grid interfaced PV inverter system without dc-dc converter implemented together in one stage. MPPT control implemented separately through dc-dc converter stage and inverter control (outer voltage control and inner current control) implemented independently for dual-stage grid connected PV inverter system. The configuration of PV module topologies discussed in chapter2 considering fundamental classification of PV system integration to grid.

PV system of rating up-to 5kW used for rooftop application and usually integrated to single-phase grid system. In this research, a three-phase dual-stage grid connected PV system of 10kW rating implemented with isolation transformer operating at grid frequency. VSI interfaced grid connected PV system implemented based upon the outer voltage control loop responsible for the dc voltage regulation and inner current control fed with generated reference current. There are various control algorithms for generation of reference quantity implemented for grid interfaced PV system. The current control based scheme is implemented more dominantly in comparison to voltage control based scheme because of high power factor obtaining capability with better transient current suppression under disturbance (percentage ratio of current and voltage controlled scheme: 81:19) [21].

Synchronization and power control strategy is required for the operation of PV system integration to grid. The various control strategy is mentioned in the literature and researches based on the power control algorithms and synchronization. The synchronous reference frame (SRF) theory implemented for control in [22-26]. The SRF based control is implementing using phased locked loop (PLL) for frequency

synchronization. In [27, 28] the instantaneous power based control for integration of PV system to grid. Earlier, the power balance theory (PBT) is applied to implement the active power filters in [29, 30]. This theory does not require PLL for grid synchronization, and power compensation and synchronization principle is simple and achieved through templates. [31]

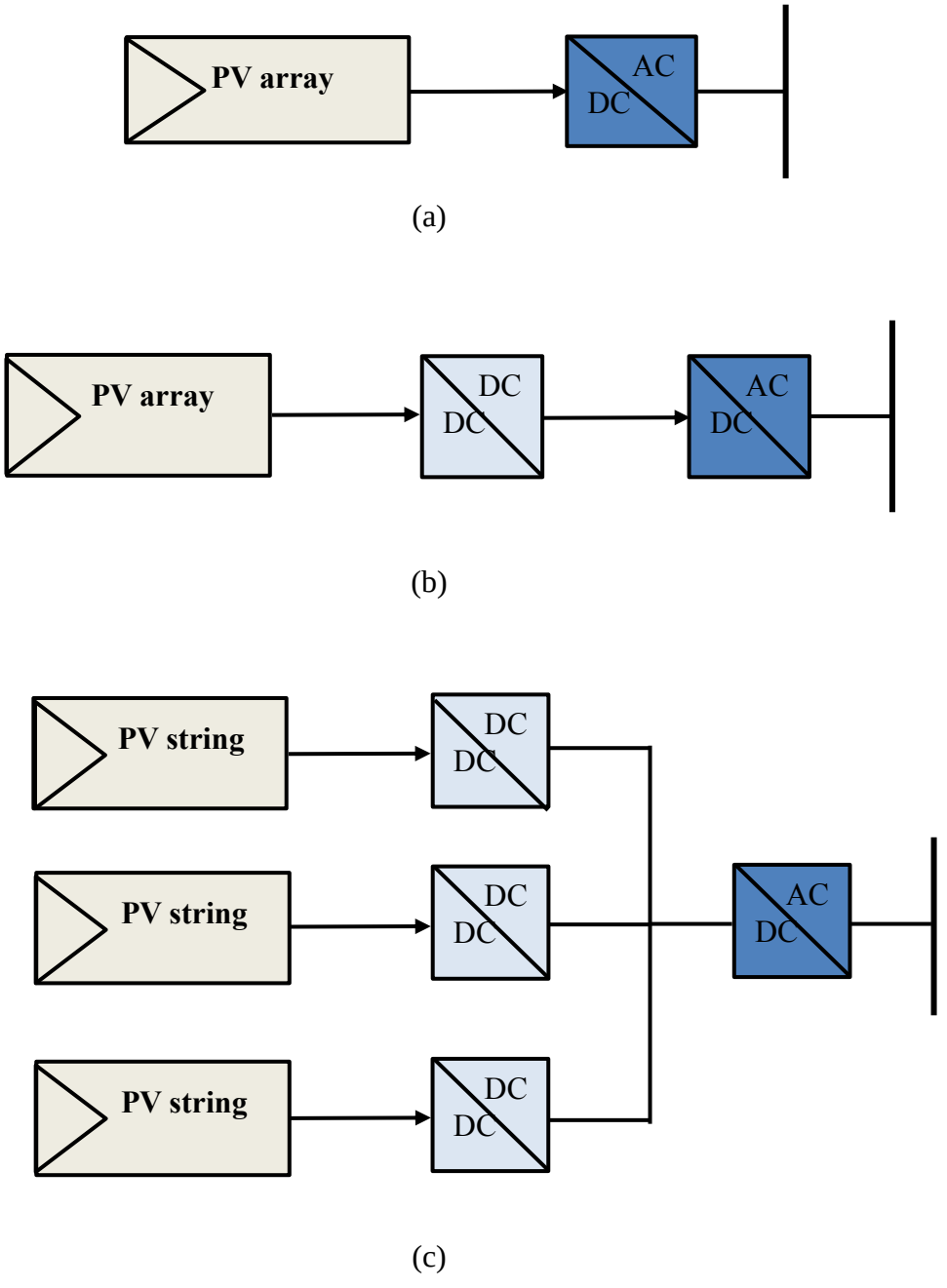

Fig 1.15 Inverter configurations considering PV configuration and control:
a) Single-stage inverter
b) Dual-stage inverter
c) Multi-stage inverter

PWM current controlled voltage source converter (VSC) used for the integration of solar PV system to AC grid. In addition, the interfacing of DER units with the grid requires the power-conditioning unit to achieve the desired standard of power quality. IEEE-519-1992 defined the limits for the power quality standards in terms of allowable ripple injection into the grid by the converters [32]. Converters used for the conversion and control of power are responsible for the generation of current harmonics/ripples on the AC side due to switching of converter. L, LC and LCL filter configuration used in the system depending up on the different power levels and problems associated with the system. The L and LC type filter are bulky and very expensive for medium and high power application (10-100 K-watts and M-watts) due to the inclusion of high value inductance. The LC filter substituted by the LCL filter. The low pass LCL filter is better option for the medium and high power application and can also be used for the low power application [31], [33], [34].

The design of LCL filter is having one of the important roles in the entire system and plays vital role for stability of the system. By taking care of cost problems, the LCL filter design is used in a way that using lower value of inductance, which is expensive and bulky too, higher value of capacitance which is cheaper [31]. The grid impedance is also having impact on the stability of the system and special care required in the design of LCL filter. The resonance frequency of LCL filter varies as the grid impedance varies i.e. stiffness of the grid [31], [35].

Dc-ac voltage source converter can be employed using PWM control switching signals. The control methods in power electronics categorized as linear and nonlinear control. The linear control is accommodated with co-ordinate transformation and modulator which fit the system to use the simple and popular proportional-integral (PI) controller, by linearizing the converter up-to an extent [36].

The non-linear controls evolved with the advancement in the power electronics control technology. Hysteresis current controller (HCC) is one of the prime example of non-linear controller and employed for power electronics control application. HCC has several advantages over linear control like as simple structure, robust and high performance dynamic response but have major drawback of variable switching frequency and not easy to extend for different converter/inverter topology. In addition, the mathematical equation derived using analysis of the electrical circuit and control shows complex relation between switching frequency, dc link voltage and hysteresis

band [37]. So, the variation of dc link voltage which in turns have variation in reference current results in variable switching frequency and high stress on switching devices. There are several researches going on to improve the performance of HCC by rectifying the drawback [38]. However, the verification of improved control is a key consideration for specific application.

There are several other control approaches developed in the recent decade with the development high performing computer technology (fast digital microprocessor unit). The control of power electronics system such as fuzzy logic control, model predictive control (MPC) and sliding mode control (SMC) evolved and received attention of the researcher [39]. However, each control method is dealing with specific disadvantage with some advantages over other control methods. Therefore, it can be concluded that no control method capable of overcome the drawbacks completely and dealing with some pros and cons of it. Therefore, there is still a lot of potential for improvement in linear controller to exploit the usefulness and advantage in much more efficient way to develop high performing controlled system.

The VSI interfaced grid connected PV system controlled through enclosed loops. The fundamental motive of the control of VSI is to feed the clean and possible in-phase sinusoidal current into the grid. The current control loop (inner current control) employed to regulate the current. In general, inner current loop implemented using proportional-integral (PI) control and generates the ac voltage reference for the inverter. The PI controller implemented for dq reference quantity obtained using synchronously rotating frame (SRF) because of incapable to track the reference signal accurately under stationary frame. abc-dq transformation converts the ac signal into dc quantity by changing from stationary frame to rotating frame. PI controller employed on constant signal in the dq reference frame can ensure to track the reference adequately with easy design and implementation. However, still there is a problem regarding filtering of ripples generated due to unbalanced quantities transformed into SRF. Another variety of controller is proportional resonant (PR) controller that is capable of regulating reference current in stationary frame. PR controller in stationary frame αβ/abc equivalent to PI controller in rotating frame dq. However, there are some differences in the performance of the system. The simplified way of system control implementation is to utilize the error current for generation of PWM signals and a proportional gain termed as modulation gain is required to improve the system performance and obtain

the trade-off between modulation index and quality of grid current and point of common coupling (PCC) voltage.

The two-level VSI consists of six switching devices to generate the three-phase ac voltage output and couple to the grid by proper generation of gate signals. The generated voltage reference/current error used to generate the gating signals fed to the switching device. Some of the common methods to generate the switching signals are sinusoidal pulse width modulation (SPWM), third harmonic injected (THI) PWM, space vector PWM and hysteresis current controlled (HCC) PWM.

In several enclosed loops, the outer voltage control loop used to regulate the dc-link capacitor voltage. The capacitor dc voltage of VSI in a grid connected PV system can be regulated using various types of controllers like proportional plus integral type controller (PI/PID), fuzzy logic controller (FLC), Fuzzy-PI. In general, dedicated PI/PID controller extensively used as single input-output system for dc voltage control and for process control in industrial applications due to ease of implementation.

It is possible to achieve regulation of the dc voltage of VSI to the desired reference voltage but there may be the possibility of not getting good transient response while connecting to the grid and under disturbance. PV system is a distributed generating system and there is a possibility that it has to deal with the islanding condition and disturbances.

The transient response is very important consideration during interconnection of PV system and disturbance/fault in the system. It is the desirable to have fast and ideal response in the system but it deals with the limitation to and nearly impossible to obtain the optimal response for the system using conventional PI controller with one degree-of-freedom (1-DOF). Therefore, it is necessary to improve the transient response of the system considering the performance of conventional 1-DOF PI controller.

The performance of the designed control structure is dependent upon the controller gains. The tuning of the controller parameter is depending upon the trade-off between response speed, stability under small disturbance and robustness of the controller under large signal disturbance and if control loops are non-linear in nature then it requires special care to select the control parameter considering various operating constraints. [40]. Controller can be tuned using trial and error method and transfer function based mathematical model criteria. Modulus optimum, symmetrical optimum and pole

placement methods are three criteria defined considering transfer function based mathematical model of control loops. Symmetric optimum (symmetric optimum-pole placement) approach is suitable for the voltage controller loop considering mathematical model transfer function [40]. The designing of mathematical model of control loop requires various system parameter [41], [42], [43] and it is not easy approach to approximate and compute the various system parameters which can be a tedious process. Two problems considered at this stage:

1) design of a controller based upon the concept of degree of freedom and
2) tuning of controller parameter.

The concept of degree of freedom for system control is widely utilized in the motor control application by using different controller configuration in the system. The number of closed loop transfer functions of a control system can be adapted independently is termed DOF [44]. The 2-DOF PI/PID control structure has been proposed and utilized under various control schemes for different type of application with significant advantage over 1-DOF PI control [45]- [49].

The 2-DOF based controller can be designed for dc voltage control in grid connected PV system [44]- [51]. However, considering 2-DOF system it is also required to have the proper controller configuration. The different system configuration used in the motor control system based upon the DOF concept. [52]

The PI/PID control structure designed to obtain the stability and good control with better transient responses. The gains of the controller need to be appropriately tuned and various tuning methods have been proposed and discussed like as iterative feedback tuning (IFT), virtual reference feedback tuning (VRFT) and fictitious reference iterative tuning (FRIT) by several researchers in [53]- [57]. These direct design approach only requires the input, output data of the controlled system, and received significant attention. The IFT tuning requires the multiple experiment data for iterative tuning to achieve the desired optimal response while VRFT required only one-time experimental data. FRIT is also used only one-time experimental data for the optimal controller gain tuning. Therefore, these tuning methods helps to achieve the optimal controller gains without any requirement of system/plant model information based upon the one-time closed loop experimental data. The basic difference between VRFT and FRIT is that in case of the VRFT minimization of function emphasizes on the input while FRIT emphasizes on the output. Therefore, the FRIT method may be more

advantageous and establishing better understanding in practical sense. FRIT method implementation and approach is better for 1-DOF as well as 2-DOF controller in comparison to VRFT [56]-[60].

FRIT method modified, studied and analysed for different application and optimal performances in [55]-[62]. It can be implemented as both online and offline system for controller tuning. The FRIT method deals with the disadvantage that it may results in local minimum for PI/PID controller tuning due to the non-linear and non-convex problem consideration. Therefore, the FRIT method required to combine with an optimization technique to mitigate the local minimum solution for non-linear and non-convex optimization problems.

1.5 Objectives

The study aims to have an insight of the controller and controller tuning method for the control loop of grid-connected PV system. Focus of this dissertation is to substantiate the application of 2-DOF controller and data driven optimized tuning method by implementing for outer voltage control loop responsible for dc voltage regulation with theoretical analysis and simulation results.

The main objective to employ 2-DOF controller is to obtain better trade-off for the response of system control under different operating conditions. Data-driven optimized tuning of controller using FRIT does not require plant information. Transfer function based mathematical model is required to analyse the stability of the system considering optimized gains obtained through data-driven method.

The 2-DOF controller structure designed and applied for dc voltage control of VSI and compared with conventional PI controller with 1-DOF. The performance of the controllers compared for the gains obtained using data-driven tuning method and trial and error method.

The important point about the controller is their performance and stability. The stability of the controllers is analysed using bode-plot and root locus technique. In addition, the performance of the controller investigated and analysed considering step response of the control loop.

1.6 Organization of Dissertation

This dissertation consists of the six chapters. The first chapter focussing on the requirement of renewable energy and especially solar energy. Moreover, why and how it is important for the society and world and followed by the present scenario of solar power generation in India, Japan and world. Later part introducing about the PV power system and a detailed literature review and objective of the dissertation considered in this chapter.

Chapter 2 aims to give an insight about the functioning of solar cell and its materials. The characteristics of the solar cell and the effect of partial shading demonstrated by modelling solar PV modules. The detailed analysis how the configuration of solar PV system is important for grid connected PV system with MPPT control.

Chapter 3 presents the modelling, control and design of grid connected solar PV system. The system design starts with filter and LCL filter discussed considering different parameter constraint affecting the design and performance of the filter. The control of the system describes about the phase locked loop (PLL), reference current generation, dc voltage control, current controller and switching scheme. The 2-DOF controller configuration introduced and designed for the voltage controller considering desired requirement.

Chapter 4 focussing on the data-driven controller tuning method. The data-driven FRIT method explained based upon the mathematical equations and model of the controller. The mathematical equations derived for 1-DOF and 2-DOF controller to implement FRIT method. FRIT combined with particle swarm optimization (PSO) method.

Chapter 5, recently digital signal processors (DSP) and field-programmable-gate-array (FPGA) are the one of the prime technology in the field of power electronics applications for motor drive and renewable energy. In addition, learning new technology from the scratch is not an easy task like as programming FPGA and DSP. In this chapter, fundamental components necessary to implement the control for integration of PV system developed using Xilinx system generator. System generator capable of generating hardware description language (HDL) files and can be used for FPGA based digitally controlled system.

Chapter 6, this chapter summarizes the work demonstrated in the dissertation and reaches to the conclusion with future scope of the work.

CHAPTER 2

Solar PV POWER GENERATING SYSTEM

2.1 General

The solar cell modeling is one of the important aspects to obtain the better and more accurate solar characteristics with reduced computational effort so that to reduce computational time. As the mathematical computational effort reduces, the computational time will reduce and better accuracy or maintaining original accuracy is a key point. The more accurate cell characteristics are important to implement the maximum power point (MPP) tracking algorithms efficiently to improve the overall efficiency of the system. Also, the solar cell characteristic changed suddenly with the change in weather condition so the robust MPP tracking algorithms can be implemented based upon the cell characteristics obtained from the solar cell modeling techniques.

The solar strings/modules connected in series and parallel combination to create a solar PV array. The series/parallel combination of PV is crucial because of partial shading effect and maximum power point tracking (MPPT). Depending upon the natural environmental conditions like as cloud, tree shadow, dust are the reasons of partial shading effect. The partial shading leads to the bad performance of the panels and it may cause the destructive effects on the panels due to hot spots. The output current of the string under the influence of partial shading is decreases significantly; therefore, the output power (peak power) is changed. To mitigate the problem of partial shading, a by-pass diode is required in parallel to solar cell/module/string [63]. The placing of bypass diode planned to have best cost effective system. Reverse flow of current from healthy string to other malfunctioned string is another problem associated with partial shading effect on string/module. This problem mitigated by putting blocking diode in series with each solar string [63].

There are several proposed modelling techniques available in literatures based upon the single diode based modelling and double diode based modelling. The single diode based modelling technique requires less computational effort and easy modelling implementation with quite good accuracy, that is why it is most commonly preferred in different papers. The double diode model offers better accuracy in comparison to single diode model and different ideas were proposed to obtain easy implementation technique and maintaining better accuracy [64]- [66]. In these research works of system

modelling, there are the techniques mentioned that how to extract electrical parameters for the model. However, still it is difficult to maintain the accuracy under low irradiance and for different combination of changes with lesser effort. The electric characteristics of PV module is analysed under several condition of irradiance and it suggests that the characteristics of the PV system becoming more complex for non-uniform irradiance/partial shading condition [67]- [71]. The complexity of characteristics depends upon the configuration of solar PV modules as the number of modules connected in series in a string decides the number of peaks in P-V characteristic under partial shading condition [13].

Incorporation of the partial shading characteristic generation capability in solar cell simulator is very important to investigate and analyze the cell characteristics under shading conditions. So, to obtain and track the best possible output power from solar PV array the characteristics should be obtained under partial shading/non-uniform irradiance condition and effects of by-pass diode and blocking diode can be investigated and analyzed based upon the PV characteristics. The PV array system poses the exponential (non-linear) I-V characteristic and also sudden and complex changes in characteristics due to weather or some other reasons. So for the modelling purpose the parameters of the system need to be tuned from experimental data sheet of practical device to obtain best possible accuracy in the simulator model. The electrical circuit model equations based mathematical modelling of PV array system can be useful and able to analyze the dynamic and complex characteristic, study of dynamic analysis of dc-dc converters based upon PV characteristic, study and analyze different array configuration and robust MPP algorithms implementation [72].

A typical solar panel converts only 30 to 40 percent of the incident solar irradiation into electrical energy. Maximum power point tracking technique used to improve the efficiency of the solar panel. According to Maximum Power Transfer theorem, the power output of a circuit is maximum when the Thevenin impedance of the circuit (source impedance) matches with the load impedance. Hence, our problem of tracking the maximum power point reduces to an impedance matching problem. In order to extract the maximum amount of energy, the PV system must be capable of tracking the solar panel unique maximum power point that varies with irradiance and temperature.

Tracking the maximum power point (MPP) of a photovoltaic (PV) array is usually an essential part of a PV system. As such, many MPP tracking (MPPT) methods have been developed and implemented. The methods vary in complexity, sensors required, convergence speed, cost, range of effectiveness, implementation hardware, popularity, and in other respects. They range from the almost obvious (not necessarily ineffective) to the most creative (not necessarily most effective). In fact, so many methods have been developed [73] that it has become difficult to determine adequately which method, newly proposed or existing, is most appropriate for a given PV system.

MPPT achieved by using a power electronics dc-dc converter inserted between the PV module and load to achieve optimum matching. It ensures that the PV module always operates at its maximum power point by using an intelligent algorithm. MPPT optimizes the power output of the solar cell by constantly tracking the varying maximum power operating point and adjusts the solar panel operating voltage [73]. In this chapter, solar PV system modelled considering different arrangements with partial shading capability. The real time data of PV system measured for 3kW PV system available in university campus also investigated and analysed. The incremental conductance MPPT algorithm utilized for the implementation of the system.

2.2 Solar PV cell materials

The solar cell can be categorized based upon technology into three groups as: crystalline solar cells, thin film solar cells, organic and hybrid solar cells. Crystalline silicon, thin film and organic solar cells are termed as first generation, second generation and third generation solar cells respectively [74]. In present scenario, more than 80% of the entire cell production belongs to crystalline silicon technologies [3] PV cell is the smallest part in PV power device that further produced as PV module.

2.2.1 Crystalline silicon solar cells (First generation)

The crystalline silicon (c-Si) solar cells are one of the most popular and efficient solar cells. It can be categorized as wafer based crystalline: single crystal (mono-crystalline) and multi-crystalline (polycrystalline). Single crystal silicon (sc-Si) are one of the oldest, much reliable and efficient among the solar cells and manufactured using single crystal growth method [3], [75]. The one of the main and distinguished method to produce sc-Si is Czochralski (CZ) method [76]. The commercially available sc-Si solar PV modules have efficiencies between 16-24% as it is developed using high

graded silicon. The multi-crystalline silicon (mc-Si) solar PV cells are fabricated using multicrystalline wafers. In general, mc-Si formed by the Bridgman method of directional crystallization: cast solidification process in which silicon melt is poured into a cast and solidified [3], [76]. It is also one of the popular type of solar cells as it is less expensive in production as compared to sc-Si solar cells but less efficient. The conversion efficiency of commercially available mc-Si collar cells is around 12-18%

2.2.2 III-V Multijunction solar cells

These type of solar cells produced using GaAs and III-V materials. GaAs and III-V material have unique combination of properties that comprised of various advantage over other materials of solar cell. The conversion efficiency of commercially available mc-Si collar cells is around 12-18%. GaAs material on the Ge substrates achieved the conversion efficiency as high as high as 40% breaking the efficiency barrier. The drawback of high cost of III-V cells forced to use for special application like concentrator PV systems and space applications.

2.2.3 Inorganic Thin-Film solar cells (Second generation) [75], [76]

2.2.3.1 Cadmium sulphide cell

Thin film solar cells fabricated by depositing thin layers of PV semiconductor materials. The primary motive behind thin film solar cell was better power-to-weight ratio instead of lower cost. The first commercially produced thin-film solar PV cell made up of cuprous sulphide/cadmium sulphide (p-Cu2S/n-CdS). This material seems to be promising as thin film cell with efficiency greater than 10% achieved but poor stability and problems related to making of ohmic contacts to Cu2S became a major issue.

2.2.3.2 Amorphous and microcrystalline thin film silicon cell

Small amorphous hydrogenated silicon (a-Si:H) PV cells of efficiency 3-4% was achieved by Japanese and commercialized for consumer goods like as calculator and watches in 1980. Stabilised efficiency of 6-8% achieved for single junction amorphous silicon modules but the one of the popularly commercialized device is termed as micromorph configuration. Stabilised efficiency of 11.9% by Oerlikon Solar in 2003.

2.2.3.3 Cadmium telluride cell

The cadmium telluride solar PV cell developed with the device structure n-CdS/p-CdTe. The one of the best solar cell efficiency reached to 16.7% and recently it has reached to 18.7% for a cell developed by first solar in 2013 and more than 11% module efficiency is achieved in general. The bandgap of CdTe is 1.44eV is nearly ideal for terrestrial solar spectrum and it may be possible to achieve efficiency above 20% but the drawback is cadmium is highly toxic (telluride is also toxic if it into the body by swallowing or absorbing) and Telluride is one of the rarest material.

2.2.3.4 Copper indium gallium diselenide (CIGS) solar PV cells

Thin-film PV solar cell produced using CIGS is also a famous technology and the best laboratory cell efficiency is achieved around 21% with 17.8% efficiency of sub-module. However, the CIGS technology also unable to cope-up with decreasing prices of c-Si technology PV modules.

2.2.4 Organic and hybrid technology solar cells (Third generation)

2.2.4.1 Organic PV cells

The electric field produced at the heterojunction between donor and acceptor properties materials in an organic photovoltaic (OPV) cell. Earlier discovered OPV cells were having very low efficiencies and to high electrical resistance, bad materials control and low internal quantum efficiency were the major factors of it. In 2012-13, the best-achieved efficiency was for Heliatek's tandem OPV cell with 10.7%. The most recent best achieved efficiency for OPV cell is 11.5% by Hong Kong UST as reported in NREL chart [10]. OPV has drawbacks off bad stability and lifetime (due to fast deterioration with time) with the edge of lightweight, bandgap adjustability and low cost.

2.2.4.2 Dye-sensitized solar cells (DSSC)

DSSC comes under the third generation PV technology. DSSC is produced using organic and inorganic materials at much cheaper production cost as compare to earlier technology, and consists of porous nanocrystalline TiO2 layer deposited onto a transparent conducting oxide (TCO) glass substrate with a monolayer of dye coated on it [DSSC modelling paper]. The various interesting prospects to design and make DSSC having different colour, shape and transparent at cheaper cost [75]. The efficiency of

12.3% achieved in 2011-12 under standard test condition (STC) and the most recent DSSC efficiency is 13.6% achieved in 2015 by AIST [10].

2.2.4.3 Perovskite solar cells

Perovskite solar cells are one of the recent trends in solar PV technology that have shown a strong prospect in terms of cell efficiency due to rapid increase. Perovskite is a hybrid technology of organic/inorganic solar cell based on methyl-ammonium-lead-halide **[76].** The most recent achieved perovskite solar cell efficiency is 22.1% by KRICT/UNIST as reported in NREL chart [10].

2.3 Solar PV system

Solar PV system formed by solar configuration of modules in series and parallel. The solar cell equations parameters modified with the module and array configuration and condition of MPP is analysed based upon the open circuit voltage condition. The MPP condition analysis generates the equation for computation of resistances without iteration. The PV system configurations Fig 2.1 connected to grid through power electronics interface and designated based on use of dc-dc/dc-ac converter.

2.3.1 Solar cell

Solar cell is the device working as to convert light into electricity and represented as an electrical equivalent model. The basic electrical equation written for ideal PV cell model modified as according to electrical equivalent model. The equation associated to the electrical models i.e. ideal model, series resistance model (single diode), shunt resistance model (single diode) and double diode model mentioned in (1) to (4) respectively. The solar cell modelled based upon the electrical model equations and parameters of the equation required for the modelling.

$$I = I_{ph} - I_o\left(e^{V/NV_t} - 1\right) \quad (1.)$$

$$I = I_{ph} - I_o\left(e^{V+IR_{se}/NV_t} - 1\right) \quad (2.)$$

$$I = I_{ph} - I_o\left(e^{V+IR_{se}/NV_t} - 1\right) - \frac{V + IR_{se}}{R_{sh}} \quad (3.)$$

$$I = I_{ph} - I_{o1}\left(e^{V+IR_{se}/NV_t} - 1\right) - I_{o2}\left(e^{V+IR_{se}/NVt} - 1\right) - \frac{V + IR_{se}}{R_{sh}} \quad (4.)$$

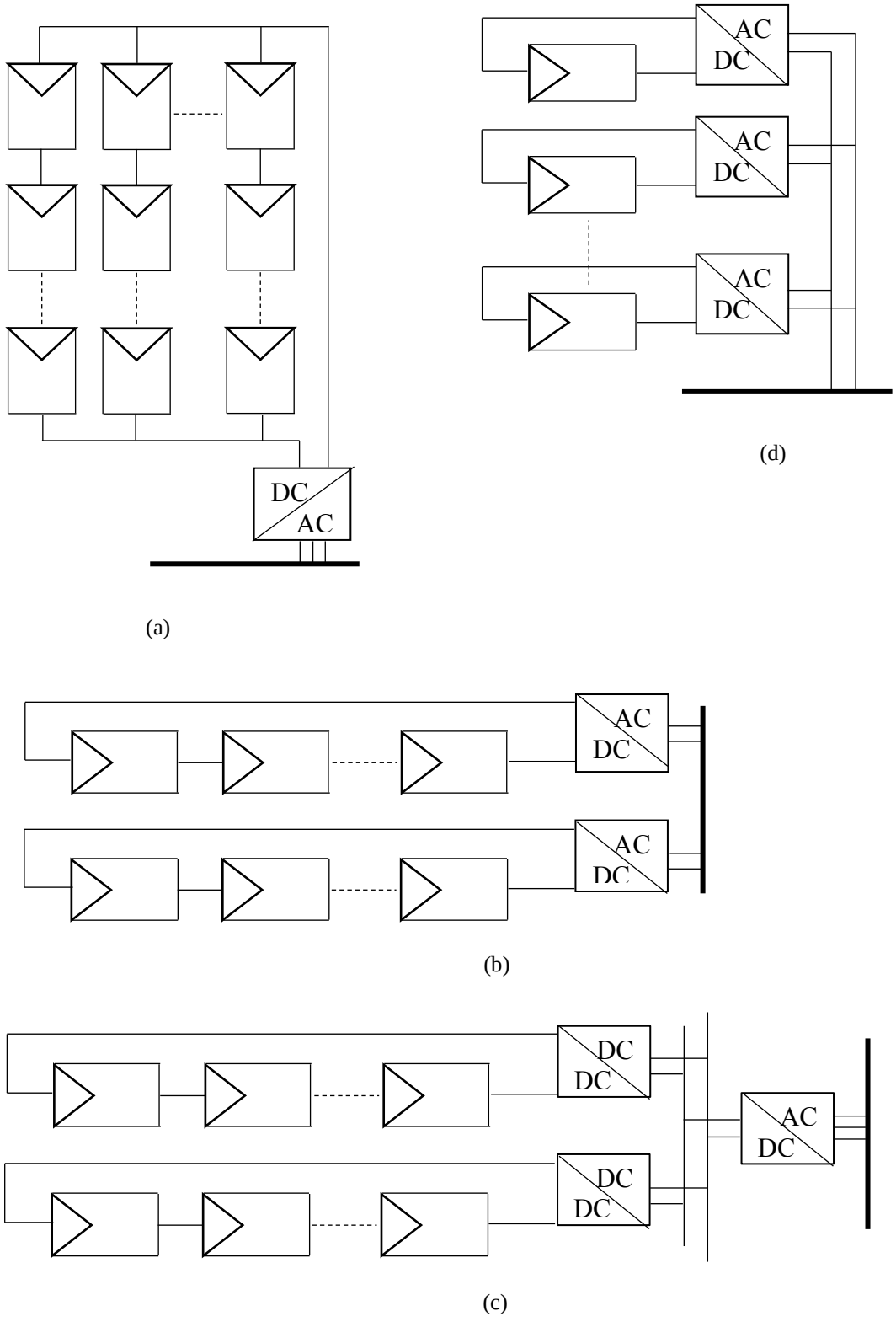

Fig 2.1 Configurations of grid-connected PV systems: (a) Central inverter (b) multiple string inverter (c) multiple string dc-dc converter (d) module integrated inverter system

2.3.2 PV array equations

The output current equation for the shunt resistance single diode equivalent circuit utilized for the modelling. To make the modelling more accurate and obtain characteristics, similar to practical solar cell the effect of maximum possible parameters to be incorporated in the model. The above-mentioned equations are specially for the modelling of single solar cell model. As the number of solar cells connected in series to form the solar module, the equation for the solar module changed with the significant change in the equation parameters. Due to connection of solar cells in series, the open circuit voltage, series, and parallel resistance of solar module will become

$$V_{OC,m} = N_s V_{OC,s,}\ R_{s,m} = N_s R_{s,s} \tag{5.}$$

PV modules connected in series and parallel fashion to develop the model of solar PV system and make the system of required/desired power rating. Therefore, it changes the fundamental solar cell equation. The series and parallel combination effect on solar cell circuit equation incorporated as

$$R_{s,a} = R_{s,m}\frac{N_{ss}}{N_{pp}}\ , R_{sh,a} = R_{sh}\frac{N_{ss}}{N_{pp}} \tag{6.}$$

$$\mathrm{I} = N_{pp}\, I_{ph} - N_{pp} I_o \left(e^{\frac{q(V+IR_{s,a})}{N_s akT}} - 1\right) - \frac{V + IR_{s,a}}{R_{sh,a}} \tag{7.}$$

2.3.3 Maximum power point (MPP)

R_{sh} assumed to be infinite for the condition $I_{ph} = I_{SC}$ and the equation for the output voltage and output current from (1) can be written as

$$\mathrm{I} = I_{SC} - I_o \left(e^{\frac{q(V+IR_S)}{N_s akT}} - 1\right) \tag{8.}$$

$$V = \frac{N_s akT}{e} ln\left(\frac{I_{ph} + I_o - I}{I_O}\right) - R_s I \tag{9.}$$

For the condition of open circuit, $\mathrm{V} = V_{OC}$ and I=0, the equation (8) become

$$V_{oc} = \frac{N_s akT}{e}\ ln\left(\frac{I_{sc}}{I_o} + 1\right) \tag{10.}$$

By substituting (11) in (9) and rearranged as

$$\frac{I}{I_{SC}} = 1 - \left(\frac{I_{SC}}{I_0}\right)^{-1}\left(\frac{I_{SC}}{I_0} \pm 1\right)^{x} \tag{11.}$$

The ratio of I_{SC} and Io is very high value because of low value of Io therefore (12) will become more simplified as

$$\frac{I}{I_{SC}} = 1 - (\alpha)^{x-1} \tag{12.}$$

where $I_{SC}/I_0 = \alpha$, $(V + IR_s)/V_{OC} = x$. The incremental conductance at the MPP is zero. Therefore, using the incremental conductance for characteristics of solar PV curve and written as

$$\frac{\mathrm{dP}}{\mathrm{dV}} = \mathrm{I} + \mathrm{V}\frac{\mathrm{dI}}{\mathrm{dV}} \tag{13.}$$

At maximum power point (MPP) condition; $dP/dV = 0$. Therefore, the above equation will be

$$\frac{\mathrm{dI}}{\mathrm{dV}}(at\ MPP) = -\frac{I_{MPP}}{V_{MPP}} \tag{14.}$$

2.3.4 Short circuit current

The solar generated current of the photovoltaic cell is having linear relation with the change in solar irradiance and affected by the change in the temperature. The effect of temperature and irradiance on current shown as

$$I_{ph} = \left(I_{ph\_N} + k_i \Delta T\right)\frac{G}{G_N} \tag{15.}$$

2.3.5 Open circuit voltage

Open circuit voltage of solar cell altered with the change in the temperature. As comparison to the effect of temperature and irradiance, the effect of irradiance is dominant on the current and the effect of the temperature is dominant on the voltage of solar PV cell. The effect of temperature on open circuit voltage given by

$$V_{OC} = V_{OC\_N} k_v (T - T_N) \tag{16.}$$

2.3.6 Reverse saturation current

The reverse saturation current is can be calculated using (8) for single diode model of solar PV system. In this equation, the temperature variation considered for calculation of current and relation between temperature and reverse saturation current computed using the temperature coefficient solar PV cell.

$$I_o = \frac{\left(I_{ph\_N} + k_i \Delta T\right)}{\exp\left[\left(V_{oc\_N} + k_v \Delta T\right)/aV_t\right] - 1} \quad (17.)$$

2.3.7 Series and parallel resistances

The solar cell resistances having conditions and for a cell considered to be having losses less than 1% due to its series and 1% due to its parallel resistance then the conditions for the resistances is defined as [63]

$$R_s < \frac{0.01V_{OC}}{I_{SC}} \quad (18.)$$

$$R_p > \frac{100V_{OC}}{I_{SC}} \quad (19.)$$

The series and parallel resistances extracted by the equations using MPP condition of solar PV cell. This is one of the simplest method proposed to find out the value of resistance without iteration. The derivative of (13) with respect to voltage (V) will also give the incremental conductance equation at MPP

$$-\frac{I_{MPP}}{V_{MPP}} = -I_{SC}\frac{1 + R_s\left(-\frac{I_{MPP}}{V_{MPP}}\right)}{V_{oc}}(\alpha)^{x-1}\ln(\alpha) \quad (20.)$$

$$\ln(\alpha) = \frac{\ln\left(1 - \frac{I}{I_{SC}}\right)}{x} \quad (21.)$$

(21) derived from the (12) by taking natural log. The value of series resistance calculated easily by using above two equations. The value of the parameters at MPP conditions under standard test condition (STC) for above equations is used. The STC condition for solar PV; Temperature=298K and irradiance = 1000W/m^2. The above equation will give the value of series resistance only. In the same way as above; derivative of (3) is calculated for MPP condition to extract the shunt resistance value. Derivative of (3) for MPP condition will be

$$\frac{I_{MPP}}{V_{MPP}} = I_{SC}\frac{1 + R_s\left(-\frac{I_{MPP}}{V_{MPP}}\right)}{V_{oc}}(\alpha)^{x-1} ln\,(\alpha) + \frac{I + R_s\left(-\frac{I_{MPP}}{V_{MPP}}\right)}{R_{sh}} \quad (22.)$$

By using, the value of series resistance calculated with help of (20) and (21), the value of shunt resistance easily calculated from (22). The value of series resistance

calculated by assuming the value of shunt resistance as infinite and once the shunt resistance calculated from same equation. This is the proposed simplified method to calculate the series and parallel resistance without iteration.

2.3.8 Double diode equation for modelling

The Double diode equation modified the implementation of proposed modelling method by replacing part of second diode by a coefficient in the equation. The solar cell characteristics is obtained using this method and tuning of ideal factor of diode (a) and coefficient use for second diode to obtain the best possible accurate result. The equation (23) represents the double diode equation considering reverse saturation current of the diodes are same. Equation (23) is can be written as in (24) and (24) is modified and proposed into (25) and based upon the equation (25)

$$\mathrm{I} = I_{ph} - I_o\left(e^{\frac{q(V+IR_S)}{a_1 kT}} - 1\right) - I_o\left(e^{\frac{q(V+IR_S)}{a_2 kT}} - 1\right) - \frac{V + IR_s}{R_{sh}} \quad (23.)$$

$$\mathrm{I} = I_{ph} - I_{d1} - I_{d2} - \frac{V + IR_s}{R_{sh}} \quad (24.)$$

$$\mathrm{I} = I_{ph} - I_{d1} - \alpha * I_{d1} - \frac{V + IR_s}{R_{sh}} \quad (25.)$$

2.4 MATLAB/Simulink Model

The Solar PV system modelled through circuit based approach in MATLAB/Simulink. The block diagram of the solar PV cell/module for single diode model with resistances in Fig 2.2(a) and 2.2(b) modelled with bypass diode. The combination of solar modules in series and parallel arrangements shown in Fig 2.3 and this arrangement can be modelled using (7). The modelled system can be modified for any type of arrangements as required for application.

This single solar cell model converted into the module by multiplying number of cells connected in series. The arrangement of this single module subsystem in series and parallel combination in Fig 2.3 results in the model of solar PV array system with the arrangements of blocking diode and bypass diode. The modelled solar PV system consists of controlled current source with the capability partial shading effect and other parameters. The partial shading curves generated as according to the shading pattern set for the PV modules.

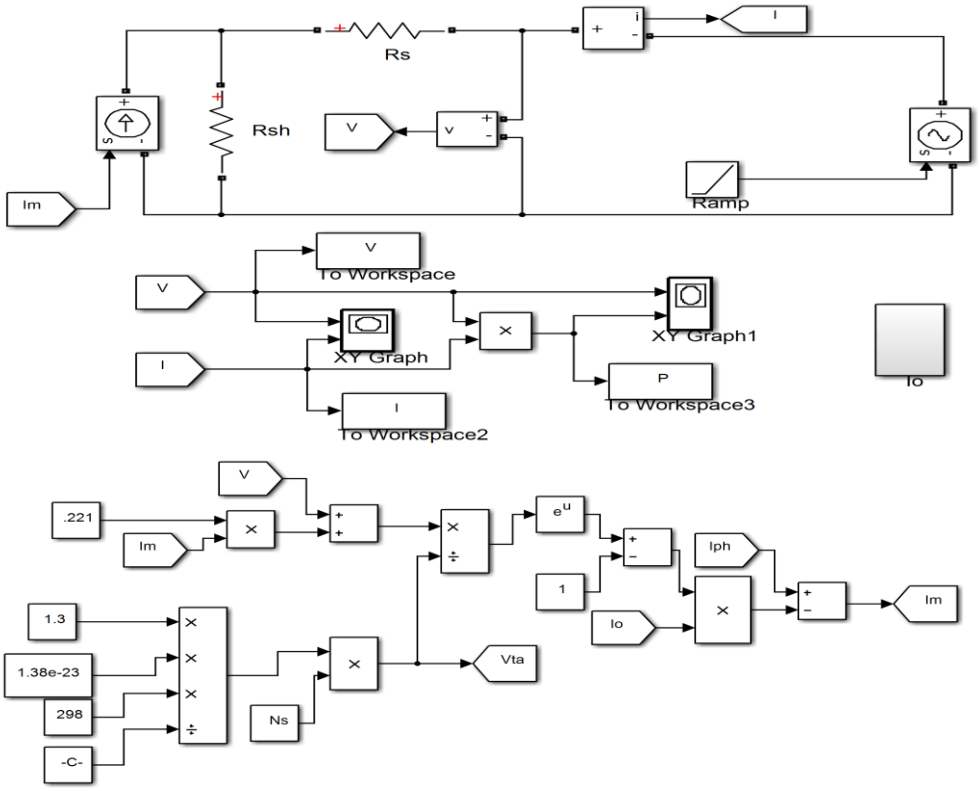

(a)

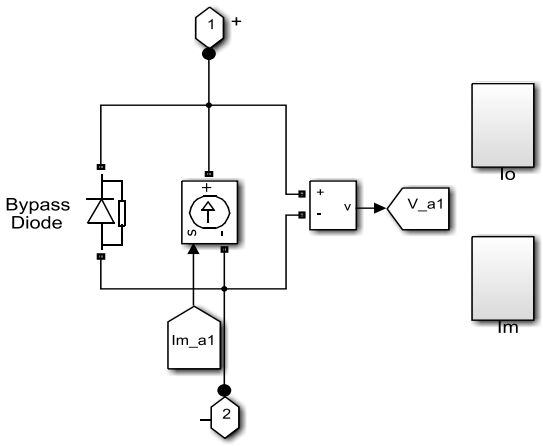

(b)

Fig 2.2 Single diode based modelling of solar PV module in Matlab-Simulink

a) Mathematical equation modelled with electrical equivalent circuit
b) Bypass diode modelling

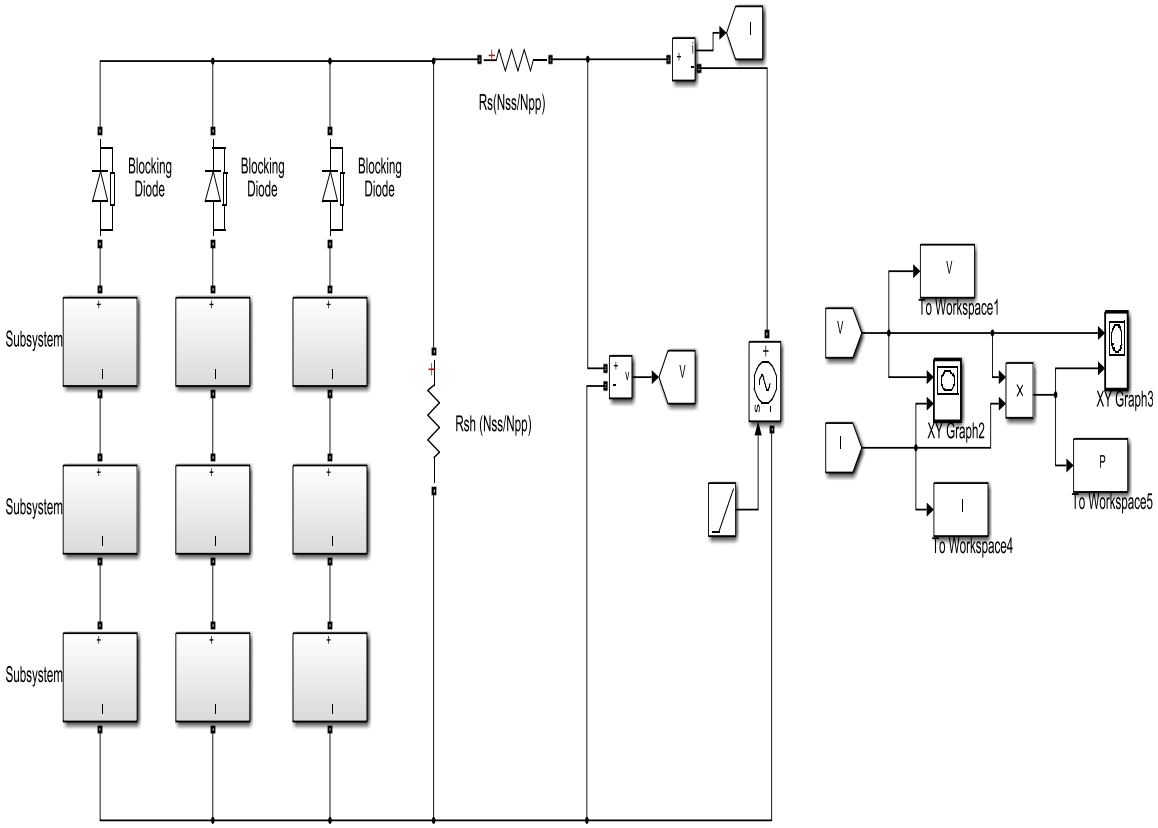

Fig 2.3 Solar PV system simulator arrangement.

The circuit equation based mathematical model for solar PV system and illustration/test method is established using ramp signal. Fig 2.2(a) and 2.2(b) illustrated the basic modelling method and rearrangements of model for the solar PV system modelling. In MATLAB/Simulink, it is not possible to plot the multiple X-Y characteristic output in same X-Y scope/plot. The Simulink block used to store the data in workspace and therefore using MATLAB commands, plotted on same plot.

2.5 Investigation and Analysis of Real Time Data of Solar PV System

The solar cell system deals with the constraints in fundamental research of solar cell materials like open circuit voltage limitation due to energy band gap constraint and efficiency limitations due to materials functioning capability over certain wavelengths of light. To develop an effective and efficient system with energy management consideration real time practical data is very important. In case of PV system, it will become more significant as the PV power generating system is dominantly dependent upon the solar irradiance condition. Based upon the real time data of solar irradiance to forecast the energy generation of solar PV system and manage the load demands for residential roof top panels. As every city weather conditions are different so the real-

time solar irradiance data obtained for the PV system will be helpful to forecast solar power generation in more precise way for Kitakyushu city and it may be helpful to obtain better energy management system for residential PV systems. It will be helpful to make the PV connected smart grid system more efficient in terms of minimizing fluctuations in the system generated due to the PV system because of variable power generation. The average solar irradiance data in terms k-W-hr/m^2 helps to develop an understanding of PV power generation under this weather condition and will be helpful to optimize the battery energy storage system solar PV power generation system and electric vehicle interconnection for both islanded and grid connected mode conditions.

2.5.1 Objective

The analysis of real-time solar irradiance data for the year 2014 is considered to compute the average solar irradiance Fig 2.4, 2.5 and 2.6 in terms of two units as k-W/m^2 and kW-hr/m^2. The real time data collected for 24 hours and data considered for the computation of average solar irradiance is from 6 am to 6 pm. The average solar irradiance helps to analyse the weather condition and average power generation from the Solar PV system installed of 2.88 kW having 16 modules Fig 2.7, installed as residential roof top application for every month that will help to forecast the power generation of each month for the upcoming years. k-W-hr/m^2 (β k-W-hr/m^2) analyse

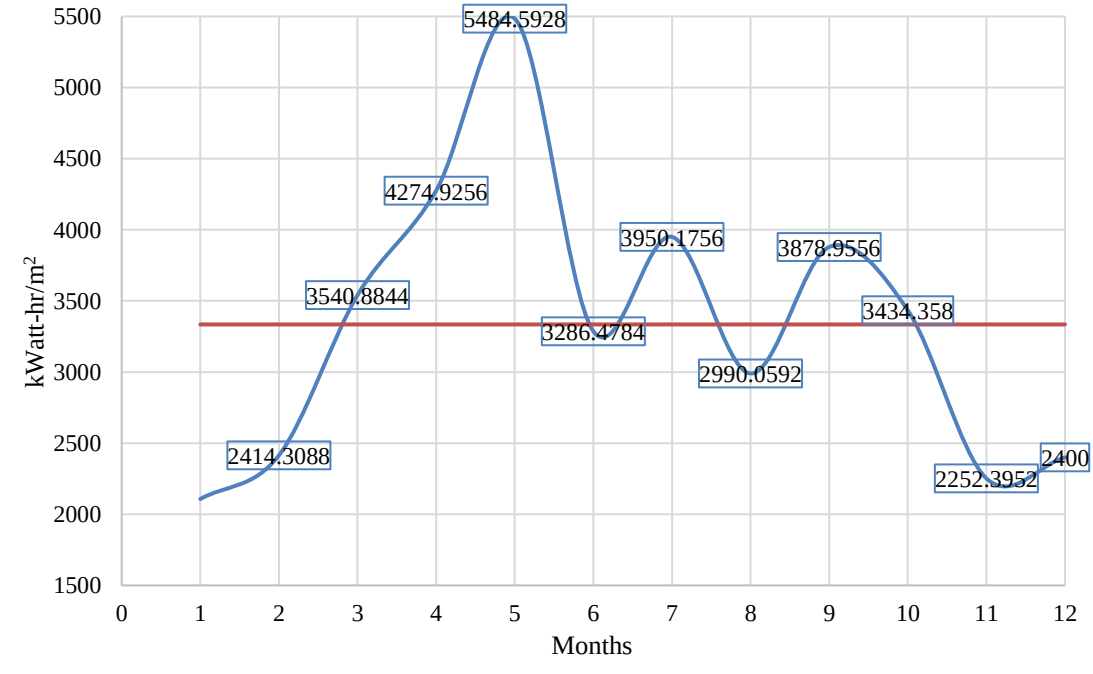

Fig 2.4: The average solar irradiance for months of year 2014 in kW-hr/m^2

the system as it can provide 1 kW of power for β hours which will be helpful in terms of battery consideration as battery rating is defined kW-hr basis.

2.5.2 Computation of power generated by solar PV based upon irradiance

Area of one panel of Kyrocera-KD180GX: 1.314*0.990 = 1.30086 m^2

Power generation from one panel: 180 Watts/ 1.30086 m^2

Power generation from one panel: 138.37 Watts /m^2

It means if 1000 kW/ m^2 falls on the 1 m^2 panel of Kyrocera-KD180GX then 138.37 Watts of power will be generated. Therefore, the efficiency of the panel is 13.837%.

So for the month of May when average irradiance of 457 W/m^2 fall on the panel the power generated by 1 m^2 panel = (457*138.37)/1000 = 63.235 Watts/ m^2

So, the power generation from the 2.88 kW solar PV panels installed through 16 panels with overall area of panel = 21.21264 m^2

The average power generated for average irradiance of 457 W/m^2 from the 2.88 kW solar PV system for the month of May = 63.235*21.21264 = 1341.38 Watts = 1.341 kW

Solar irradiance and PV module parameters summarized in Table 2.1 and 2.2 respectively. Calculation of average power generation for single module and for overall 2.88 kW PV system listed in Table 2.3.

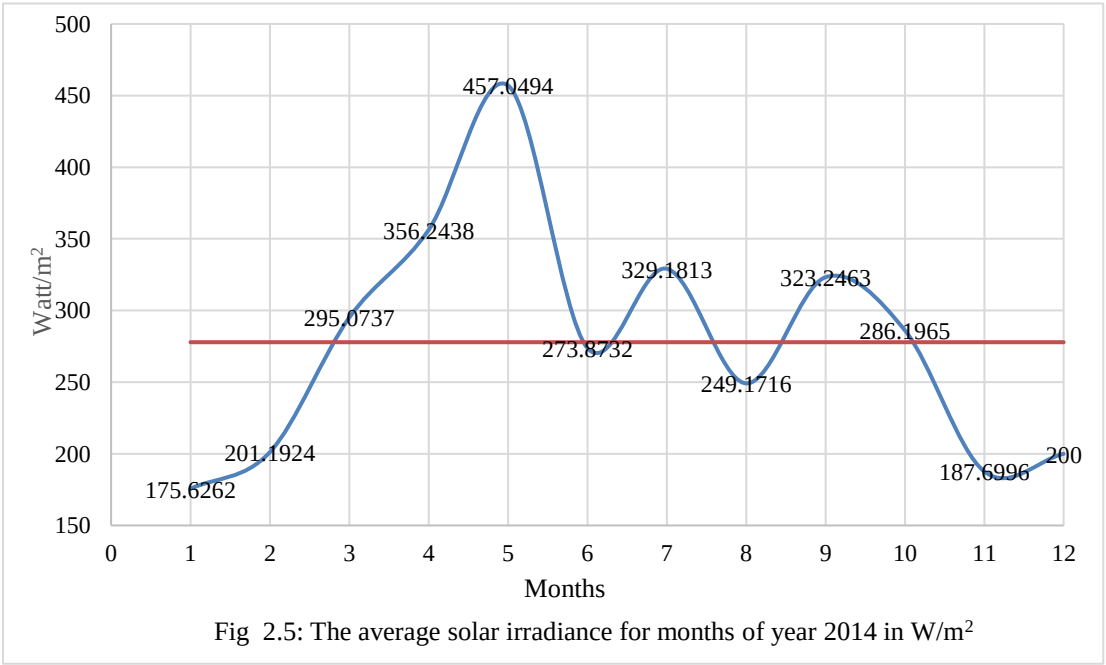

Fig 2.5: The average solar irradiance for months of year 2014 in W/m^2

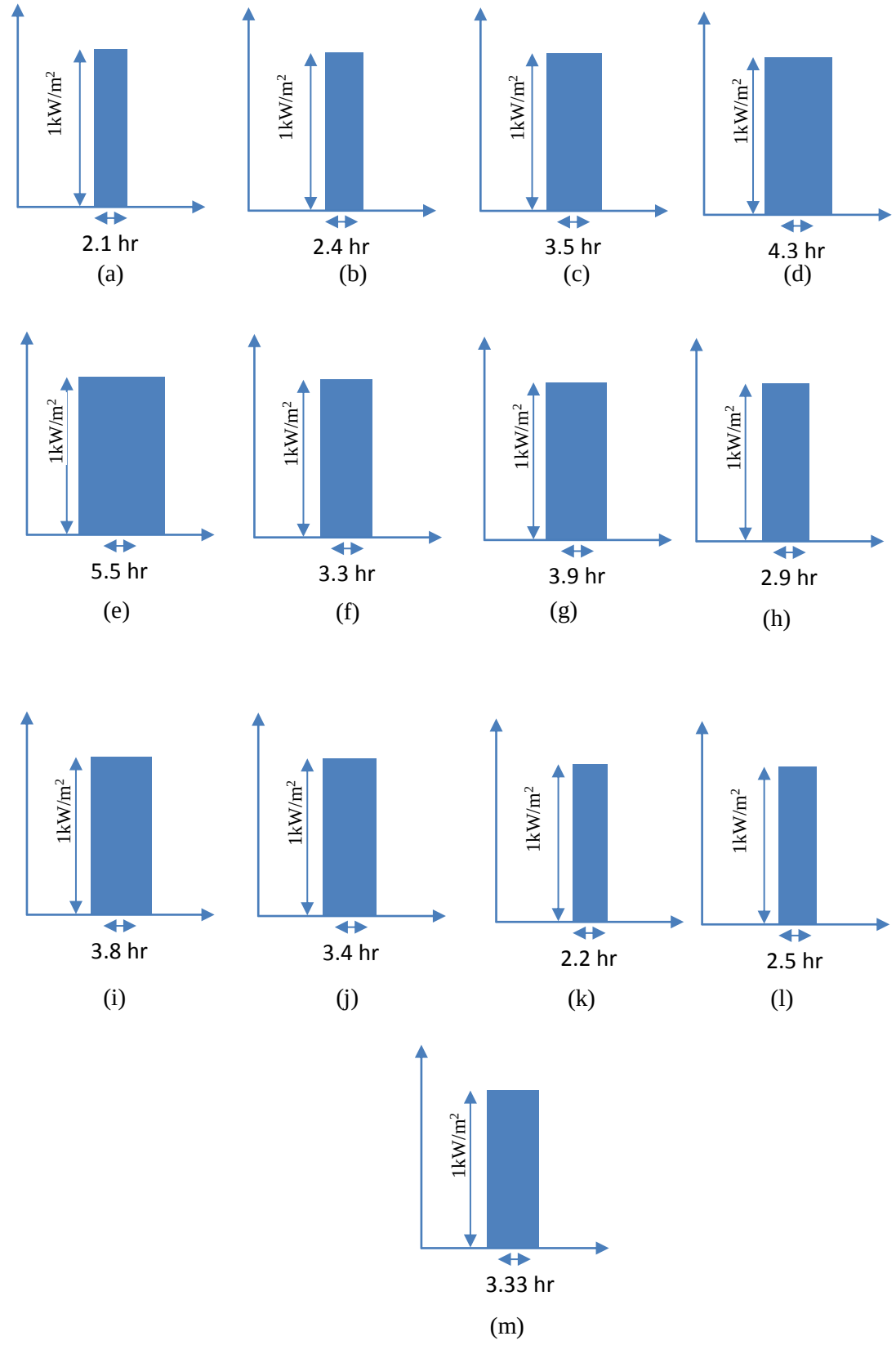

Fig 2.6. kW-hr/m^2 monthly characteristic for 1kW/m^2 and time in hour: a) January, b) February, c) March, d) April, e) May, f) June, g) July, h) August, i) September, j) October, k) November, l) December, m) average of year.

Table 2.1. Average Solar irradiance monthly.

Month	Irradiance W/m^2	Irradiance $W\text{-}hr/m^2$
January	175.6262	2107.514
February	201.1924	2414.309
March	295.0737	3540.884
April	356.2438	4274.926
May	457.0494	5484.593
June	273.8732	3286.478
July	329.1813	3950.176
August	249.1716	2990.059
September	323.2463	3878.956
October	286.1965	3434.358
November	187.6996	2252.395
December	200	2400

Table 2.2 Parameters of the Kyocera (KD180GX)

I_{SC}	**8.35 A**
I_{mpp}	7.63 A
V_{OC}	29.5 V
V_{mpp}	23.6 V
P_{mpp}	180 W
N_S	48
k_V	-0.106 V/K
k_I	.005 A/K
Length (l)	1342mm (52.8 inch)
Width (b)	990mm (39.0 inch)
Depth (t)	36mm (1.4 inch)

Table 2.3 Monthly average power generation data calculated for single module and for overall 2.88 kW PV system in Watts and kW-hr.

Months	Avg. Irradiance (kW/m^2)	Average power from each panel (Watts)	Total average power (Watts)	Total Average power (kW-hr)
January	175.6262	24.3014	515.4967923	6.185961508
February	201.1924	27.83899	590.5385235	7.086462282
March	295.0737	40.82935	866.0982578	10.39317909
April	356.2438	49.29345	1045.644307	12.54773168
May	457.0494	63.24193	1341.528198	16.09833838
June	273.8732	37.89583	803.8706987	9.646448384
July	329.1813	45.54882	966.2106464	11.59452776
August	249.1716	34.47787	731.3667353	8.776400824
September	323.2463	44.72759	948.790276	11.38548331
October	286.1965	39.60101	840.0419625	10.08050355
November	187.6996	25.97199	550.9345514	6.611214617
December	200	27.674	587.0385994	7.044463192

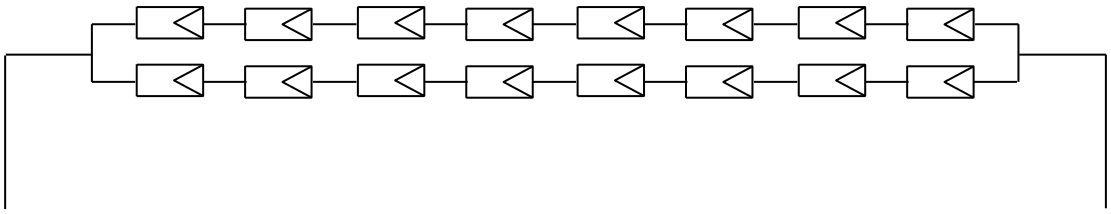

Fig 2.7: Installed solar PV array configuration of 2.88 kW having 16 modules.

2.6 Model Validation

The solar PV module/array model is validated by comparing the developed model and the experimental (provided by the manufacturer or extracted from the datasheet) data of PV curves which will further justify the parameter extraction method.

2.6.1 For single diode equivalent model

2.6.1.1 PV module

The experimental data and simulated data are matched considering $(V_{OC} = 0, I_{SC})$, (V_{MPP}, I_{MPP}), $(V_{OC}, I_{SC} = 0)$ and $(V_{OC} = 0, P = 0)$ (V_{MPP}, P_{MPP}) for I-V and P-V curve of Kyocera KC200GT PV module at STC as Table 2.4 and 2.5 and Fig. 2.8(a) have illustrated. I-V and P-V curve both should have to match the experimental data showing same V_{MPP} corresponding to I_{MPP} and P_{MPP} to validate the model with better accuracy. I-V and P-V curve obtained successfully matching the experimental data at STC shown as shown in Fig 2.8(a).

Validation of the simulated model will be acceptable, if it matched with experimental data at different irradiance and temperature level other than STC. The mathematical I-V and P-V curve was compared and matched with the experimental data provided by manufacturer at normal operating cell temperature (NOCT=47^0C) and 800W/m^2 as in Table 2.6 and Fig 2.8(b). The mathematical I-V and P- V curves of KC200GT PV module is using simulated model at five different irradiance condition and three different temperature condition following the experimental electrical characteristic curve provided by the manufacturer. The experimental data of I-V curve was extracted from the electrical characteristic and plotted with the simulated data of I-V at different irradiance and generated temperature in Fig 2.8(c) and 2.8(d) respectively. Even though some points not matched properly, most of the points of extracted experimental data matched with simulated data curve. The extracted experimental data from datasheet provided manufacturer added in appendix [77].

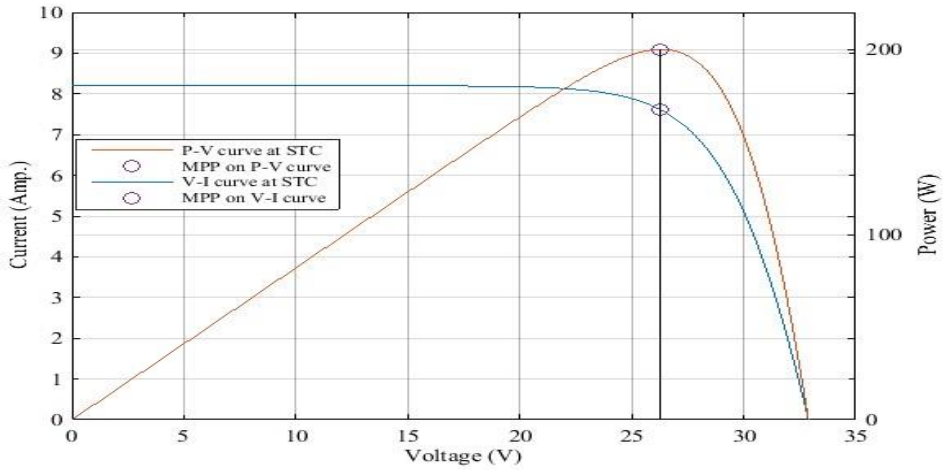
P-V curve at STC
MPP on P-V curve
V-I curve at STC
MPP on V-I curve
Current (Amp.)
Power (W)
Voltage (V)

(a)

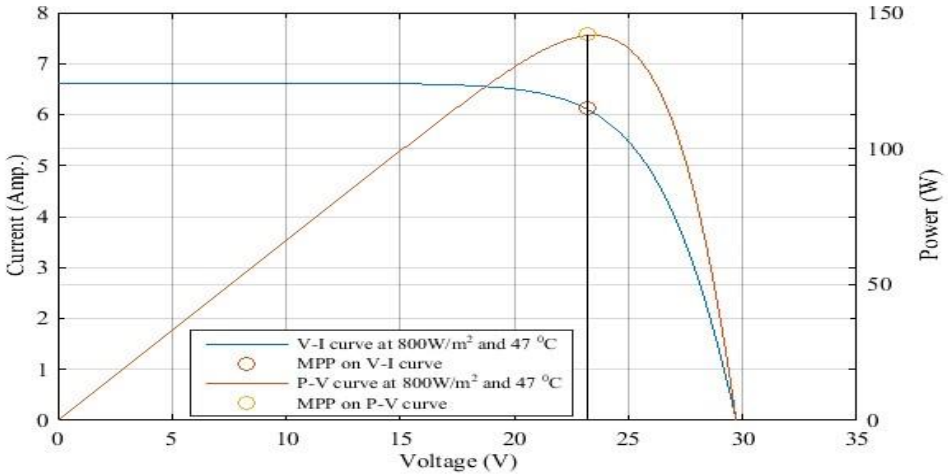
V-I curve at 800W/m² and 47 °C
MPP on V-I curve
P-V curve at 800W/m² and 47 °C
MPP on P-V curve
Current (Amp.)
Power (W)
Voltage (V)

(b)

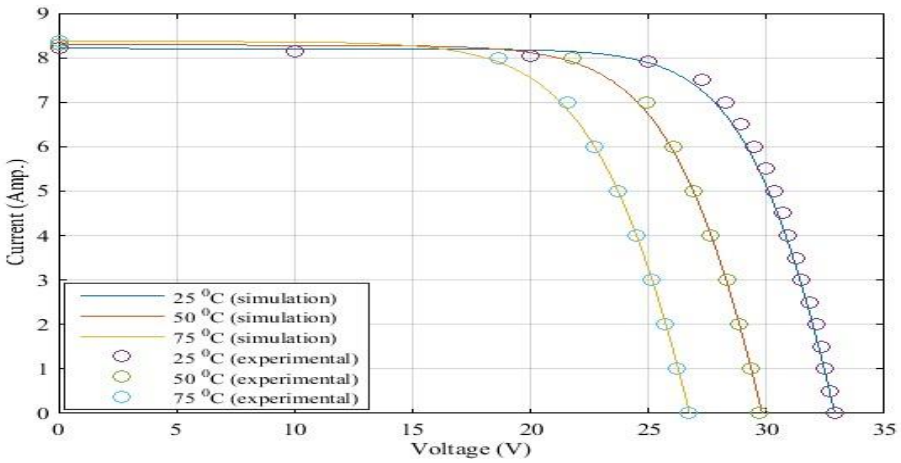
25 °C (simulation)
50 °C (simulation)
75 °C (simulation)
25 °C (experimental)
50 °C (experimental)
75 °C (experimental)
Current (Amp.)
Voltage (V)

(c)

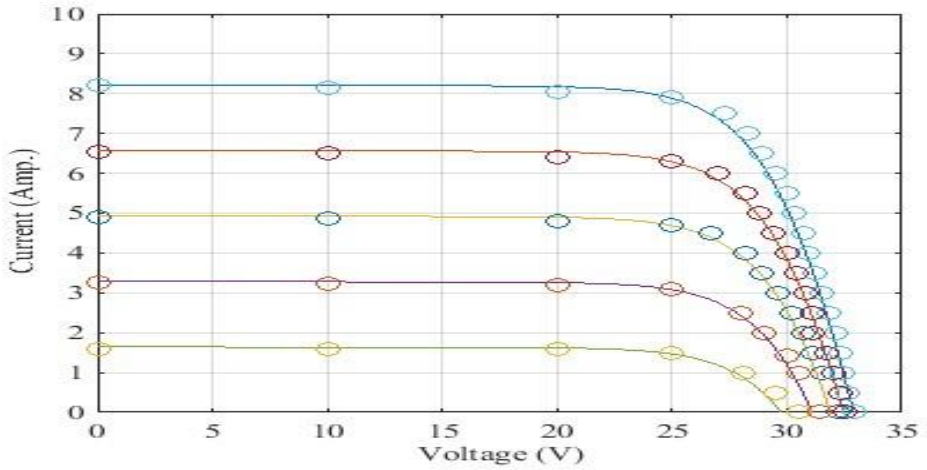

(d)

Fig 2.8 Solar PV characteristic for KC200GT module
a) I-V and P-V curve of PV module at STC.
b) I-V and P-V curve of PV module at 800W/m2 and NOCT.
c) I-V curve of a PV module at different temperature.
d) I-V curve of a PV module at different irradiance.

2.6.1.2 PV array

The mathematical I-V and P-V curves matched and plotted for a PV module and PV array is simulated using validated PV modules. The PV array consists of three series connected modules in a string (N_{ss}=3) and 3 parallel string of modules (N_{pp}=3) i.e. 3×3 arrangement is considered. I-V and P-V curves are plotted for different irradiance and temperature using PV array simulator model as in Fig 2.9(a) and (b). In order to test and analyse the performance of the PV array model the mathematical I-V and P-V curve plotted under partial shading condition. The different condition of partial shading as in Table 2.7 and 2.8 considered to generate the PV characteristics under non-uniform condition. I-V and P-V curves under partial shading condition in Table 2.7 was plotted as illustrated in Fig 2.10 (a) and 2.10 (b) respectively and in Table 2.8 was plotted as illustrated in Fig 2.10 (c) and 2.10 (d) respectively.

The PV array performance get deteriorated under partial shading condition and efficiency of PV module also reduced corresponding to change in irradiance as reported in datasheet by manufacturer [77]. The PV array performance improved by using the bypass diode connected in parallel to each module and a blocking diode connected in series with each string under partial shading. The effect of shading on I-V and P-V characteristics illustrated with and without bypass diode. The effect of bypass diode on I-V and P-V curve of PV array observed as shown in Fig 2.10(c) and 2.10(d).

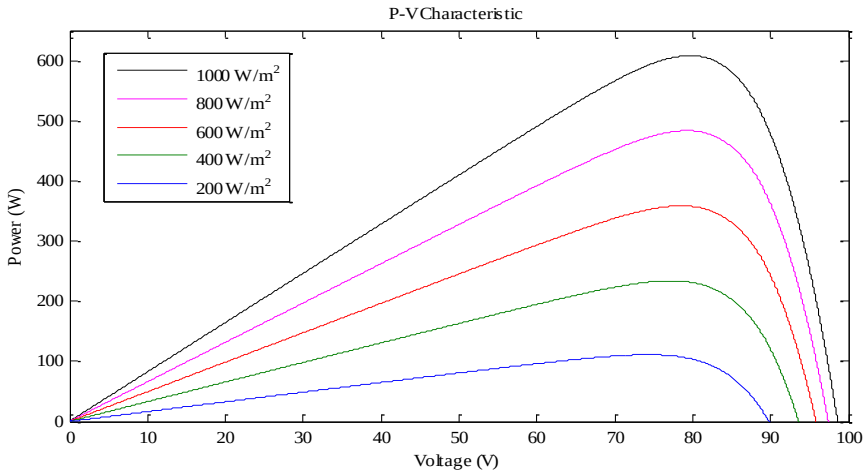

(a)

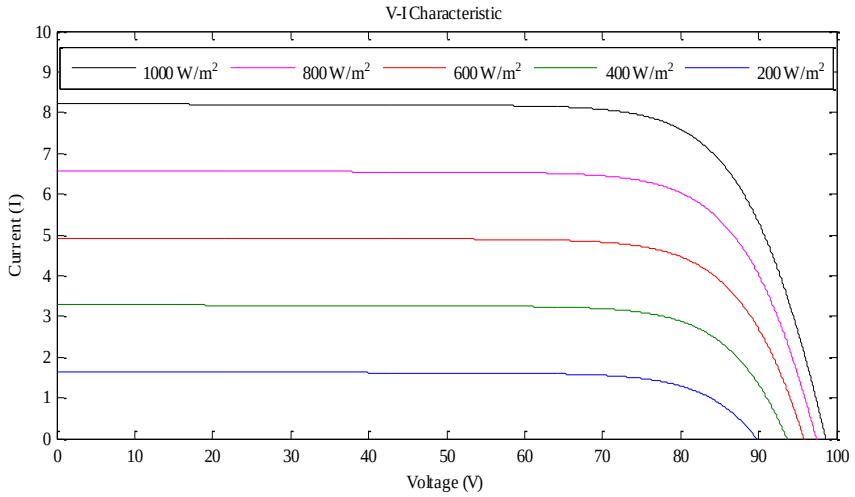

(b)

Fig. 2.9 Solar PV characteristic for array
a) P-V curve of PV array at different irradiance.
b) I-V curve of PV array at different irradiance.

It can be analysed from the Fig 2.10(a) to 2.10(d) that the use of bypass diode improves the performance of PV system under non-uniform weather case and provides better output power. It also leads to the damage of shaded module due to hot spot effect. After that, cumulative effect comes into the picture and shaded module string started acting as load. The current started to flow from the healthy string to damaged string. Therefore, overall performance of the system will be disturbed and chance of the module damage may become very high. The bypass diode prevents the shaded modules and bypass the current through diode and the blocking diode prevents the reverse flow of current from healthy string to shaded/damaged string. The number of maxima and

minima in a PV characteristic is depend upon the number of series connected modules. The effect of blocking diode on I-V and P-V curves observed in Fig 2.10(e) and 2.10(f) respectively. In Fig. 2.10(e) and 2.10(f), the dotted red line is I-V and P-V curve with blocking diode and continuous blue line is I-V and P-V curve without blocking diode. There is a difference in open circuit voltage and peak power for I-V and P-V characteristics respectively.

Table 2.4 Parameters of the the KC200GT at STC W/m^2

I_{SC}	8.21 A
I_{mpp}	7.61 A
V_{OC}	32.9 V
V_{mpp}	26.3 V
P_{mpp}	200.143 W
N_S	54
k_V	-0.1230 V/K
k_I	.0032 A/K

Table 2.5 Parameters of the simulated model of KC200GT at STC

$I_{o,N}$	9.825*10^{-8} A
Rs (reference)	0.221
Rp (reference)	415
Rs (module)	0.185 Ω
Rp (module)	583 Ω
Pmpp (simulator)	606.91 W
Pmpp	600.429 W

Table 2.6 Parameters of KC200GT at 47^{0}C, 800

I_{SC}	6.62 A
V_{OC}	29.9 V
I_{mpp}	6.13 A
V_{mpp}	23.2 V
P_{mpp}	142 W

Table 2.7 Shading pattern for illustrated test model with 3×1 arrangement

Irradiance of modules for single string characteristic (W/m^2)		
600	1000	400

Table 2.8 Shading pattern for illustrated test with 3×3 model arrangement

Irradiance 1st String Modules (W/m^2)	Irradiance 2nd String Modules (W/m^2)	Irradiance 3rd String Modules (W/m^2)
400	600	600
1000	200	1000
800	400	400

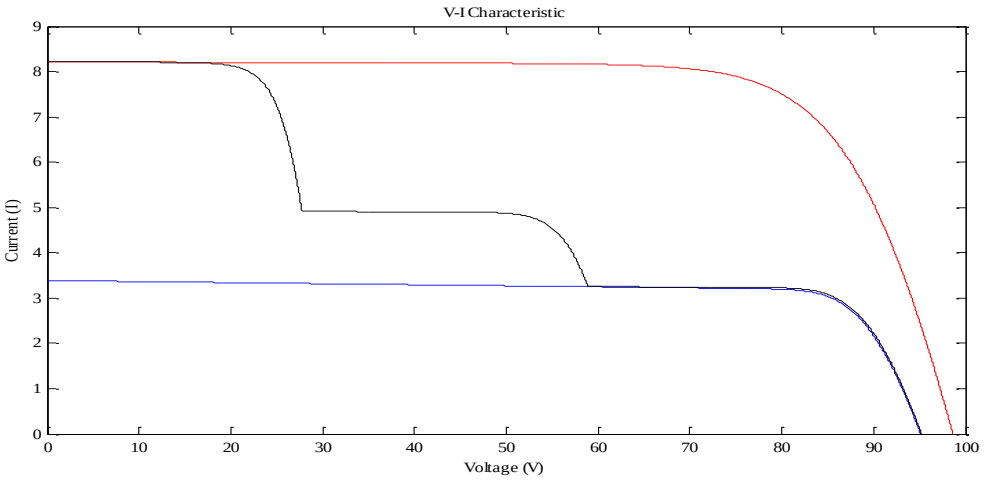

(a)

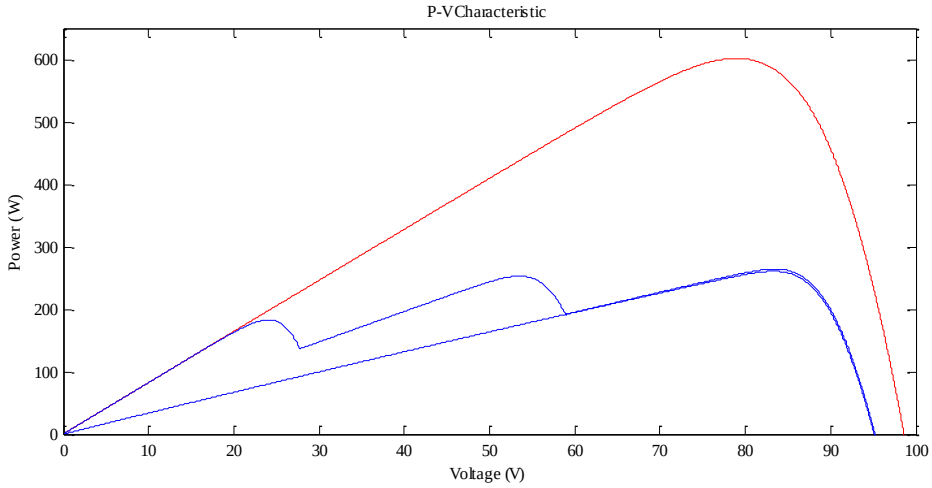
P-V Characteristic
Power (W)
Voltage (V)
0
100
200
300
400
500
600
0
10
20
30
40
50
60
70
80
90
100

(b)

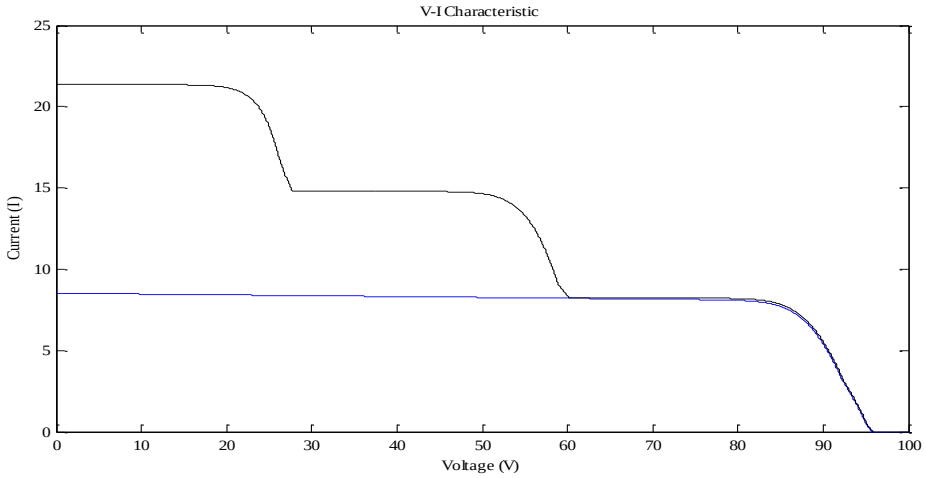
V-I Characteristic
Current (I)
Voltage (V)
0
5
10
15
20
25
0
10
20
30
40
50
60
70
80
90
100

(c)

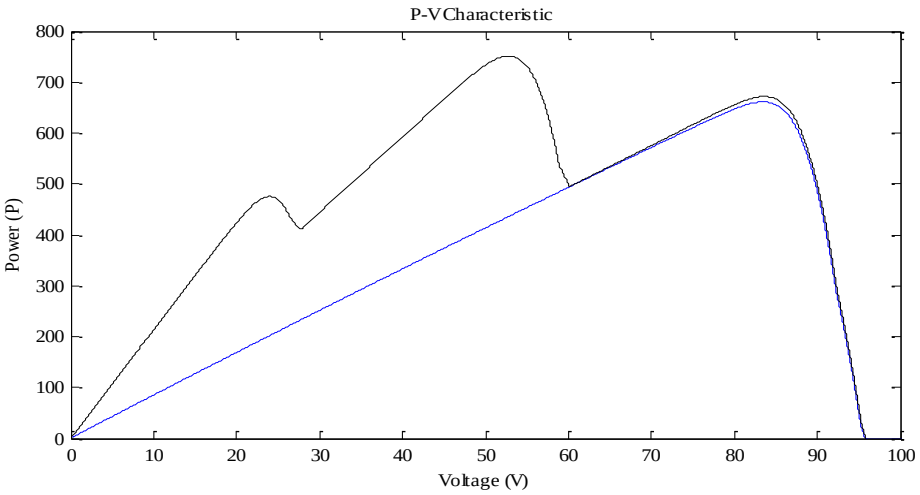
P-V Characteristic
Power (P)
Voltage (V)
0
100
200
300
400
500
600
700
800
0
10
20
30
40
50
60
70
80
90
100

(d)

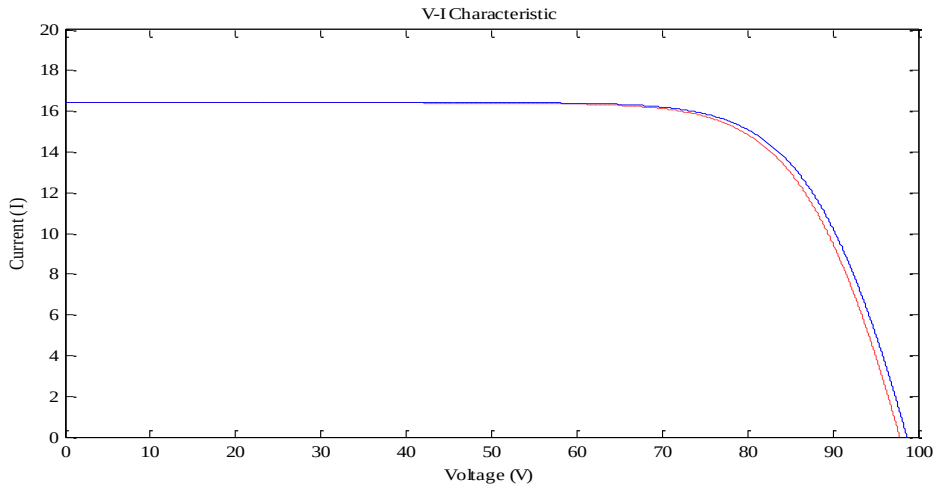

(e)

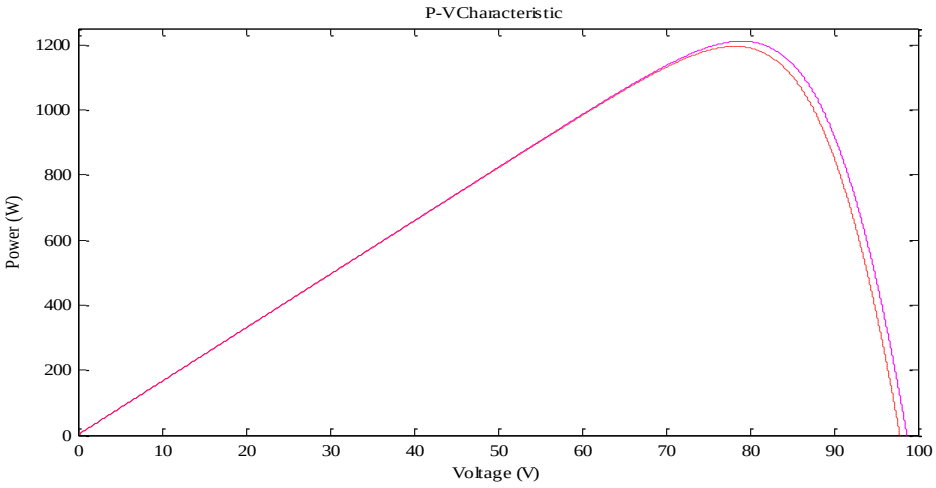

(f)

Fig. 2.10 Solar PV characteristic with partial shading capability
a) V-I curve for KC200GT by PV simulator (3×1)
b) P-V curve for KC200GT by PV simulator (3×1)
c) V-I curve for KC200GT by PV simulator (3×3)
d) P-V curve for KC200GT by PV simulator (3×3)
e) V-I curve with blocking diode and without blocking
f) P-V curve with blocking diode and without blocking

To analyse and test the effect of strings connected in parallel, the characteristics obtained in Fig. 2.10(a) and 2.10(b) is for single string under partial shading condition as in Table 2.7. And, the characteristics obtained in Fig. 2.10(c) and 2.10(d) is for the strings connected in parallel under partial shading condition as in Table 2.8. The number of peaks (maxima-minima) of P-V curve was remained same in Fig. 2.10(b) and 2.10(d). Therefore, the number of modules connected in series governs the number

of peaks in P-V curve of PV array. Even though the number of peaks are same but the interesting key point is position of global maxima and minima might be changed in Fig. 2.10(b) and 2.10(d).

2.6.2 Propose Two-diode Modelling Method

The proposed two diode based solar PV simulator model and parameters computed from the method discussed in this paper is validated under various conditions for KD180GX Table9 and the accuracy of the PV simulator is validated based upon the error in model results and manufacturer data sheet. This method of modelling only requires the tuning between diode ideality factor and the coefficient used for computation of second diode. The overall computational procedure is reduced as in (25) for mathematical model of solar current.

2.6.2.1 Different irradiance levels

The standard irradiance level is 1000 W/m^2 and the data provided by the manufacturers specified for the standard test condition (STC). Standard test conditions are irradiance= 1000 W/m^2, T= 25^{0}C (298K), AM 1.5. I-V and P-V curves for different irradiance level is shown in Fig. 2.11(a) and 2.11(b) and the error in reference to maximum power and open circuit voltage corresponds to maximum power under different irradiation level condition is shown in Fig. 2.11(c) and 2.11(d). The PV data is also specified for the case irradiance= 800 W/m^2, T= 49^{0}C (322K). The error is defined for the difference in simulate value and measured value for P_{mp} and V_{oc} corresponding to each P_{mp}.

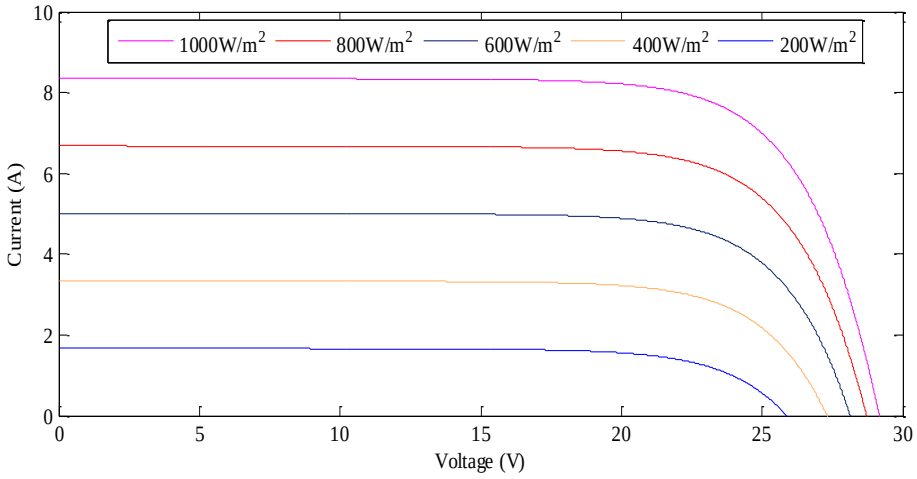

(a)

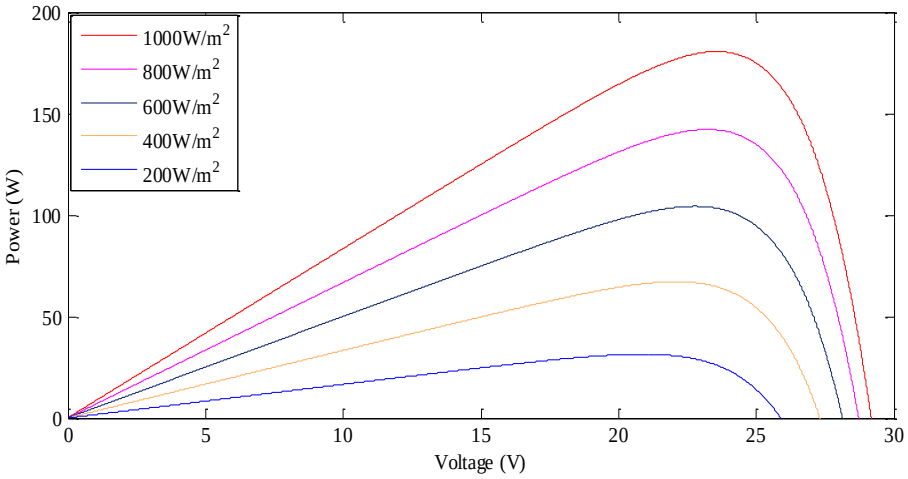

(b)

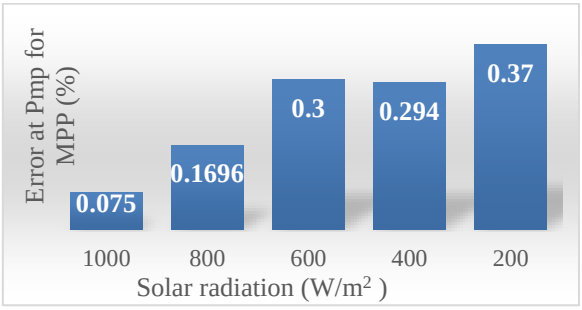

(c)

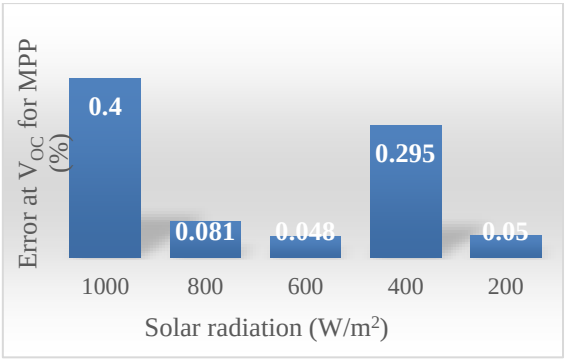

(d)

2.6.2.2 Different temperature levels

The PV system affected by the temperature of panel and changed due to losses and heat generated by radiation. I-V characteristics obtained for the change in temperature levels Fig. 2.11(e).

The combined effect of temperature and irradiance is specified in PV data is the case irradiance= 800 W/m^2, T= 49^{0}C (322K) and the error under this condition is shown Fig.

2.11(f). The combined effect of irradiance and temperature provides better information about the accuracy how simulator is behaving for the change in radiation and temperature simultaneously.

2.6.2.3 Partial shading condition

To generate the characteristics for illustration, the controlled voltage source with ramp signal shown in Fig. 2.3 used to run the simulation model and validate the PV characteristics. For the validation of PV array curve under non-uniform condition 3 modules in series (N_{ss} = 3) and 2 parallel string (N_{pp} =2) i.e. 3×2 arrangement is considered. The different condition of shading taken to generate the PV characteristics

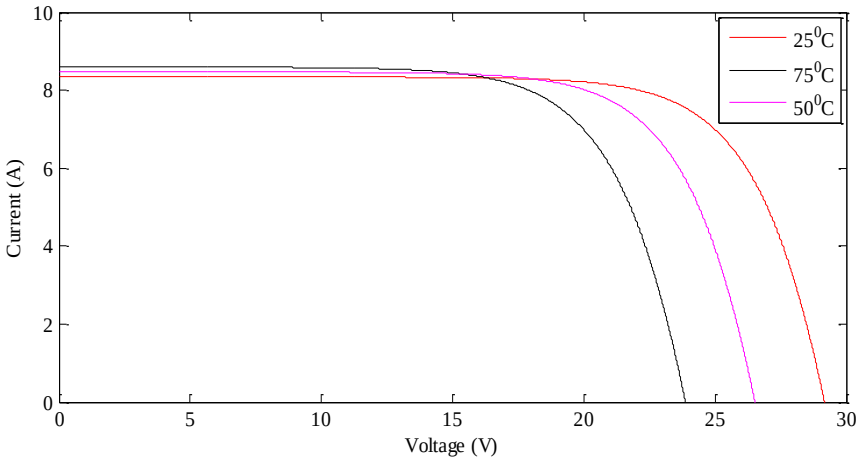

(e)

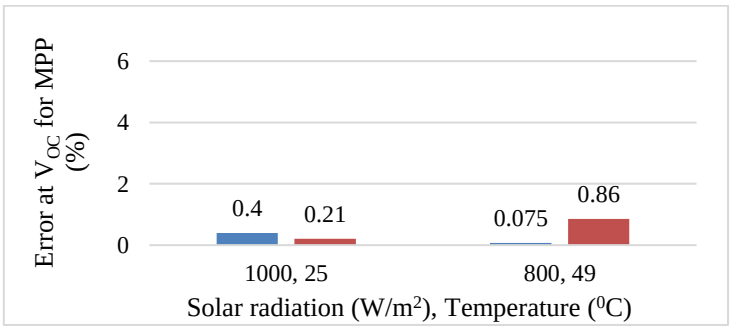

(f)

Fig. 2.11 Solar PV characteristic for KD180GX
a) I-V characteristic
b) P-V characteristic
c) error for MPP power,
d) error for Voc relative to MPP,
e) I-V characteristic for temperature change
f) error in PMPP and V_{oc} for 1000W/m^2 and 250C and 800W/m^2 and 49^{0}C.

for non-uniform condition. The conditions of partial shading mentioned in Table 2.10 and 2.11 corresponding results shown in Fig. 2.12 (a), (b), Fig. 2.12(c), and (d). The improvements in the characteristics of PV array under partial shading is achieved by using the bypass diode connected in parallel to each module and blocking diode connected in series with each with each string. The bypass diode effect in Fig. 2.12(a) and (b) and Fig. 2.12(c) and (d) validated using PV simulator. The characteristics obtained in Fig. 2.12(a) and (b) is for the 2 string connected in parallel, each having 3 modules in series. The number of peaks for the PV characteristics changes as the configuration is changes from 3 series connected modules to 2 modules Fig 2.12(c) and (d). Therefore, it is very important for practical designing of PV array to decide the number of modules connected in series should be minimum.

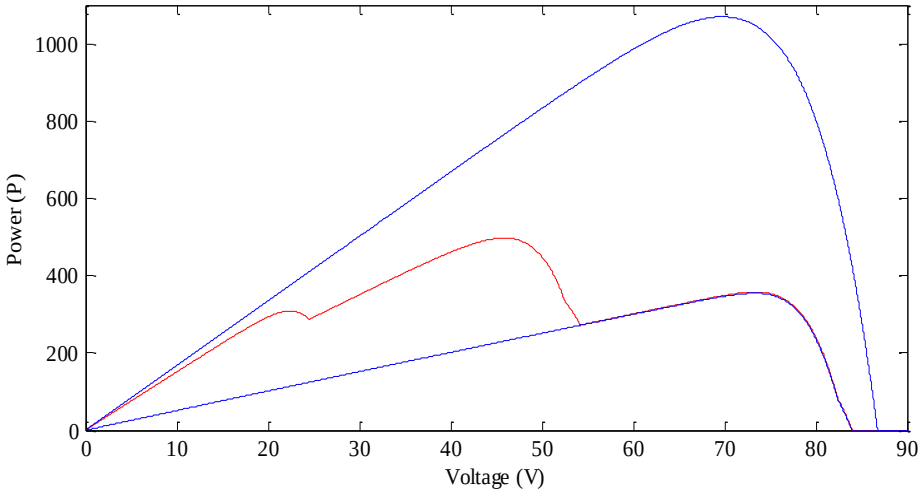

(a)

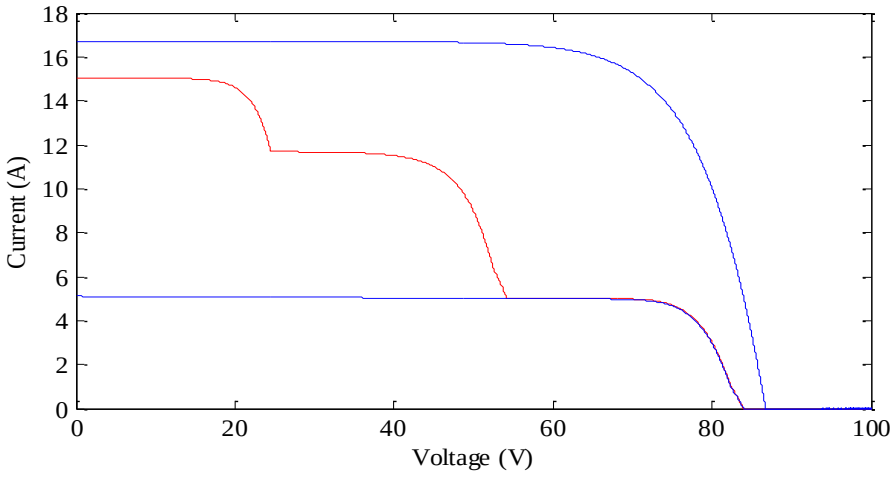

(b)

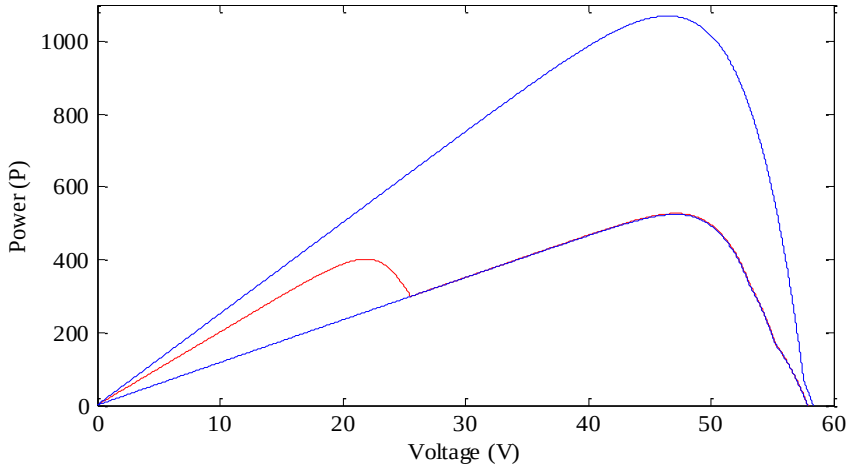

(c)

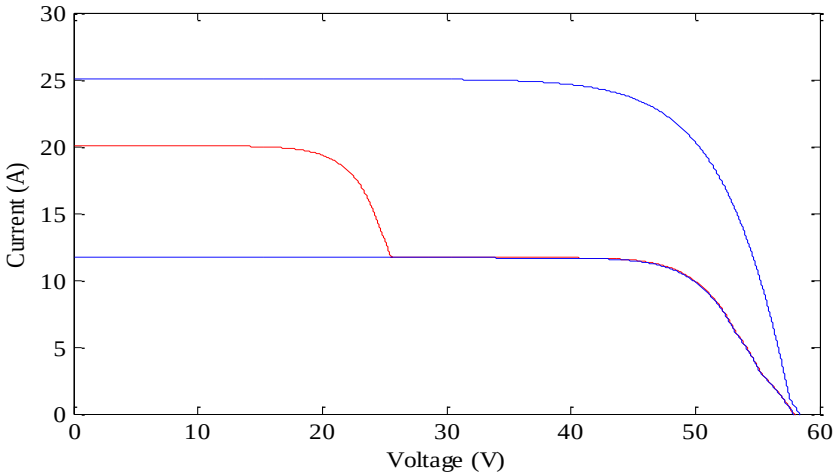

(d)

Fig. 2.12 Solar PV characteristics under partial shading for KD180GX
a) P-V characteristic for 3×2 array
b) I-V characteristic for 3×2 array
c) I-V characteristic for 2×3 array
d) P-V characteristic for 2×3 array

Table 2.9. Parameters of the Kyocera under partial shading

I_{SC}	8.35 A
I_{mpp}	7.63 A
V_{OC}	29.5 V
V_{mpp}	23.6 V
P_{mpp}	180 W
N_S	48
k_V	-0.106 V/K
k_I	.005 A/K

Table 2.10. Irradiance level for 3×2 array (KD180GX).

Irradiance (W/m^2) 1st string	Irradiance (W/m^2) 2nd string
600	800
200	400
1000	800

Table 2.11. Irradiance level for 2×3 array under partial shading

Irradiance (W/m^2) 1st string	600	200
Irradiance (W/m^2) 2nd string	800	400
Irradiance (W/m^2) 3rd string	1000	800

It inferred from the Fig.2.12 (a) to (d) that use of bypass diode improves the performance of PV system much significantly and provides better output power under non-uniform weather case. The shaded modules behave as a load and causes heavy drop in the resultant output current whenever shading occurs so the performance of output power get reduced.

2.7 Conclusion

The solar PV characteristics investigated considering partial shading capability of simulated model in MATLAB/Simulink. The impact of PV system configuration during partial shading is also illustrated and by-pass diode and blocking diode utilized to show the improvement in solar characteristic. First, the single diode solar cell equivalent model utilized for modelling. Further double diode model utilized to model the solar cell to obtain the characteristic at low irradiance level with better accuracy. The real time data of rooftop solar PV system and PV panel parameters utilized to investigate the installed rooftop system.

CHAPTER 3

GRID PV SYSTEM INTEGRATION: 2-DOF CONTROLLER

3.1 General

The solar power production is growing at very fast rate in India and world also. The distributed generation in grid-connected mode is mostly desirable with grid following power export control to cater the power demand with the increasing rate of consumption, [78], [79] and lowers the possibility of energy storage problems. The PV system can be coupled to the grid using inverter to convert the dc into ac as power generated by PV system is dc in nature [31].

The integration of solar PV generation to the grid causes some very important technical issues and challenges that affect the quality of power. These include voltage fluctuations, harmonics, reactive power, low power factor (PF), load management etc. and therefore an integration of renewable energy source to the electric grid should fulfil standards of power quality and power quality requirements [80], [81]. Solar PV generation mainly developed in standalone mode or isolated mode and the main drawback of the isolated mode is that it is limited to very low rating of power generation. In addition, it requires very large storage capacity; but in recent years the focus is also shifting to grid connected solar PV generation to augment the grid capacity.

The rapid growth and research in solar industry has led to the development of PV systems, which are more reliable and efficient, especially for utility power in distributed generation (DG) at medium, and low voltages power systems. Several research projects dealing with smart grids increasingly carried out in India and abroad. Implementing distributed energy resources (DER) into interconnected grids could be part of the solution to meet the rising electricity demand [82]- [83].

There are different techniques to control the grid connected photovoltaic (PV) system to synchronize the PV system with utility grid. The grid-following power export control strategy is often used to control the DER (in this case PV) output power within the voltage and frequency limits as determined by the micro-grid or utility grid. The grid-following approach employed when direct control of voltage and/or frequency is not required [82]

The grid connected PV systems as DER deals with the evacuation of solar PV power generated by the solar system in daytime with proper tracking of maximum power point (MPP). The maximum power point tracking algorithms implemented with dc-dc converter. [57]

In general, a photovoltaic grid-connected system considered as a two stage grid-connected inverter. The first stage is a dc-dc converter controlled in such a way that the photovoltaic system operates in optimal condition i.e. seeking maximum power point tracking (MPPT). The second stage is a dc-ac converter that controlled in a way that allows PV to be grid connected. Control is achieved for unity power factor (PF) correction, which means that the output current (entering into the grid) must be sinusoidal and in phase with the grid voltage. The dc-dc and dc-ac converters operate independently making the entire control system easier to implement. Two-level VSI is widely used for grid-connected PV systems, regardless of the disadvantages such as high switching losses and relative low-quality output voltage waveforms [83]. In grid-connected mode, it is necessary to control power flow between the PV and the utility. This system requires power conditioning unit for smooth operation and control algorithm for grid synchronization and power control. The LC filter used for reduction of ripples as power conditioner but it is expensive for medium and high power application due to the inclusion of high value inductance [34]. The LC filter substituted by an LCL filter.

Therefore, the current control strategy of the PWM-VSI system is one of the most important aspects of the modern power electronics converters. There are two main categories for current controllers: nonlinear controllers based on closed loop current type PWM, and linear controllers based on open loop voltage type PWM. Both categories of controllers utilize the inner current feedback loop. In the nonlinear controller, hysteresis current control (HCC) commonly used for three-phase grid-connected VSI systems. The HCC compensates the current error and generates PWM signals with acceptable dynamic response. While the current controlled independently with a control delay, zero voltage vectors cannot be generated, resulting in a large current ripple with high total harmonic distortion (THD). The linear current controller based space vector PWM is an adequate controller, which compensates the current error either by the proportional-integral (PI) regulator or predictive control algorithm while

the compensation and PWM generation can be done separately. This controller yields an excellent steady-state response, low current ripple, and a high quality sinusoidal waveform [84].

In this chapter, the LCL interfaced VSI based grid integrated PV system is designed and modelled. The two-degree-of-freedom (2-DOF) controller structure utilized for the improved dc voltage regulation [85], [86].

3.2 PV and Grid System: Defined Requirements for Integration

PV configuration with dc-dc/dc-ac converters is an important point to take care of in the grid coupled PV system Fig 3.1. Inverters used for PV power conversion from dc-ac classified considering the PV plant structure Table3.1 [80].

Table 3.1 Classification of PV inverters considering to PV plant configuration (power rating).

50-400 W	Module Integrated inverter	Usually one PV module
0.4-2 kW	Roof-top PV string inverter	String of series connected modules
1.5-6 kW	Medium large roof-top inverter	One or two strings
6-100 kW	Three phase topology of inverters (Mini central inverters)	Multistring/array configuration with plant sizes of 6, 8, 10, 15 kW
>100kW	Three phase topology inverters and modular design (Central Inverters)	Multistring/array configuration with plant sizes of 100,150, 250, 500, 1000 kW

The PV power output fed to the grid and ac load through dc-ac inverter in a grid connected PV system. The defined standards followed to maintain the power quality of the system as according to the standards defined by the agencies (grid connection standards by IEC, IEEE). The power quality of the delivered power PV regulated by standards and practices related to voltage, DC-injection, flicker, frequency, distortion/harmonics and power factor at the point of common coupling (PCC). [12], [80], [87].

The response of the PV inverter to any abnormal grid condition within certain time limit is an important factor as in general grid coupled PV system do not control the utility grid voltage. So, the inverter must act depending upon the voltage (allowed to operate in

Table 3.2 Trip time for grid connected PV system.

Voltage (nominal voltage at PCC in RMS)	Maximum trip time (Time between occurrence of abnormality and inverter ceasing)
V < 50%	0.1s
50% ≤V< 85%	2.0s
85% ≤V< 110%	Continuous operation
110% ≤ V< 135%	2.0s
135% ≤V	0.05s

specific voltage range) level to prevent unwanted islanding condition during abnormal grid conditions by detecting it. The response time defined as in Table 3.2. [12], [80], [87]

The allowable injected dc current into the utility grid, should not be >0.5% of rated inverter output current for any operating condition and constraints (IEEE 929 and IEC 61727 standards).

The current harmonic distortion desired to be as low as possible maintaining other constraints. The dc-ac converters for the coupling of PV to grid generated harmonics and it is limited by the standards (IEEE 929 and IEC 61727 standards). The limits of the allowable current distortion inject into the grid in Table3 is defined based on odd harmonics order and defined as a percentage of the rated fundamental component of current. The even harmonics are limited to 25% of corresponding to limits of odd harmonics order. [12], [80], [87].

The power factor of the grid-coupled system defined based upon the output of the PV inverter. The converter should operate at >0.85(lagging) and >0.9(lagging) power factor for the >10% and >50% of the rated output of the converter respectively. Some of the major key points related to grid integration of PV summarized in Table 3.4 [12] for a 50 Hz and 60 Hz utility grid system.

There are some demands required by the PV system too for a better combination of the overall system. MPPT algorithm implemented to track the MPP and extract the maximum generated power from the PV system. The output voltage/current of the tracked MPP is having ripple and maximum allowable ripple of PV is defined for the voltage as [12], [88]

Table 3.3 THD limitation for grid connected PV system.

Odd harmonic order	THD of odd harmonics order
THD	5%
$3^{rd} – 9^{th}$	<4%
$11^{th} – 15^{th}$	<2%
$17^{th} – 21^{st}$	<1.5%
$23^{rd} – 33^{rd}$	<0.6%
Above 33^{rd}	<0.3%

Table 3.4 IEEE and IEC standards for grid connected PV system.

	IEC61727	IEEE1547
Rated power	10kW	30kW
THD in current	5%	5%
Power factor for >50% of rated power	0.90	0.90
Voltage range under normal operating condition	85%-110%	88%-110%
Frequency	50±1 Hz	59.3 – 60.5 Hz
DC current injection	< 1% I_{out}	< 0.5% I_{out}

$$\hat{V} = \sqrt{\frac{2\,(K_{PV}-1)P_{MPP}}{3\alpha V_{MPP} + \beta}} = 2\sqrt{\frac{(K_{PV}-1)P_{MPP}}{d^2p_{pv}\Big/d^2v_{pv}^2}} \quad (1.)$$

$\hat{V}$ is the maximum desired voltage ripples, P_{MPP} and V_{MPP} are the power and voltage at MPP, α and β are the coefficient of the second order equation $i_{PV} = \alpha V_{PV}^2 + \beta V_{PV} + \gamma$ (used for curve fitting of the I-V characteristic) and K_{PV} utilization ratio i.e. defined as ratio of generated power and theoretical maximum power provided by manufacturer. Based upon the voltage ripple equation, the ripple voltage of <8.5% is required to achieve the $K_{PV} \geq 98\%$ [12], [87].

3.3 Design and Selection

3.3.1 Selection of DC link capacitor voltage

The dc link voltage of grid connected PV system controlled by an outer voltage control loop that operates on the dc voltage error. The dc voltage controller generates references for the grid current in case of direct current controlled grid connected PV system. The selection of reference dc link voltage and dc link capacitor is an important parameter of VSI for grid interfacing of PV system. The selection of peculiar reference dc input voltage (V_{dc}) is essential for operation and control of three-phase output

voltage of pulse width modulated (PWM) VSI. The dc link voltage limitation and selection is important due to switching losses and losses due to filter resistance. The dc link capacitor charged upto certain voltage level through the anti-parallel diode of switching device when the VSI is been connected to grid and switching devices were not controlled by the PWM pulses. The reference dc link voltage rating for VSI selected based upon the criteria mentioned in **[42]** based upon the voltage level obtained by the uncontrolled natural charging of dc link capacitor. The reference dc link voltage should be selected 10-15% higher of the charged capacitor voltage level. If the line-to-line rms grid voltage V_{LL} is 415V then uncontrolled VSI output voltage is 680V. The hysteresis current controlled (HCC) VSI based system is considered therefore 15% criteria is chosen and reference dc voltage is selected as V_{dc} = 800V. V_{LL} is obtained through VSI in terms of dc link voltage (V_{dc}) and modulation index (m) can be computed as

$$V_{LL} = \frac{(\sqrt{3}V_{dc}m)}{2\sqrt{2}}\ (SPWM)\ ;\quad V_{LL} = \frac{V_{dc}m}{\sqrt{2}}\ (THIPWM, SVPWM) \tag{2.}$$

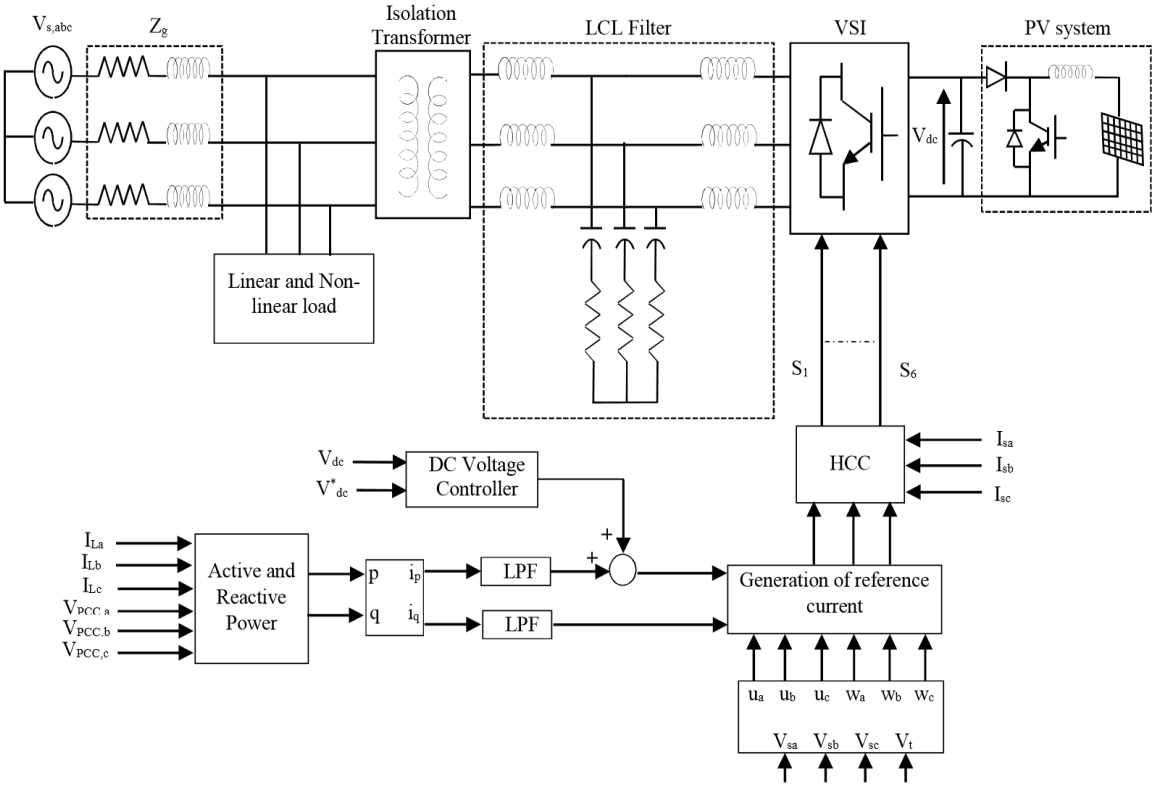

Fig 3.1 Grid interfaced solar PV system (LCL filter and isolation transformer).

where V_{LL} is the line to line voltage, and m is modulation index. According to Eq. (2), the dc link voltage should be greater than twice of the peak of the phase voltage of the system. DC link voltage of system considered under investigation; selected as 800V for modulation index of 0.9 and V_{LL} is 415V.

3.3.2 Design and selection of DC link capacitor

The size of the decoupling capacitor can be determined when knowing that the power into the DC-link is constant, and that the power drawn from the DC-link follows a $\sin^2$(wt) waveform [84], [87]

$$C_{dc} = \frac{I_d}{2 * \omega * \tilde{v}_{dc}} = \frac{P_{dc}}{2 * \omega * \langle V_{dc} \rangle * \tilde{v}_{dc}} \quad (3.)$$

where P_{dc} is the average DC-link power, ω is the grid frequency), $\langle V_{dc} \rangle$ is the average DC-link voltage and $\tilde{v}_{dc}$ is the amplitude of the ripple voltage (5% of the dc link voltage). The flow of current cannot be controlled if the dc link voltage is less than the peak grid-voltage plus the drop in between grid and inverter (i.e. filter loss and semiconductor loss in inverter).

The other method of design of DC link capacitor (C_{dc}) of VSC depends upon the instantaneous energy available to the VSC at the time of transient. Based on the principle of energy conservation principle, the value of DC capacitor given below as

$$\frac{1}{2} C_{dc} \left[V_{dc}^2 - V_{dc1}^2 \right] = 3V\alpha It \quad (4.)$$

where V is the phase voltage, I is the phase current, t is the time by which dc link voltage is to be recovered, V_{dc} is the reference DC link voltage and V_{dc1} is the minimum DC link voltage level of DC bus. Taking, V_{dc} = 800 V, V_{dc1} = 790 volt, α= 1.2, t=350 microsecond, the calculated value of C_{dc} is obtained to be 1500 μF.

3.3.3 Power conditioner: Grid-connected filter

The power conditioner is required and connected in between dc-ac inverter and grid to fulfill three main requirements: minimize the noise at high frequency, protecting the inverter under transient situations of the system and conversion of voltage generated by VSI in current. The LCL filter became very popular since last decade due to inherent advantages over L and LC filter.

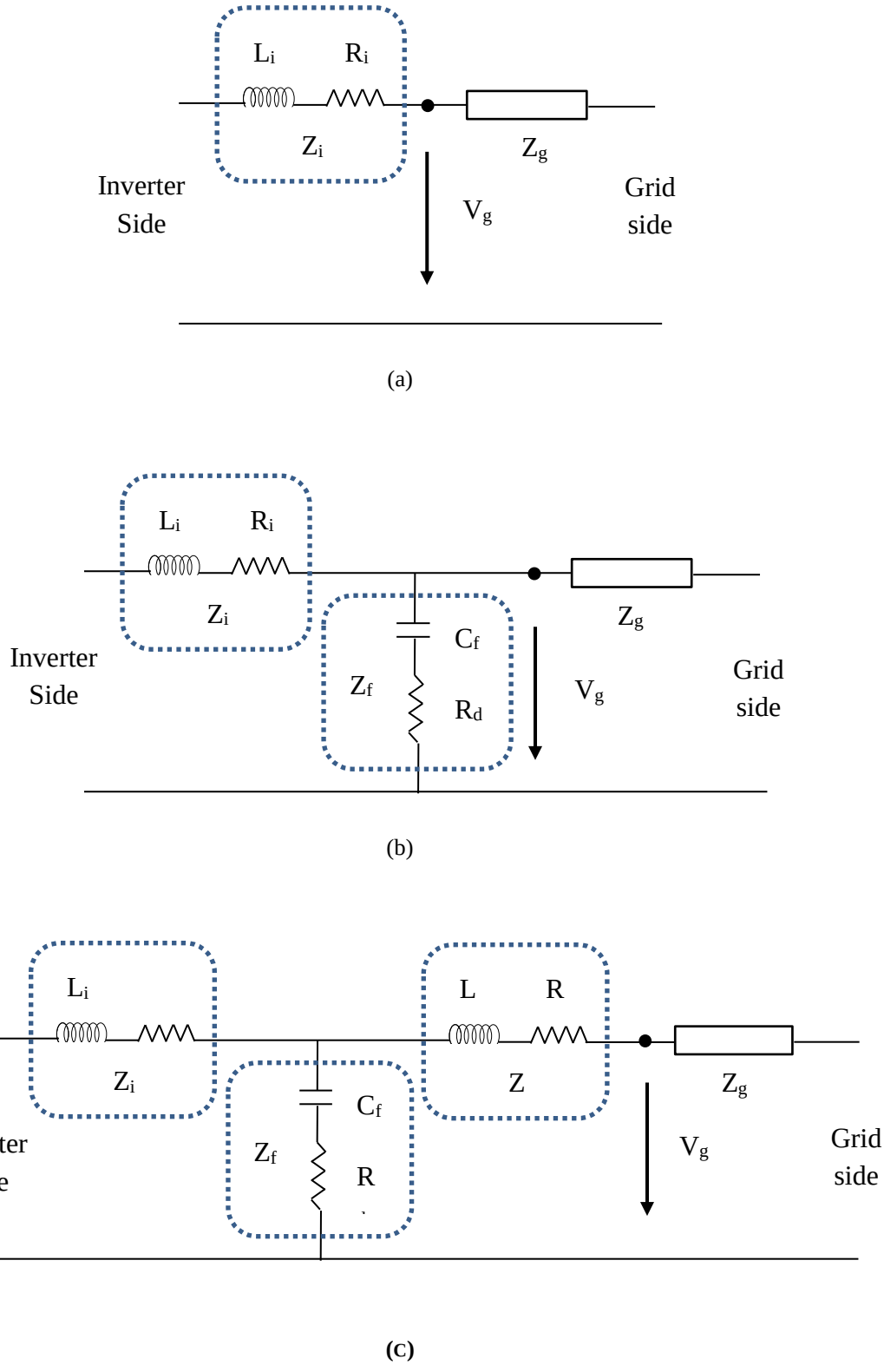

Fig 3.2 Grid connected inverter with filter circuit
a) Circuit with L Filter
b) Circuit with LC filter
c) Circuit with LCL filter

The system circuit consists of L filter in Fig. 3.2a have to deal with the drawback of bad system dynamics caused due to large value of inductance. The L filter is capable

of converting voltage into current with good performance but unable to minimize the high frequency noise. The LC filter in Fig. 3.2b having an inductance in series with the inverter and a capacitance in shunt so using capacitance in shunt the value inductance is decreased which in turn affects the loss and cost positively. Similar to L filter, LC filter is capable of voltage to current conversion with good performance and can minimize the high frequency noise up-to certain level (grid impedance considerably high in comparison capacitive reactance). But, again the constraint is there that we cannot choose very high value of capacitance which will results in other adverse effects like high inrush current (capacitor exposed to voltage ripples) and grid inductance is significantly dominant.

The transfer function of the LCL filter Fig. 3.2c is changed according to the control parameters (inverter voltage and current; grid current and voltage). The one of the most commonly used control parameter combination is inverter voltage and grid current.

The single-phase equivalent of LCL filter in Fig. 3.3 represented as transfer function block in Fig. The circuit equations written using fundamental laws of electrical circuits as:

$$i_i = i_g + i_c \tag{5.}$$

$$v_i = v_c + i_i(sL_i + R_i) \tag{6.}$$

$$v_c = v_g + i_i(sL + R) \tag{7.}$$

$$v_c = i_c\left(\frac{1}{sC_f} + R_d\right) \tag{8.}$$

The transfer function of LCL filter considering inverter voltage and grid current is

$$G_{LCL} = \frac{i_g}{v_i} \tag{9.}$$

$$G_{LCL} = \frac{(sR_dC_f + 1)}{\begin{aligned}&(s^3L_gLC_f + s^2C_f(L(R_d + R_i) + L_i(R_d + R)) + \\ &s\left(L + L_i + C_f(R_dR + R_dR_i + RR_i)\right) + (R + R_i))\end{aligned}} \tag{10.}$$

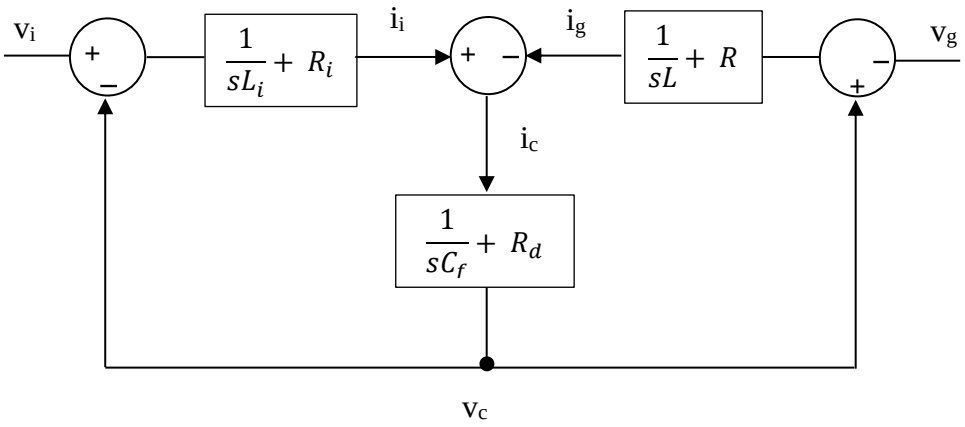

Fig 3.3 LCL filter represented as block diagram using transfer function

3.3.3.1 Constraints for designing LCL filter: [31], [33], [34], [35], [42], [85]

- The resonance frequency (f_{res}) should be less than half of the switching frequency (f_{sw}) and more than ten times of the fundamental grid frequency (f) (to avoid interference).

$$10f < f_{res} < (f_{sw}/2) \quad (11.)$$

- The capacitance value should be less than 5% of base capacitance at the rated power (due to decrease in power factor).

$$C_f \leq .05C_{base} \quad (12.)$$

- The total value of inductance value should be less than 0.1pu (to limit the ac voltage drop for low power filters). The maximum value of inductance is very much dependent upon the power rating of the system and based upon application it can be varied.

$$(L_i + L) \leq 0.1Z_{base} \quad (13.)$$

- Considering digital control for the system: the sampling frequency (f_s) should be adopted as twice of f_{sw} (to avoid aliasing). The ratio of f_{res} and f_s (f_{res}/f_s) is play an important role in LCL filter stability. And, f_s should be four times or more of f_{res} for grid current based inverter control.

$$f_s \geq 4f_{res}\,;\; f_s \geq 2f_{sw} \quad (14.)$$

3.3.3.2 Design equations

Inverter side inductor (L_i)

$$\frac{i_i(h_{sw})}{v_i(h_{sw})} \approx \frac{1}{w_{sw}L_i} \tag{15.}$$

$$\Rightarrow L_i = \frac{v_i(h_{sw})}{w_{sw} * i_i(h_{sw})} \tag{16.}$$

Capacitance (C_d)

$$C_f \leq 0.05C_{base};\ C_{base} = \frac{P_{rating}}{2 * pi * f * V_{gLL}^2} \tag{17.}$$

Grid side inductor (L)

$$\frac{i_g(h_{sw})}{i_i(h_{sw})} \approx \frac{z_{LC}^2}{| w_{res}^2 - w_{sw}^2 |} \tag{18.}$$

$$z_{LC}^2 = \frac{1}{LC_f}\ ;\ w_{res} = \sqrt{\frac{L_i + L}{L_i * L * C_f}}\ ;\ w_{sw} = a * w_{res}\ (a \geq 2) \tag{19.}$$

3.4 Control Design

The control design can be divided into steps according to control algorithm and ease of implementation. The general categorization can be as:

1) Grid synchronisation
2) Voltage Controller
3) Reference current generation
4) Current control (Switching scheme)

The control design categorization explained as follows:

3.4.1 Grid synchronisation

In general, phase locked loop (PLL) is used for grid frequency synchronization with phase locking of the signal. The generalized fundamental structure of PLL consists of phase detector, loop filter and voltage controlled oscillator (VCO) as shown in Fig. 3.4a. The accurate detection of phase and frequency utilized for proper generation of

reference signals responsible for compensation of different quantitates. The synchronous reference frame (SRF) is used to implement PLL by converting three phase quantity into two phase rotating frame (abc→dq) and reference quantity (V_d^*) is set to zero. Generally, PI controller used as a filter to control the system variable. The output of the PI controller is fundamental grid frequency further passed through VCO realized by an integrator. The

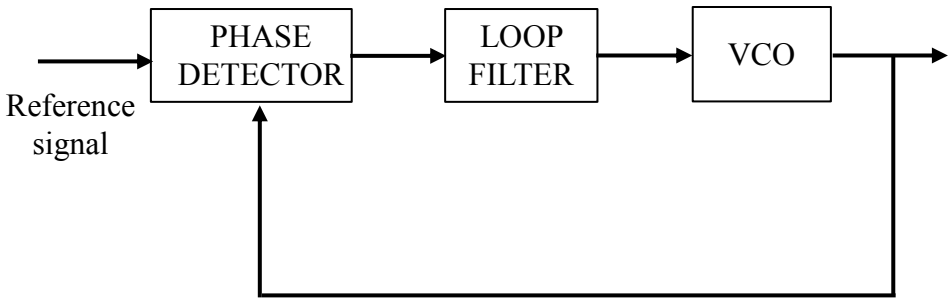

(a)

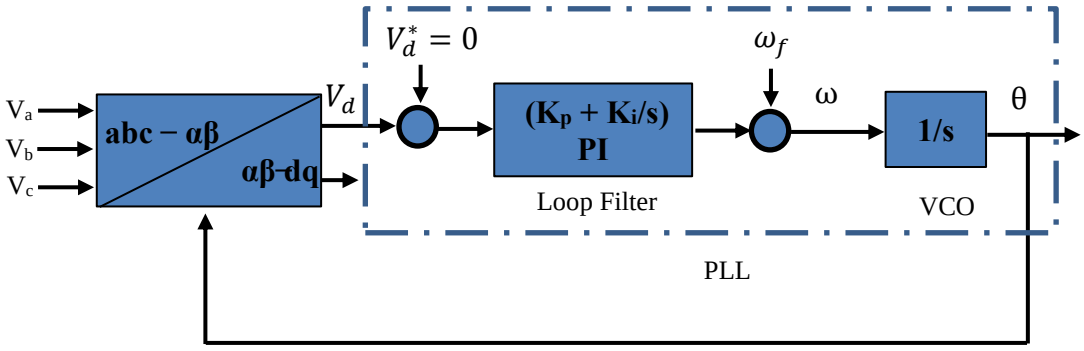

(b)

Fig 3.4 Phase locked loop (PLL)
(a) Block diagram
(b) Implementation and design of PLL algorithm in power system

output of the integrator is an angle and fed into the transformation block as shown in Fig. 3.4b. PLL transfer function can be written as:

$$M_{PLL}(s) = \frac{sK_p + K_i}{s^2 + sK_p + K_i} = \frac{sK_p + \frac{K_p}{T_i}}{s^2 + sK_p + \frac{K_p}{T_i}} \quad (20.)$$

Second order standard transfer function given as:

$$M(s) = \frac{s(2a\omega_n) + \omega_n^2}{s^2 + s(2a\omega_n) + \omega_n^2} \quad (21.)$$

$$\omega_n = \sqrt{\frac{K_p}{T_i}}\ ;\ \zeta = \frac{K_p}{2\omega_n} \quad (22.)$$

The damping factor (ζ) selected as .707 considering standard case with overshoot less than 5% for a step response. Considering settling time (T_{set}), filtering and tracking performance $k_p$and T_i and can be tuned.

3.4.2 Voltage controller

The voltage controller is used for regulation of DC-link voltage of VSI. The dc voltage controller generates the equivalent d-axis quantity fed to the inner control loop for generation of reference signal. The generalized dc voltage control loop in Fig. 3.5 is consists of conventional PI controller, current control block (can be considered as response delay of current), dc coefficient (K_{dc}) (to balance the power in between dc quantity and d-q co-ordinate) and dc link capacitor. The sampling block is also considered for digital control analysis and can put in feedback loop or in forward loop only.

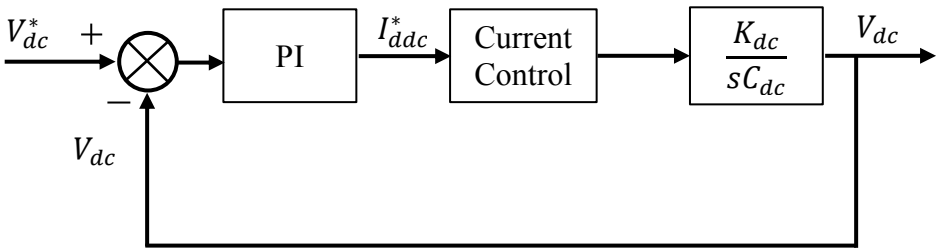

Fig 3.5 Block diagram of dc voltage controller.

The dc coefficient computed using the relationship between direct components of current fed to VSI and dc current. The relationship of input and output power in terms of direct component and dc component written as (23)

$$V_{dc} * I_{dc} = \frac{3}{2} V_d * I_d \quad (23.)$$

So, the dc coefficient (K_{dc}) can be computed as

$$K_{dc} = \frac{I_{dc}}{I_d} = \frac{3}{2}\frac{V_d}{V_{dc}} \quad (24.)$$

The relation of dc link voltage (V_{dc}) and line-to-line grid voltage (V_{LL}) in (23) and (24) gives an expression

$$\frac{V_d}{V_{dc}} = \frac{m}{2} \tag{25.}$$

Therefore,

$$K_{dc} = \frac{3}{4}m \tag{26.}$$

Modulation index (m) is in between zero to one for sinusoidal carrier based PWM switching and in between zero to 1.155 for SVPWM and THI-PWM.

The PI controller based dc link voltage control shown in Fig. 3.5. The reference current quantity for the voltage error generated for current controlled VSI and considered as an active power component of current. This active power current regulates the dc link voltage to reference dc level by feeding losses of VSI.

The conventional PI control structure in Fig. 3.6a consists of controller and plant/system transfer function block where, P(s): PI controller ($k_p + k_{int}/s$) and G(s): transfer function of the plant/system. The 1-DOF PI controller may not achieve satisfactory response considering multi-objective viewpoint of the system control and therefore 2-DOF controller have natural advantage over conventional PI controller [21]. In this study, the 2-DOF PI control instrumented first time for dc voltage control.

The number of independent closed loops in control structure decides the DOF of the system control and considered as two-input and one output system. The 2-DOF controller designed and discussed in [16,21] with various configuration stated as feed-forward type (FF), feedback type (FB), filter type, filter and preceded derivative type and component separated type depending upon the application and objective of system control. The 2-DOF feedback compensating (2-DOF FB) controller in Fig. 3.6b implemented for dc voltage regulation. The 2-DOF PI control configuration used for dc voltage control consists of proportional gain (k_p) and integral gain (k_{int}) same as conventional PI controller and additional feedback proportional gain (k_{pfb}) as a feedback compensation. Therefore, it is having two proportional control gain and one integral control gain and represented as PI-P (2-DOF PI) controller. The reference input signal (r) and controller output signal (y) are the input signal and the modified output

signal (u) output signal. The closed loop transfer function of conventional PI control structure in Fig. 3.6a, from reference input r to controlled output y and from disturbance d-y are given respectively as

$$M(s) = \frac{G(s)P(s)}{1 + G(s)P(s)} \tag{27.}$$

$$M(s) = \frac{G(s)}{1 + G(s)P(s)} \tag{28.}$$

The transfer function shown in (1) and (2) having only one tunable element as P(s) for optimal system performance. As it includes only one tuning element it cannot be tuned independently. The closed loop transfer function of 2-DOF FB control structure shown in Fig. 3.6b from reference input r to controlled output y and from disturbance d to y given respectively as

$$M(s) = \frac{G(s)P(s)H(s)}{1 + G(s)\mathrm{H(s)}(P(s) + 1)} \tag{29.}$$

$$M(s) = \frac{G(s)}{1 + G(s)(P(s) + \mathrm{H(s)})} \tag{30.}$$

Here, the function shown in (3) and (4) having two tuning elements as P(s) and H(s). It will help to achieve the optimal performance for the system with feedback compensating terms tuning to accommodate the effect of P(s) on other performance like disturbance case.

r is reference input quantity as V_{dc}^{*}, y is output quantity as measured dc link voltage V_{dc} and output of the controller u is equivalent quantity as the active power component of current for dc link i_{ddc} for dc link voltage control. This closed loop system is consists of PI controller transfer function P(s,k) and plant transfer function G(s) representing the response delay of current controller/regulator, dc coefficient to keep the balance of power in dc-ac system and capacitor.

The controller system analyzed for the step change in r and response of the y and termed as reference point (set point) response. The reference dc voltage 'V_{dc}^{*}' is the reference input signal 'r' and measure dc voltage 'V_{dc}' which have to be regulated to reference level is considered as output for dc voltage control scheme.

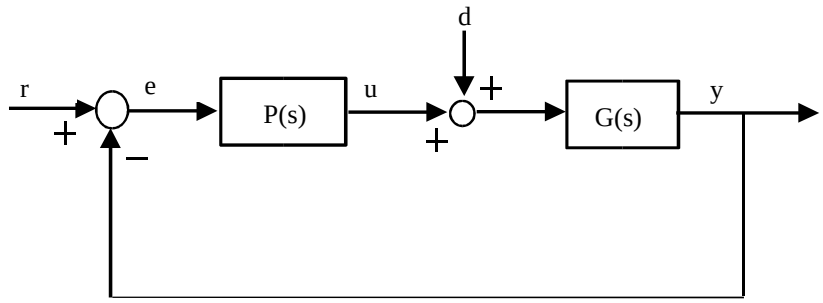

(a)

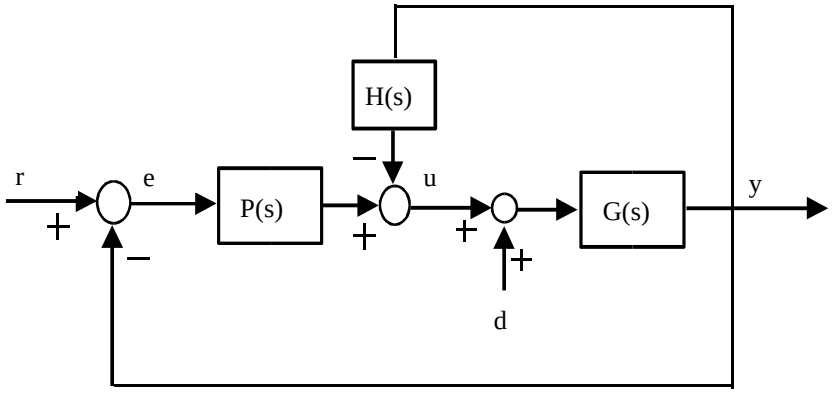

(b)

Fig 3.6 Generalized configuration of controllers.
(a) Conventional PI controller (1-DOF) PI configuration.
(b) 2-DOF controller configuration.

The 1-DOF and 2-DOF controller response for dc voltage control analyzed for the step change in V_{dc}^{*}. The control method in the form of equations for dedicated PI controller used for dc link control is been shown as (31) and (32). The difference in reference voltage and measured voltage for dc link shown in (31) and the output after the PI controller shown in (32).

$$E = V_{de}(k) = V_{dc}^{*}(K) - V_{dc}(K) \quad (31.)$$

where $V_{dc}^{*}(K)$ and measured voltage $V_{dc}(K)$of dc link The output quantity after the PI control is current as current control method have been used which is considered in terms of losses. So, the active power component of current required to compensate the losses and regulate the DC link voltage to the reference level and can be computation as:

a) The dedicated dc voltage PI controller regulates the dc bus voltage to desired reference level & provides the active power component of current for dc link (i_{ddc}) to

compensate losses. The value of output current quantity after the PI controller needed compensate the losses computed as

$$i_{d,dc}(K) = i_{d,dc}(K-1) + k_p\big(v_{de}(K) - v_{de}(K-1)\big) + k_{int}(v_{de}(K)) \quad (32.)$$

k_p & k_{int} are proportional and integral gain of the PI controller. $i_{d,dc}(K)$ and $i_{d,dc}(K-1)$ are the loss component of current at kth and k-1th sampling.

b) The dedicated dc voltage PI controller replaced by PI-P controller for regulation of the dc bus voltage to desired reference level by feeding losses of VSC. The equation for the value of output current quantity is modified based upon the PI control (32) and given by (33) as

$$i_{d,dc}(K) = i_{d,dc}(K-1) + k_p\big(v_{de}(K) - v_{de}(K-1)\big) + k_{int}\big(v_{de}(K)\big) - k_{fbp}\big(v_{de}(K)\big) \quad (33.)$$

k_p , k_{int} , k_{fbp} are proportional, integral gain and proportional gain of the PI-P controller.

3.4.3 Reference current generation

The reference current can be generated using different algorithms. There are various control algorithms mentioned in literature like instantaneous reactive power theory (IRPT), synchronous reference frame theory (SRFT), Fryze conductance theory and power balance theory (PBT). In this study, SRFT, PBT and fryze conductance theory implemented and each algorithm has its own advantage over other. SRFT algorithm requires transformation of control parameters and PLL for synchronisation. The compensation of the different components like harmonics, negative sequence is easier as compared other algorithms. PBT algorithm does not required PLL for grid frequency synchronisation. Unit templates computed using system control parameters and utilized for synchronisation and generation of reference currents. The control parameter transformation is not required for Fryze conductance algorithm but selective harmonic compensation is not an easy task.

3.4.3.1 Synchronous reference frame theory (SRFT)

The synchronous reference frame theory (SRFT) control employed in indirect current control mode. The references for three phase ac grid currents are generated for the control of VSI. The fundamental approach of SRF theory is to convert the three phase

control parameters synchronously rotating d-q frame using transformation equations. The transformation equation used for abc to dq0 conversion is

$$\begin{bmatrix} x_q \\ x_d \\ x_0 \end{bmatrix} = \frac{2}{3}\begin{bmatrix} \cos\theta & \cos(\theta - 2\pi/3) & \cos(\theta + 2\pi/3) \\ \sin\theta & \sin(\theta - 2\pi/3) & \sin(\theta + 2\pi/3) \\ 1/2 & 1/2 & 1/2 \end{bmatrix}\begin{bmatrix} x_a \\ x_b \\ x_c \end{bmatrix} \quad (34.)$$

$$\begin{bmatrix} x_a \\ x_b \\ x_c \end{bmatrix} = \begin{bmatrix} \cos\theta & \sin\theta & 1 \\ \cos(\theta - 2\pi/3) & \sin(\theta - 2\pi/3) & 1 \\ \cos(\theta + 2\pi/3) & \sin(\theta + 2\pi/3) & 1 \end{bmatrix}\begin{bmatrix} x_d \\ x_q \\ x_0 \end{bmatrix} \quad (35.)$$

where cosθ & sinθ are generated through three phase PLL and x can be voltage or current. The dq component of current and voltage may consist of average component (dc component) and oscillating component (harmonic component).

The selective compensation employed by decomposing the load current using SRF algorithm. Selective compensation requires intermediate transformation of quantities i.e. αβ components.

$$\begin{bmatrix} i_{L\alpha} \\ i_{L\beta} \end{bmatrix} = \sqrt{\frac{2}{3}}\begin{bmatrix} 1 & -\frac{1}{2} & -\frac{1}{2} \\ 0 & \frac{\sqrt{3}}{2} & -\frac{\sqrt{3}}{2} \end{bmatrix}\begin{bmatrix} i_{La} \\ i_{Lb} \\ i_{Lc} \end{bmatrix} \quad (36.)$$

$$\begin{bmatrix} i_{Ld} \\ i_{Lq} \end{bmatrix} = \sqrt{\frac{2}{3}}\begin{bmatrix} \cos\theta & \sin\theta \\ -\sin\theta & \cos\theta \end{bmatrix}\begin{bmatrix} i_{L\alpha} \\ i_{L\beta} \end{bmatrix} \quad (37.)$$

The dq component of load current computed using above equation are positive components. The negative component of load current computed by rotating the frame in opposite direction and mathematically by changing sign of angle.

$$\begin{bmatrix} i_{Ld}^{-} \\ i_{Lq}^{-} \end{bmatrix} = \sqrt{\frac{2}{3}}\begin{bmatrix} \cos\theta & -\sin\theta \\ \sin\theta & \cos\theta \end{bmatrix}\begin{bmatrix} i_{L\alpha} \\ i_{L\beta} \end{bmatrix} \quad (38.)$$

The dc component of dq quantities of load current extracted by passing through low pass filter (LPF) for positive and negative sequence component both. The positive sequence fundamental component calculated using d-q components while transformation into three phase reference quantities.

$$\begin{bmatrix} i_{LP\alpha} \\ i_{LP\beta} \end{bmatrix} = \sqrt{\frac{2}{3}}\begin{bmatrix} \cos\theta & -\sin\theta \\ \sin\theta & \cos\theta \end{bmatrix}\begin{bmatrix} 0 \\ i_{Ldc,q} \end{bmatrix} \quad (39.)$$

$$\begin{bmatrix} i_{LQ\alpha} \\ i_{LQ\beta} \end{bmatrix} = \sqrt{\frac{2}{3}} \begin{bmatrix} \cos\theta & -\sin\theta \\ \sin\theta & \cos\theta \end{bmatrix} \begin{bmatrix} i_{Ldc,d} \\ 0 \end{bmatrix} \quad (40.)$$

$$\begin{bmatrix} i_{LPa} \\ i_{LPb} \\ i_{LPc} \end{bmatrix} = \sqrt{\frac{2}{3}} \begin{bmatrix} 1 & 0 \\ -\frac{1}{2} & \frac{\sqrt{3}}{2} \\ -\frac{1}{2} & -\frac{\sqrt{3}}{2} \end{bmatrix} \begin{bmatrix} i_{LP\alpha} \\ i_{LP\beta} \end{bmatrix} ; \quad \begin{bmatrix} i_{LQa} \\ i_{LQb} \\ i_{LQc} \end{bmatrix} = \sqrt{\frac{2}{3}} \begin{bmatrix} 1 & 0 \\ -\frac{1}{2} & \frac{\sqrt{3}}{2} \\ -\frac{1}{2} & -\frac{\sqrt{3}}{2} \end{bmatrix} \begin{bmatrix} i_{LQ\alpha} \\ i_{LQ\beta} \end{bmatrix} \quad (41.)$$

The negative sequence components and harmonics undergo phase/frequency shift during transformation so it is a key point to be careful.

$$\begin{bmatrix} i^{-}_{L\alpha} \\ i^{-}_{L\beta} \end{bmatrix} = \sqrt{\frac{2}{3}} \begin{bmatrix} \cos(\theta+\phi) & \sin(\theta+\phi) \\ -\sin(\theta+\phi) & \cos(\theta+\phi) \end{bmatrix} \begin{bmatrix} i^{-}_{Ldc,d} \\ i^{-}_{Ldc,q} \end{bmatrix} \quad (42.)$$

$$\begin{bmatrix} i^{-}_{La} \\ i^{-}_{Lb} \\ i^{-}_{Lc} \end{bmatrix} = \sqrt{\frac{2}{3}} \begin{bmatrix} 1 & 0 \\ -\frac{1}{2} & \frac{\sqrt{3}}{2} \\ -\frac{1}{2} & -\frac{\sqrt{3}}{2} \end{bmatrix} \begin{bmatrix} i^{-}_{L\alpha} \\ i^{-}_{L\beta} \end{bmatrix} \quad (43.)$$

3.4.3.2 Power balance theory (PBT)

The fundamental mechanism to implement PBT is generation of in-phase and quadrature unit templates shown in Fig. 3.7.

A. Unit templates generation

Unit templates generated based upon their phase orientation in reference to the grid voltage. The in-phase templates and quadrature phase templates generated by (44) and (45)

$$u_{sa} = \frac{V_{sa}}{V_{PCC,t}}, u_{sb} = \frac{V_{sb}}{V_{PCC,t}}, u_{sc} = \frac{V_{sc}}{V_{PCC,t}} \quad (44.)$$

where u_{sa}, u_{sb}, u_{sc} are the in-phase templates and $V_{PCC,t}$ is amplitude of three phase point of common coupling (PCC) voltage and calculated as

$$V_{PCC,t} = \left(\frac{2}{3}\right)^{\frac{1}{2}} (v^2_{sa} + v^2_{sb} + v^2_{sc})^{1/2} \quad (45.)$$

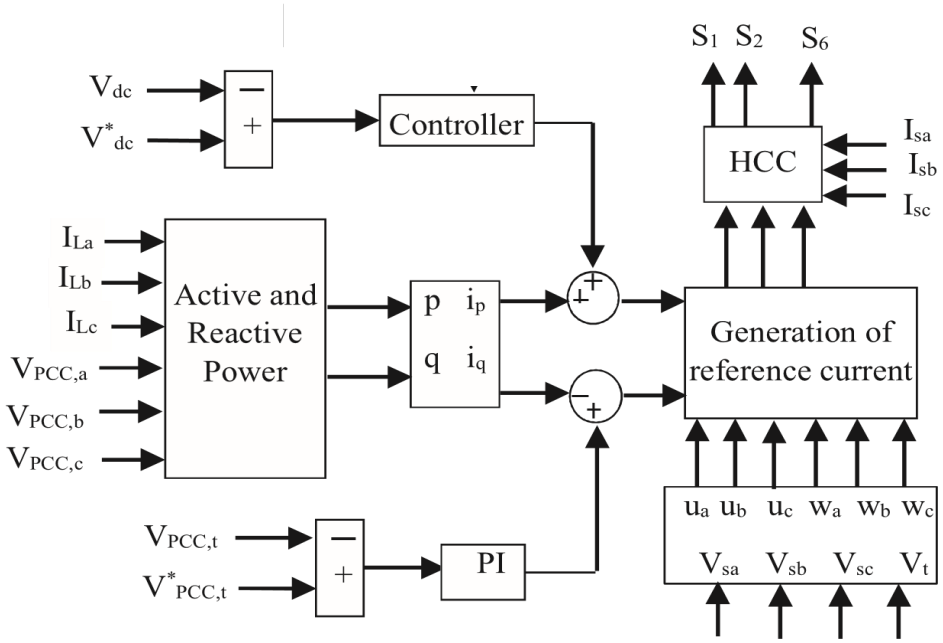

Fig 3.7 Reference current generation using power balance theory (PBT) algorithm

w_a, w_b, w_c are quadrature phase templates.

$$\frac{u_c - u_b}{\sqrt{3}} = w_a \tag{46.}$$

$$\frac{u_a}{\sqrt{2}} + \frac{u_b - u_c}{\sqrt{6}} = w_b \tag{47.}$$

$$\frac{u_b - u_c}{\sqrt{6}} - \frac{u_a}{\sqrt{2}} = w_c \tag{48.}$$

B. Reference current generation

The equivalent active and reactive component of current can be compute by using (49)-(52)

$$i_{Lp} = \frac{2}{3}\frac{p_L}{V_t} \tag{49.}$$

$$q_{Lp} = \frac{2}{3}\frac{q_L}{V_t} \tag{50.}$$

$$p_L = v_{PCC,a} * i_{L,a} + v_{PCC,b} * i_{L,b} + v_{PCC,c} * i_{L,c} \tag{51.}$$

$$q_L = (v_{PCC,a} - v_{PCC,b}) * i_{L,a} + (v_{PCC,b} - v_{PCC,c}) * i_{L,b} + (v_{PCC,c} - v_{PCC,a}) * i_{L,c} \tag{52.}$$

Therefore, the reference current generated for ‘d’ component/active power current of grid current is given as

$$i_{Lp}^{*} = i_p + i_{d,loss} \quad (53.)$$

Active power components of reference grid currents are

$$I^{*}_{spa} = I^{*}_{Lp} * u_{sa},\ I^{*}_{spb} = I^{*}_{Lp} * u_{sb},\ I^{*}_{spc} = I^{*}_{Lp} * u_{sc} \quad (54.)$$

The reference current generated in terms of q component current is given as

$$i_q^{*} = i_q - i_{qPCC,t} \quad (55.)$$

Reactive power components of reference grid currents are

$$I^{*}_{sqa} = I^{*}_{Lq} * w_{sa},\ I^{*}_{sqb} = I^{*}_{Lq} * w_{sb},\ I^{*}_{sqc} = I^{*}_{Lq} * w_{sc} \quad (56.)$$

So, the reference current for grid given by (57)

$$I^{*}_{sa} = I^{*}_{spa} + I^{*}_{sqa}, I^{*}_{sb} = I^{*}_{spb} + I^{*}_{sqb}, I^{*}_{sc} = I^{*}_{spc} + I^{*}_{sqc} \quad (57.)$$

3.4.3.3 Fryze conductance theory

The control based on calculation of conductance termed as fryze conductance using the load current and point of common coupling (PCC) voltage. The reference current using fryze conductance minimization method Fig. 3.8 is generated in such a way that the grid current should follow the average active reference current. The concept behind the minimization is to minimized the r.m.s. value of source current for supplying the same amount of average active power which will reduces the over-all line losses and heat generation in the system [4], [16].

A. Conductance computation

The fryze conductance based current minimization algorithm is based on the computation of conductance using the three-phase load current and three phase PCC voltage. The conductance computed by using equation (8). The computation of conductance for the average active current obtained by passing it through the low pass filter. The control algorithm considers that utility grid must supply active power component of current required to regulate the DC bus voltage to the reference level & feed VSC losses (Gloss). The dedicated dc voltage PI controller regulates the dc bus voltage to desired reference level & provides the active power transfer for compensation of VSC losses.

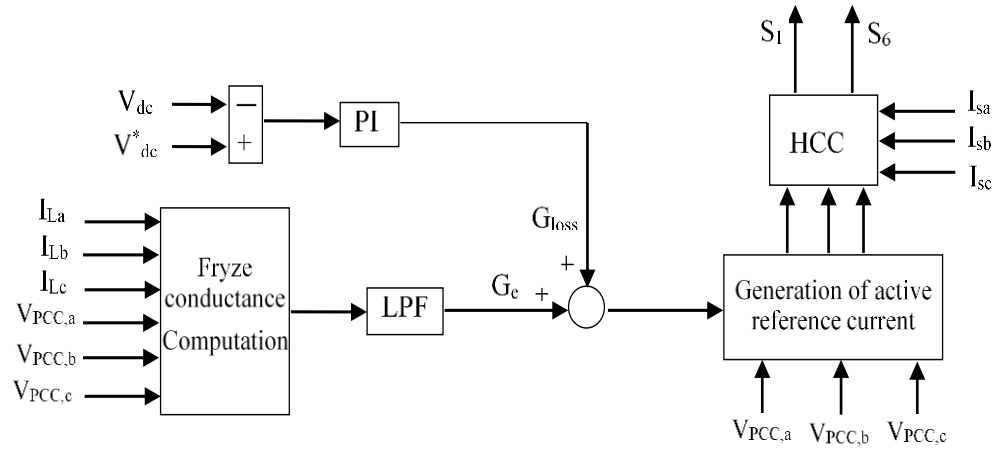

Fig 3.8 Reference current generation using Fryze conductance theory.

$$G_e = \frac{v_{pcc,a} i_{La} + v_{pcc,b} i_{Lb} + v_{pcc,c} i_{Lc}}{v_{pcc,a}^2 + v_{pcc,b}^2 + v_{pcc,c}^2} \quad (58.)$$

B. Average active reference current generation

The conductance equivalent to average active current obtained after the low pass filter added with the conductance equivalent to the losses at dc link. The parameter equivalent to the losses (G_{loss}) at the dc link obtained through the PI controller used for regulation of dc link voltage. The average active reference current generation obtained using the following equations

$$i_{Lpa} = (\bar{G}_e + G_{loss})\, v_{pcc,a} \quad (59.)$$

$$i_{Lpb} = (\bar{G}_e + G_{loss})\, v_{pcc,b} \quad (60.)$$

$$i_{Lpc} = (\bar{G}_e + G_{loss})\, v_{pcc,c} \quad (61.)$$

3.4.4 Current Control (Switching scheme)

The dc-link voltage control employed as an outer voltage loop and current control block is part of it. Therefore, the current regulator/control termed as an inner control loop. The generalized current regulator loop in Fig. 3.9a is consists of controller, control delay, inverter block and filter. The sampling block can also be considered for digital control analysis and can put in feedback loop or in forward loop only.

The current regulator loop simplified by merging the blocks and considered as delay of the system. The overall delay considered for the system is $1.5T_s$ **[reference 2-DOF controller].** The current regulator loop simplified as in Fig. 3.9b

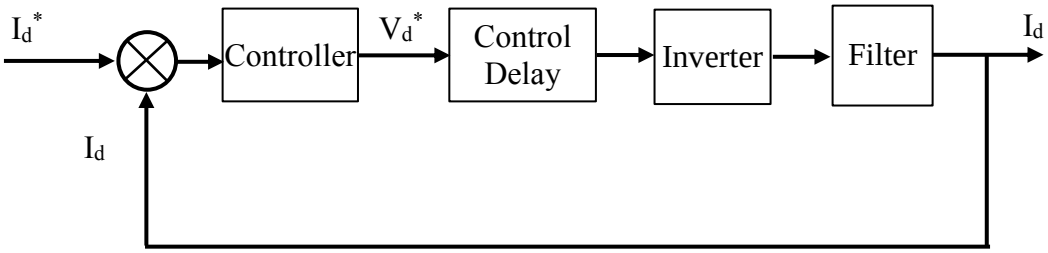

(a)

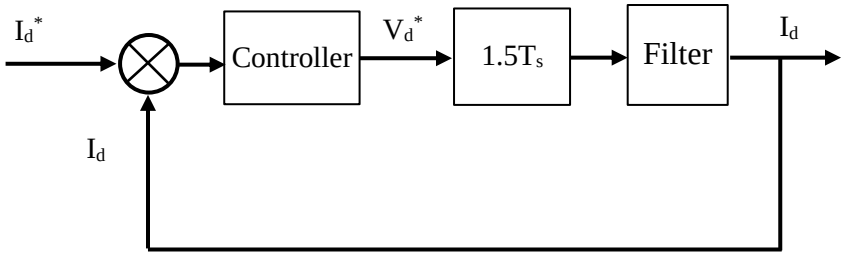

(b)

Fig 3.9 Block diagram of current controller.
(a) Generalized controller blocks diagram.
(b) Simplified block diagram of controller.

$$G_{OLTF} = G_{controller} * G_{control} * G_{inverter} * G_{filter} \quad (62.)$$

The control of VSI based active rectifiers and power generating system interfacing with grid is an important issue. The implementation and extension of conventional control like as SPWM is simple for inverters. HCC is a non-linear control and robust with good tracking but it possesses variable switching frequency and extension to different inverter topologies is difficult. These controllers are having distinctive advantages and disadvantages Table 3.5 and Table 3.6 [36].

The SPWM has advantages as having fixed switching frequency and well established control in industry for commercial purposes. However, it is difficult to obtain best trade-off between modulation index, THD for point of common coupling (PCC) voltage and grid current. The proportional gain/proportional-integral gain used to improve the system performance under SPWM current control. Still, a constraint in

between modulation index and proportional gain affects the source current and PCC voltage.

HCC: variable and constant frequency (non-linear controllers) and PI/PR current control (linear controllers) are the most commonly used current regulators. Pulse width modulation (PWM) is generally used for switching of VSIs. The most common method of PWM modulation is carrier based PWM (CB-PWM) and space vector PWM (SV-PWM). Hysteresis controlled PWM scheme is also one of the commonly used switching scheme. Sinusoidal PWM, third harmonic injected PWM (THI-PWM) and HCC-PWM are employed for the study.

Table 3.5 Advantages and disadvantages of non-linear controllers.

ADVANTAGES	DISADVANTAGES
Non-linear controller and robustness is good	Variable switching frequency
Fast dynamics (no need of modulator)	Resonance problems.
Easy and simple design	High sampling rate for digital implementation
Well established method	Quite difficult to extend for different topologies of converter.

Table 3.6 Advantages and disadvantages of linear controllers.

ADVANTAGES	DISADVANTAGES
Fixed Switching Frequency	Slower dynamics due to modulator
Bandwidth is known through design	Requires co-ordinate transformation
Easier to extend to different topologies	Robustness is an issue for non-linear system
Well established method	Quite difficult to adopt under constraints (special requirements).

3.5 Results and Discussion

3.5.1 DC voltage control

The grid connected PV system performance is analyzed for dc link voltage control. The dc link voltage is controlled using PI and PI-P controller. The transient response of proposed novel configuration of PI-P controller is compared and analyzed in respect of PI controller transient response for dc link voltage control. The proposed controller have advantage over PI controller in terms of increased degree of freedom

for controller tuning which also widen the tuning range for controller gains. With increased degree of freedom and wider range of gains there may be better possibility to obtain the transient response for dc link voltage near idle one. This can be considered in two cases: first is response while connecting to grid and other one is response when there is perturbation/disturbance in reference dc voltage. The proposed novel controller configuration minimizes the error by using another proportional gain which is added to the output of conventional PI control scheme with negative polarity.

3.5.1.1 Coupling to Grid System

The transient response of dc link voltage control for conventional PI and PI-P (2-DOF PI) controller is been compared as shown in Fig. 3.10a while PV system is coupled to the utility grid. The 2-DOF PI controller response as shown in Fig. 3.10a is showing more smooth response possessing no overshoot. The conventional PI response is dealt with the overshoot during interconnection to the grid. So, 2-DOF PI controller is performing better and showing highly improved transient response which is quite similar to idle one. The PI-P controller response shown in Fig. 3.10a is for the gains K_{p1}= 0.12, K_{int}=1.5, K_{pfb}=0.03.

The response of the dc voltage regulation can also be examined for the settling time of the response. The keen examination of the dc voltage control response shown in Fig. 3.10a is showing slightly better settling time for 2-DOF PI. It also shows quick response after reaching to certain voltage limit governed by voltage rating of grid.

3.5.1.2 Disturbance in Reference dc Voltage

The response of controllers is shown in Fig. 3.10b for the condition of disturbance in reference dc voltage. The reference dc voltage is perturbed from 800 volt to 840 volt at t=0.25 sec. The PI-P controller gains for the response shown in Fig. 3.10b are K_{p1}= 0.18, K_{int}=1, K_{pfb}=0.028. The PI-P controller response is been analyzed for the step disturbance in the system. There is a change in reference voltage level by applying step disturbance at t=0.25. PI-P controller response can be compared to PI controller response for step change in reference of dc link voltage as shown in Fig. 3.10b. Improved fast response is achieved using PI-P controller in comparison to conventional PI controller under disturbance condition also.

The disturbance responses are shown in Fig. 3.10b and can be observed the difference in responses clearly. The PI-P controller showing quite improved fast response with no

overshoot and less settling time. This response is nearly similar to ideal response of the system for dc link voltage control.

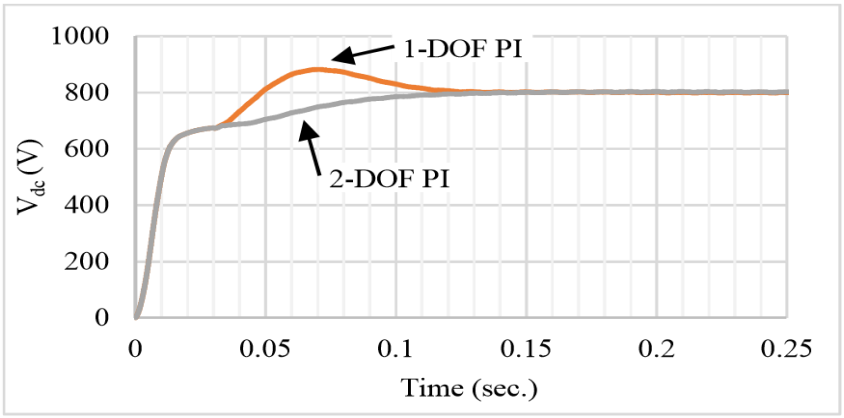

(a)

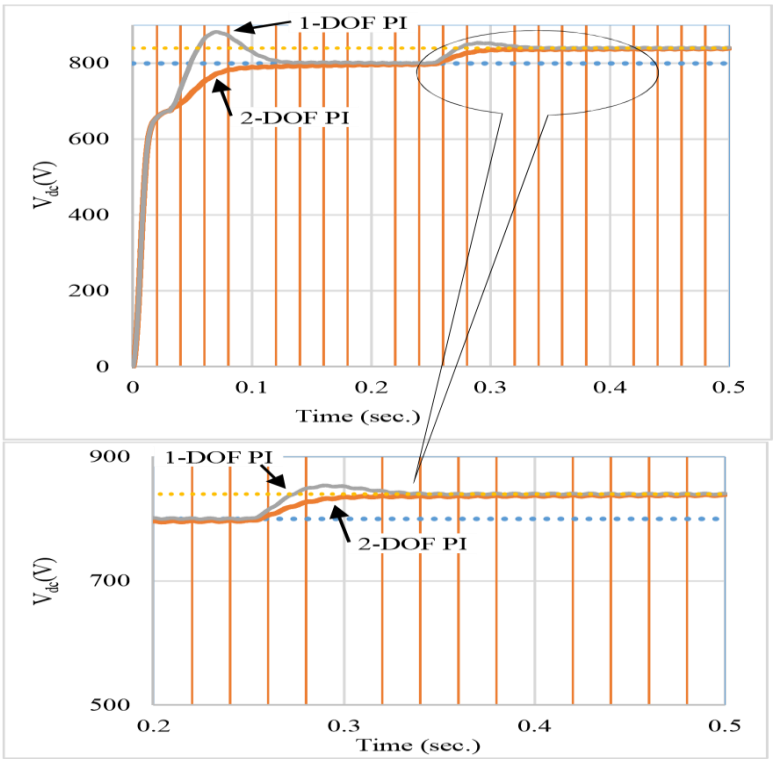

(b)

The response of 2-DOF controller for two different controller gains obtained using trial and error method compared and analyzed as illustrated in Fig. 3.10c. The technique behind the trial and error based tuning of 2-DOF PI controller is to keep the

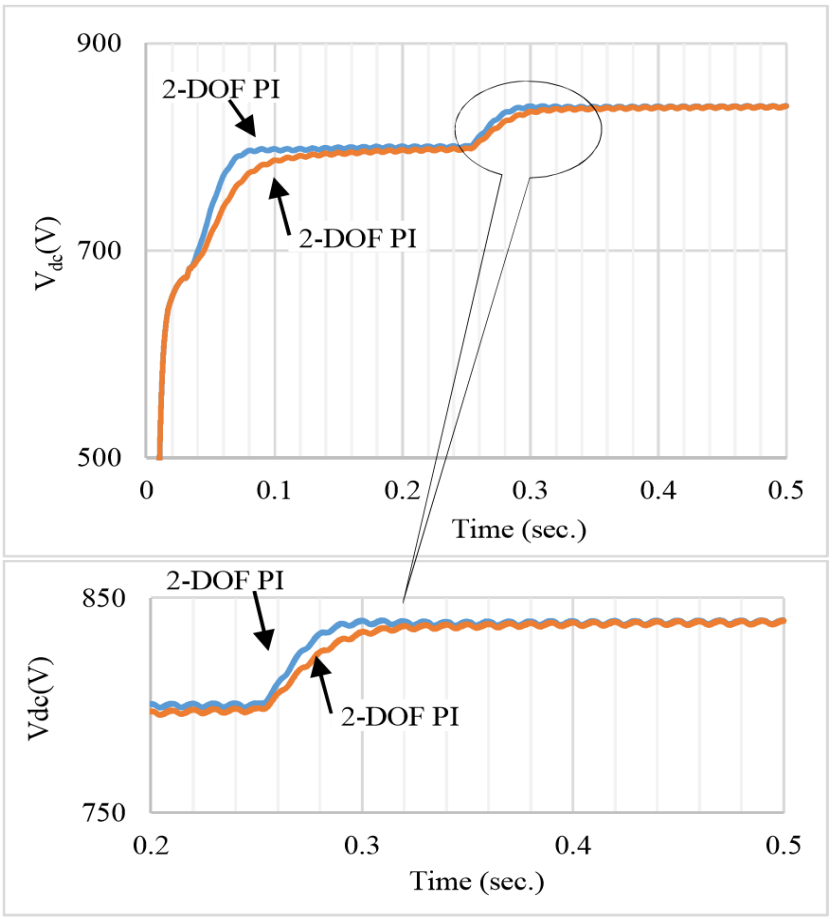

(c)

Fig 3.10 Response of DC voltage controller
(a) DC voltage controller response while PV is connected to grid.
(b) DC voltage control response under disturbance in reference dc voltage and grid integration.
(c) Comparison of DC voltage controller response for two different controller gains.

addition of proportional gains Kp1 and Kp2 closer to the proportional gain K_p of conventional PI controller. As in this case, the addition of K_p and K_{pfb} is 0.208, which is closer to 1-DOF PI gain K_p=0.3 in comparison to addition of earlier proportional gains addition 0.15. The performance of 2-DOF controller validated for voltage regulation in Fig.3.10b. The 2-DOF controller showing better response for new controller gains K_p= 0.18, K_{int}=1, K_{pfb}=0.028 as compared to previous gains K_p= 0.12, K_{int}=1.5, K_{pfb}=0.03 for both the cases of coupling to grid system and disturbance.

3.5.2 Reference current generation using fryze method

The grid connected solar PV system is analyzed for considering linear and non-linear loads using fryze conductance current minimization algorithm in MATLAB-Simulink. The results are demonstrated using following terms: grid current (I_s), grid voltage (V_s), point of common coupling (PCC) voltage (V_{PCC}), load current (I_{load}), inverter current (I_{inv}), dc link voltage (V_{dc}). The results for the linear load system is shown in Fig. 3.11a

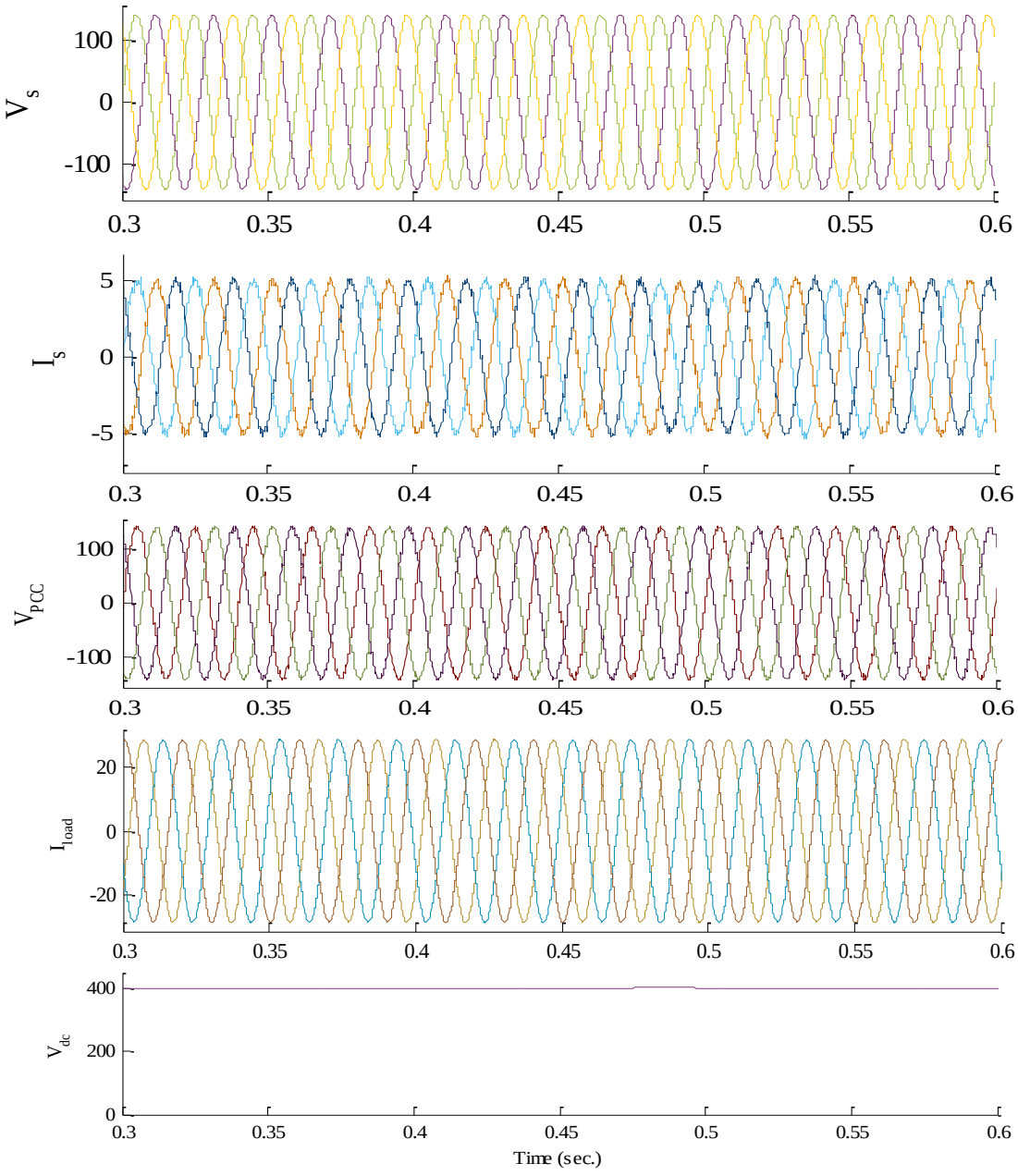

(a)

from t=0.3sec. to t=0.6 sec. The system performance and capability is also demonstrated using the non-linear load connected to grid connected PV system in balanced and unbalanced condition. The results for the non-linear load system is demonstrated in Fig. 3.11b and c from t=0.3 sec. to t= 0.9 sec. At t=0.35 sec. system is operating for non-linear load in balanced condition. It is switched to the unbalanced condition by disconnecting phase 'b' of the load. The dc link voltage (V_{dc}) is maintained to the reference level for the unbalanced condition. The source current (I_s) is maintained in balanced condition Fig. 3.11b as the unbalanced component of current is supplied by the inverter (I_{inv}) current Fig. 3.11c. So, the PV power converted from dc-ac using voltage source inverter (VSI) delivered as compensating power in the grid connected system under unbalanced condition. For non-linear load operation, even in balanced case harmonics are generated by the load. The inverter current supplied the harmonics content of load current and the source current is maintained as like in the linear load condition.

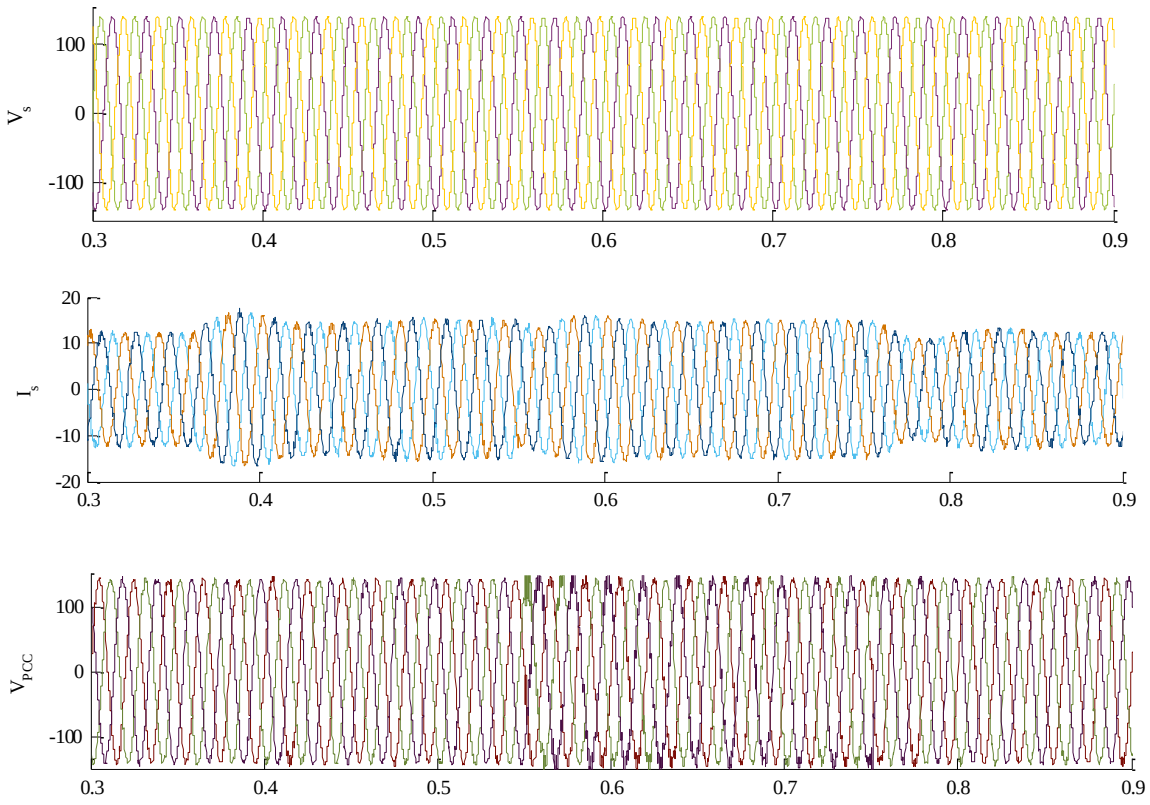

(b)

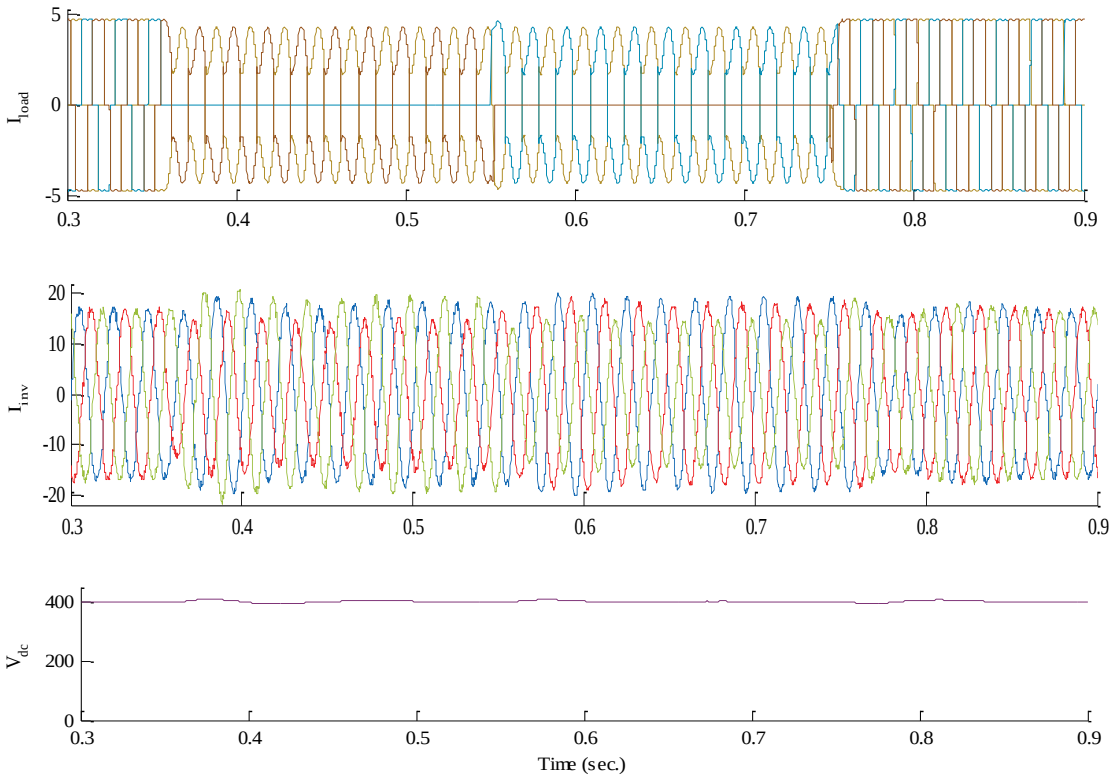

(c)

Fig 3.11 Performance of the grid connected PV system for fryze conductance theory
(a) System performance under linear load condition.
(b) System performance (V_s, I_s, V_{PCC}) under non-linear load and load unbalancing.
(c) System performance (I_{load}, I_{inv}, V_{dc}) under non-linear load condition and load unbalancing.

The unbalancing in the inverter current can be seen after t=0.35 sec. which makes the source current balanced by supplying unbalanced component. At t=0.55 the phase 'c' of the non-linear load is also disconnected for the load unbalancing condition and at t=0.75 the system brought back to the balanced condition. The dc link voltage of the system is maintained to the reference level during unbalanced condition as shown in Fig. 3.11c.

The harmonic spectrum of the source current under linear load condition, load current and source current for non-linear load condition is shown in Fig. 3.12 a, b and c respectively. The source current THD for linear load condition is well within the limits. THD of the load current and source current for non-linear condition is shown in Fig. 3.12b and 3.12c clearly shows that the grid connected PV system is capable of improving power quality of the system by eliminating harmonics as the source current THD is maintained as according to the IEEE-519-1992 standards under non-linear load

also. The fryze current minimization algorithm extracts the reference component of current from the distorted current and the average active power of the loads can be supplied from the grid side with minimum r.m.s. value of current.

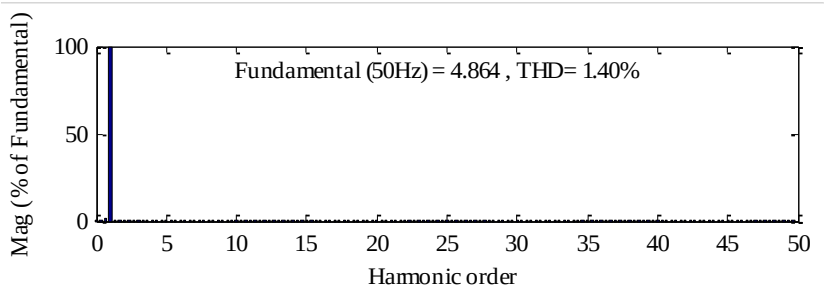

(a)

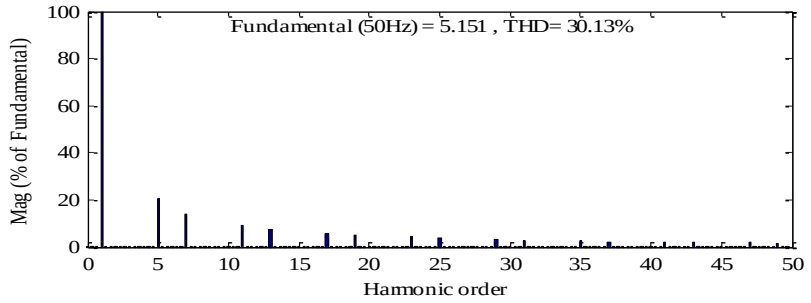

(b)

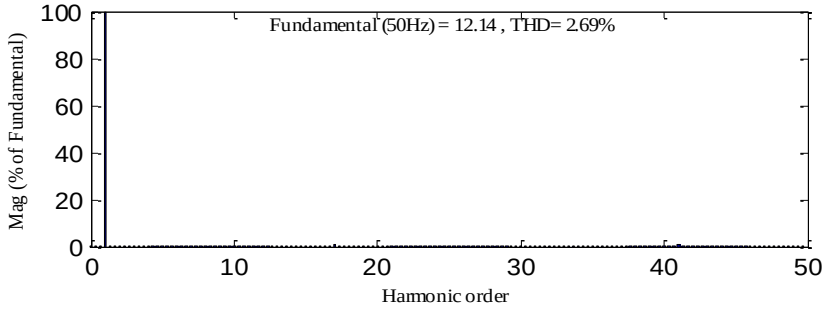

(c)

Fig 3.12 Harmonic spectrum of the system
(a) Harmonic spectrum for I_s under linear load condition.
(b) Harmonic spectrum for I_{load} under non-linear condition
(c) Harmonic spectrum for I_s under non-linear load condition.

AC line voltage: 172V, 50Hz; DC bus voltage: 400V; DC bus Capacitance: 1500μF; Grid impedances i.e. R_s = 0.05 Ω and L_s = 0.5mH; LC filter L = 4.2 mH, C= 8 μF; 3-phase diode rectifier, R load varies from 18-60Ω and L = 100mH; K_p = 0.001, K_{int} = 0.05; HCC is adopted.

3.5.3 Reference current generatio using PBT

The in phase and quadrature phase templates generated in the simulation for the phase ‘a’, ‘b’ and ‘c’ is shown in Fig. 3.13 a,b, and c respectively.

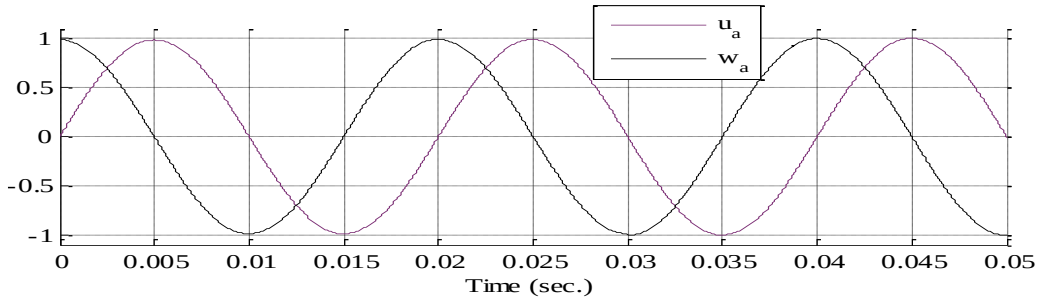

(a)

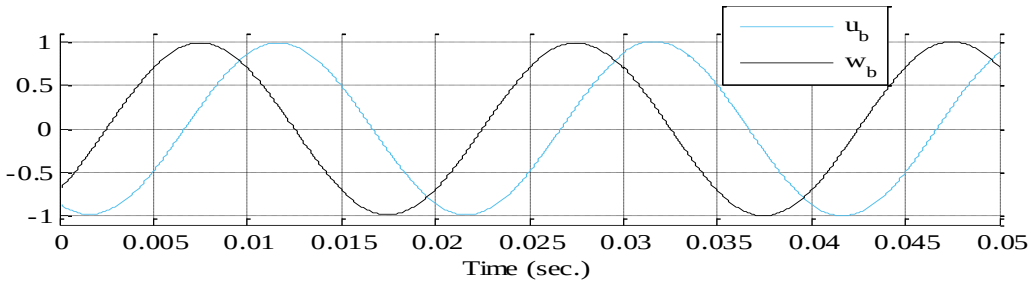

(b)

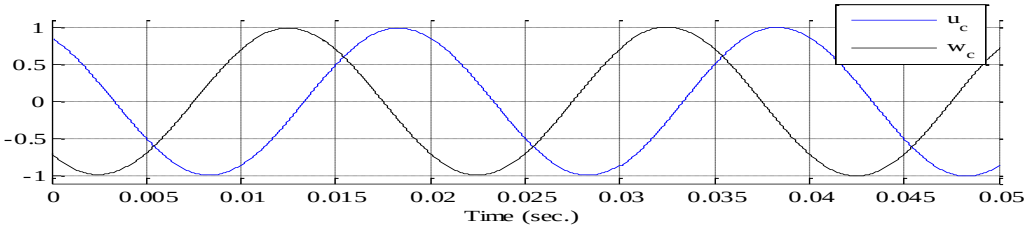

(c)

Fig 3.13 In-phase and quadrature templates
(a) phase ‘a’
(b) phase ‘b’
(c) phase ‘c’

3.6 Conclusion

The design and selection requirement for the integration of PV system to grid discussed and explained. The novel controller configuration proposed in this chapter based upon degree of freedom concept is implemented as 2-DOF PI (PI-P) for dc voltage regulation of grid connected PV and response of controllers were compared under grid coupling of PV system and disturbance in reference dc voltage. The controller performance

observed and investigated based upon the overshoot, settling time and response of grid current in respect to dc voltage regulation. The different algorithms for the generation of reference current implemented.

CHAPTER 4

DATA DRIVEN OPTIMIZED TUNING OF CONTROLLER

4.1 General

The grid connected PV system is to be controlled based upon the different control algorithms mentioned in introduction chapter1 and chapter3. The overall control of the system implemented with the dedicated PI controller for the regulation of dc-link voltage to the reference voltage. The tuning of PI controller requires generating the equivalent quantity for dc link voltage regulation. In fundamental approach, the PI controller gains are tuned using trial and error method or using optimization criteria (modulus and symmetrical optimum) to obtain the appropriate response desired for the dc link voltage control. The methods are having limitation (due to assumed approximations) and it may not search the best possible controller gain that can provide the best response for dc voltage control. Fictitious reference iterative tuning (FRIT) is a data driven method used to find optimized gains of the PI controller. The FRIT method implemented based upon the data obtained using trial and error method based PI controller gains [56].

The performance of the controller is dependent upon their gains so the parameter tuning is one of the significant consideration for better performance. Conventionally, controller design method required dynamic model and system/plant information with system stability using bode plot or other methods. FRIT is data-driven parameter tuning method so it only requires one shot input and output data. Using this input and output data it can optimize the controller gain parameter without any mathematical model of system. The input and output data is required to generate reference signal and closed loop response obtained using the optimized controller parameter should follow a presumed reference model output. Therefore, initial data and reference model assumption is primarily essential part of this method.

The DOF based control with optimal tuning methods of controller gains widely applied and implemented specially in motor control application and process industry. Sometimes, numerical examples considered to show the effectiveness of DOF controllers and tuning method. This is the first time that the optimal tuning method and DOF based controller introduced for grid connected PV system in Fig. 4.1a application to regulate the dc link voltage through optimal tuning in Fig. 4.1b of conventional PI controller and proposed 2-DOF structure.

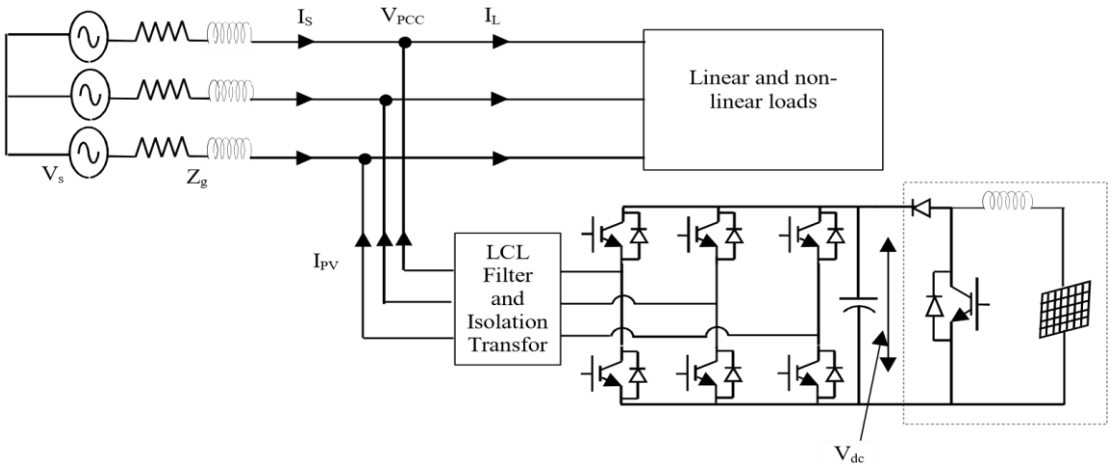

(a)

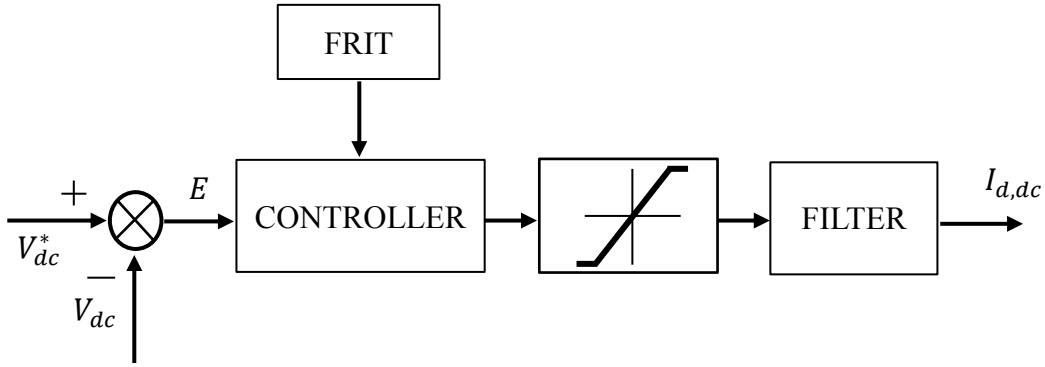

(b)

Fig. 4.1 Grid integrated solar photovoltaic system
a) system circuit diagram considered for the study and control analysis.
b) block diagram of voltage control loop implemented for the regulation of dc voltage.

4.2 Fictitious Reference Iterative Tuning (FRIT)

The performance of the controller is dependent upon gains so the parameter tuning is one of the significant consideration for better performance. FRIT is data-driven parameter tuning method so it only requires one shot input and output data. Using this input and output data it is possible to optimize the controller parameter without any mathematical model of the system.

4.2.1 Reference signal generation

The reference signal is generated by using the input and output data for initial parameter $k_0$of controller. The k_0 was obtained using trial and error method and represented as $[k_{p0} \quad k_{int0}]^T$. The one shot data as: intermediate output u_0 as input data and controlled output y_0 as output data.

$$u_0 = \begin{bmatrix} k_{p0} \\ k_{int0}/_s \end{bmatrix} [(r - y_0)] = \begin{bmatrix} k_{p0} & k_{int0}/_s \end{bmatrix}^T [(r - y_0)] \quad (1.)$$

The reference signal generated using the input and output data by using k_0 of the controller. The one shot data obtained in the form as: intermediated output u_0 as input data and controlled output y_0 as output data using k_0 as controller gains. The reference signal generation for 1-DOF controller and 2-DOF controller computed as:

4.2.1.1 Conventional PI (1-DOF) controller

The fictitious reference signal can be generated based upon the system configuration shown in Fig. 4.2a. The mathematical evaluation of reference signal for conventional PI controller is as follows

$$\tilde{r}(k) = P(s, k_0)^{-1} u_0 + y_0 \quad (2.)$$

$$\Rightarrow \tilde{r}(k) = e_0 + y_0 \quad (3.)$$

e_0 is the error in between r and y_0 for the initial response and data obtained using k_0. So, the performing one-shot experiment using $P(s, k_0)$ in Fig. 4.2a is used to obtain initial input-output data set (u_0, y_0). The reference signal computed using initial data set (u_0, y_0) in (3).

4.2.1.2 2-DOF controller (PI-P)

The fictitious reference signal computation modified as the additional feedback compensator Fig. 4.2b is included. The reference signal for 2-DOF FB PI controller configuration computed by using transfer function from r →y

$$(\tilde{r}(k, k_{fb}) - y_0) P(s, k) - y_0 H(s, k_{fb}) = u_0 \quad (4.)$$

$$\Rightarrow \tilde{r}(k, k_{fb}) - y_0 = \left(u_0 + y_0 H(s, k_{fb}) P(s, k)^{-1}\right) \quad (5.)$$

$$\Rightarrow \tilde{r}(k, k_{fb}) = \left(u_0 + y_0 H(s, k_{fb})\right) P(s, k)^{-1} + y_0 \quad (6.)$$

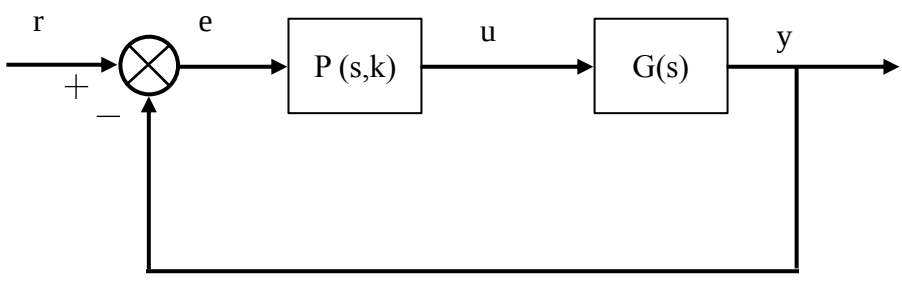

(a)

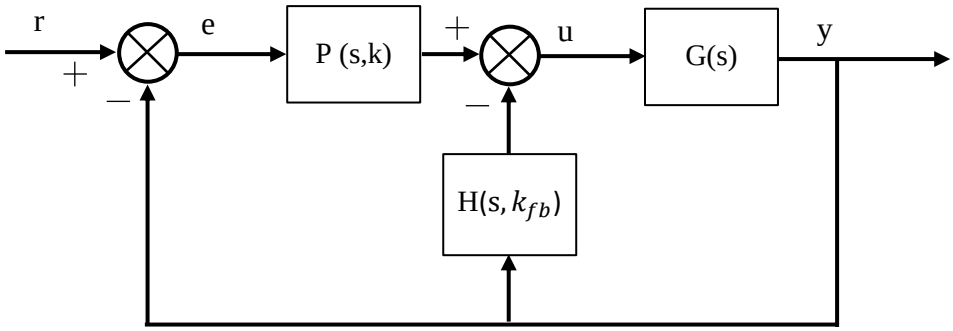

(b)

Fig. 4.2 Outer voltage control loop
a) Consists of conventional PI controller transfer function block and plant transfer function.
b) Consists of 2-DOF feedback (FB) type controller transfer function block and plant transfer function.

Where,

$$\mathrm{k} = [k_p \quad k_{int}]^T \tag{7.}$$

$$\mathrm{P}\,(\mathrm{s},\mathrm{k}) = \; k_p + \frac{k_{int}}{s} \tag{8.}$$

$$\mathrm{H}\left(\mathrm{s}, k_{fb}\right) = \; C_{fb}(s,k) = k_{pfb} \tag{9.}$$

k_{fb} : Feedback controller gain, k_{pfb} : proportional gain of feedback controller and initial controller gain for FB is k_{fb0}. The reference generated by performing one-time experiment using $P(s,k_0)$ and $\mathrm{H}\left(\mathrm{s}, k_{fb0}\right)$ with the initial parameter k_{p0}, k_{int0} and k_{pfb0} illustrated in Fig. 4.3.

4.2.2 Optimization function and reference model

The generation of fictitious reference signal used to make the optimization function in terms of performance index function. The controller parameters/gains k-kfb tuned and optimized to minimize the performance index function. The performance index optimization function is represented as mathematical equation and defined based upon the reference model response. As the FRIT method does not require any mathematical or dynamical model of the system so a reference model have to be assumed as transfer function with or without dead time consideration. The generalized transfer function for reference model setting shown as

$$\mathrm{M(s)} = \frac{1}{(Ts+1)^n} e^{-\tau s} \tag{10.}$$

The system configuration with reference model M(s) shown Fig. 4.3. The controlled output y_0 generated using initial parameters compared with the output generated using fictitious reference signal and reference model to obtain the optimized controller parameters so that closed loop response of the system should follow the presumed reference model output. The optimization function based on the initial data set defined as

$$\tilde{e}(\mathrm{k}, k_{fb}) = y_0 - M(s)\tilde{r} \tag{11.}$$

$$I(\mathrm{k}, k_{fb}) = \sum(\tilde{e})^2 \tag{12.}$$

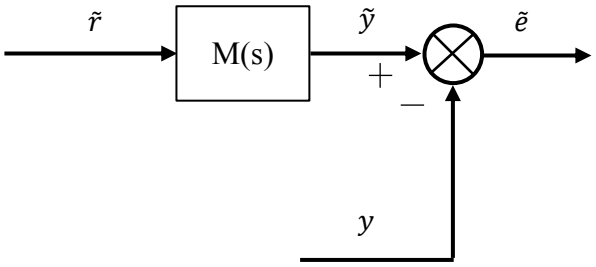

Fig. 4.3 Reference model based configuration for performance index function.

In FRIT method, fictitious reference signal generated by (2) and (5) utilized to generate objective function for optimization and the performance index function defined considering the system configuration. The performance index considering fictitious reference signal defined as the following

$$\tilde{e}(\mathrm{k}) = y_0 - \tilde{y} \tag{13.}$$

$$\Rightarrow \tilde{e}(\mathrm{k}, k_{fb}) = y_0 - M(s)\,\tilde{r}(k, k_{fb}) \tag{14.}$$

$$\tilde{I}(\mathrm{k}, k_{fb}) = \sum\left(\tilde{e}(\mathrm{k}, k_{fb}, \mathrm{s})\right)^2 \tag{15.}$$

$$\Rightarrow \tilde{I}(\mathrm{k}, k_{fb}) = \sum\left(y_0 - M(s)\,\tilde{r}(k, k_{fb})\right) \tag{16.}$$

Therefore, the objective function for optimization of gain parameters is to minimize the performance index error function (16) and represented in terms of controller gains as

$$(k, k_{fb})_{opt.} = \arg\min \tilde{I}(\mathrm{k}, k_{fb}) \tag{17.}$$

4.2.3 PSO based FRIT

The optimization algorithm is essential to implement FRIT method to avoid local minimum solution. The PSO based FRIT (PSO-FRIT) proposed for the computation of optimized controller parameters of 2-DOF PI used for dc voltage control. Therefore, an objective function is required as an optimization problem to achieve optimized controller gains. The optimization method based upon the behaviour of particle to imitate the potential solution of neighbouring particle and related to the neighbourhood best/local best, and its own achieved solution related to the person best solution.

4.2.3.1 Generalized PSO

PSO method search the possible potential solutions as a swarm of particles that move in virtual space. It is a stochastic approach and swarm population based search method considering the behaviour of bird flocks. The position and velocity vector is associated with each particle and updated at each iteration. Therefore, the position of a particle is dependent upon the personal best (p_{best}) and neighborhood best which leads to the global best (g_{best}). Therefore, the particle velocity modified as follows

$$\rho_i^{\alpha+1} = \varphi\rho_i^{\alpha} + c_1 w_1 (p_{besti} - x_i^{\alpha}) + c_2 w_2 \left(g_{best} - x_i^{\alpha}\right) \quad (18.)$$

The velocity of particle updated considering following three terms

1) Acceleration coefficient/cognitive component (c1), which is related to the personal best solution (p_{best}) of each particle.

2) Acceleration coefficient/social component (c2), which relates with the best position of particle in whole solution and termed as global best solution (g_{best}).

3) An inertia weight (φ), which controls the velocity of particle.

The value of w_1 and w_2 should be decided in between 0 and 1. The position of each particle modified based upon the changes in velocity of each particle. The position update shown as

$$x_i^{\alpha+1} = x_i^{\alpha} + \rho_i^{\alpha+1} \quad (19.)$$

4.2.3.2 PSO-FRIT

The general PSO method can be modified for the FRIT method implementation. The position of particle is defining as the controller gain parameter and update of the velocity will represent the perturbation in controller gains. So, the position update of each particle in eq. modified for controller parameter as follows

$$k_i^{\alpha+1} = k_i^{\alpha} + \rho_i^{\alpha+1} \quad (20.)$$

The controller gain parameter update in (20) is adjusted for 2-DOF PI controller gains (k_{p0}, k_{int0} k_{pfb0}) as

$$k_{p,i}^{\alpha+1} = k_{p,i}^{\alpha} + \rho_{p,i}^{\alpha+1} \quad (21.)$$

$$k_{int,i}^{\alpha+1} = k_{int,i}^{\alpha} + \rho_{int,i}^{\alpha+1} \quad (22.)$$

$$k_{pfb,i}^{\alpha+1} = k_{pfb,i}^{\alpha} + \rho_{pfb,i}^{\alpha+1} \quad (23.)$$

The PSO application for FRIT method iillustrated in the following steps:

Step 1: The number of particles (N) based solution vector of controller parameter is defined as follow

$$\mathrm{k} = [k_1\ k_2\ k_3 \ldots\ldots k_j] \quad (24.)$$

$$\mathrm{j} = 1, 2, 3, \ldots\ldots, \mathrm{N} \quad (25.)$$

The solution vector of controller parameter in (24) is applicable to the all the three gains (k_{p0}, k_{int0} k_{pfb0}) of 2-DOF PI controller. The position of each particle with random controller gains is initialized considering range constraint for gains based upon the earlier experience of trial and error method.

$$k_i(0) = [k_{p,i}(0), k_{int,i}(0)] \quad \text{for 1-DOF PI controller} \quad (26.)$$

$$k_i(0) = [k_{p,i}(0), k_{int,i}(0), k_{pfb,i}(0)] \quad \text{for 2-DOF PI controller} \quad (27.)$$

$$k_{imax} > k_i > k_{imin} \quad (28.)$$

The velocity of the particle initialized and range constraint applied too for proper convergence.

$$\rho_i(0) = [\rho_{p,i}(0), \rho_{int,i}(0), \rho_{pfb,i}(0)] \quad (29.)$$

$$\rho_{imax} > \rho_i > \rho_{imin} \quad (30.)$$

The p_{best} and g_{best} of the particle i and swarm population initialized.

Step 2: The one-time data (input u_0 , output y_0) is collected using initial parameters k_0 obtained by trial and error method. The fictitious reference signal generated and updated for each particle. Therefore, the performance index relates to the reference signal and error signal for each particle. The updated equation for reference, error and performance are

$$\tilde{r}(k_i) = P(s, k_i)^{-1} u_0 + y_0 \quad (31.)$$

$$\tilde{e}(k_i) = y_0(n) - M(s)\tilde{r}(k_i) \quad \text{for 1-DOF PI controller} \quad (32.)$$

$$I(k_i,) = \sum \left(e(k_i)\right)^2 \quad (33.)$$

$$\tilde{r}\left(k_i, k_{fbi}\right) = \left(u_0 + y_0 H\left(s, k_{fbi}\right) P(s, k_i)^{-1}\right) + y_0 \quad (34.)$$

$$\tilde{e}\left(k_i, k_{fbi}\right) = y_0 - M(s)\tilde{r}\left(k_i, k_{fbi}\right) \quad \text{for 2-DOF PI controller} \quad (35.)$$

$$I\left(k_i, k_{fbi}\right) = \sum \left(e\left(k_i, k_{fbi}\right)\right)^2 \quad (36.)$$

Reference, error and performance index equation for 1-DOF PI and 2-DOF PI controller shown from eq. to eq. and from eq. to eq. respectively. So, the objective function of PSO-FRIT method for 2-DOF PI in (36) represented as

$$(k_i, k_{fbi})_{opt.} = \arg\min \tilde{I}\left(k_i, k_{fbi}\right) \quad (37.)$$

Objective function of (37) evaluated based upon p_{best} of each particle and personal best position is updated for iteration.

if

$$p_{best\,i} < l_{best\,i} \quad (38.)$$

then

$$l_{best\,i} = p_{best\,i} \quad (39.)$$

and

$$k_{local\,best} = k_i \quad (40.)$$

Step 3: The global best position updated based upon the personal best of each particle.

if

$$p_{best\,i} < g_{best\,i} \quad (41.)$$

then

$$g_{best\,i} = p_{best\,i} \quad (42.)$$

and

$$k_{global\,best} = k_i \quad (43.)$$

Step 4: The velocity and position of particle has been updated as

$$\rho_\alpha^{\alpha+1} = \varphi\rho_i^\alpha + c_1 w_1 (p_{besti} - k_i^\alpha) + c_2 w_2 (g_{besti} - k_i^\alpha) \quad (44.)$$

$$k_i^{\alpha+1} = k_i^{\alpha} + \rho_i^{\alpha+1} \quad (45.)$$

The iteration repeated until the good fitness value not achieved considering the constraint of number of iterations as

$$\alpha = \alpha_{max} \quad (46.)$$

4.3 Results and Discussion

The grid connected PV system designed and modelled in the MATLAB-Simulink environment and the input(u_k) and output (y_k) data collected for the FRIT method. Input data (u_k , y_k) obtained using the proportional and integral gains obtained using trial and error method. PSO-FRIT program developed in MATLAB-mfile and data is called for the program from excel/note file. The response of traditional PI controller (optimized and non-optimized) have been investigated and compared with 2-DOF PI controller (optimized and non-optimized). The transient response of the system during interconnection of solar system to grid and for the disturbance in dc voltage reference have been illustrated, analyzed and discussed considering simulation results for 1-DOF and 2-DOF PI control. The simulation results of the system collected for dc voltage response and exported in the form of data. Further, the results plotted using MS-excel. The results analyzed and discussed considering following cases:

4.3.1 Conventional PI controller (1-DOF structure)

4.3.1.1 Optimized and non-optimized response during grid integration

The controller gains obtained using trial and error method initially. The response for the trial and error gains improved using an optimized tuning method and it may improve the system response. The transient response of the dc voltage control Fig. 4.4a compared for the optimized controller gains obtained using FRIT-PSO and trial and error method gains. In the Fig. 4.4a, at t=0.7 the optimized response settled as for non-optimized response settled at t=0.11 sec. and the peak overshoot is also reduced from V_{dc} (overshoot) = 882.79 to 865.94. The optimized and non-optimized controller gains for traditional PI controller shown in Table 4.1. FRIT-PSO method applied considering the assumed reference model for the plant/system. The controller gains are optimized using FRIT-PSO method for two different cases of reference model settings. In Fig., 4.4a controller gains optimized using FRIT for reference model considered as second order system. FRIT based optimized gains are showing better transient response in

terms of settling time, rise time and peak overshoot. The FRIT method have tried to use with reference model of higher order. Controller gains optimized using FRIT for reference model considered as third order system Fig. 4.4b. The optimized proportional and integral gains were different but the transient response for both the cases is quite similar and showing better transient response in comparison to gains achieved by trial and error method.

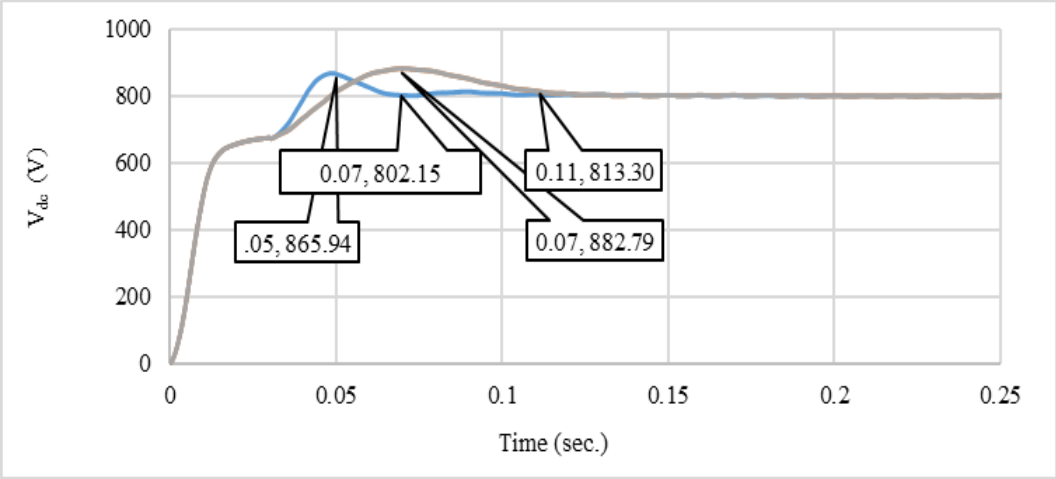

(a)

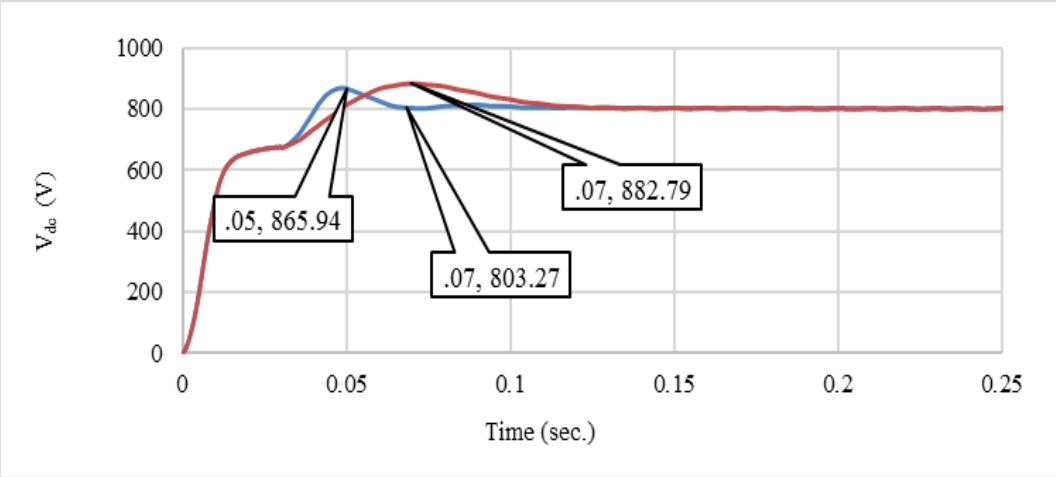

(b)

Fig. 4.4 DC voltage response of conventional PI controller
a) optimized response obtained for second order reference model.
b) optimized response obtained for third order reference model.

4.3.1.2 Optimized and non-optimized response for linear load

The grid interfaced PV system with linear load is considered to compare the performance of controller response. The response of dc link voltage control is illustrated in Fig. 4.5a for the trial and error gain (initial gain) and optimized gain

obtained using FRIT-PSO. At t=0sec. the PV system is interfaced to the grid therefore the dc link voltage of the VSI has to be regulated to reference dc voltage. The dc voltage controller is showing fast response with reduced overshoot for optimized gains in comparison to the response for initial gains. The source current response is dependent

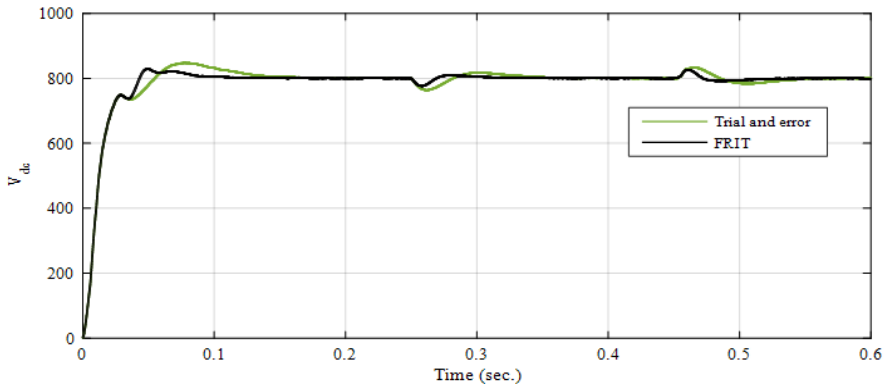

(a)

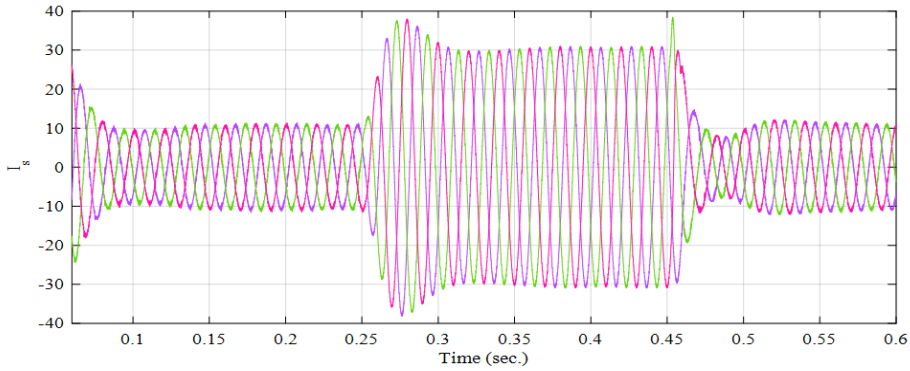

(b)

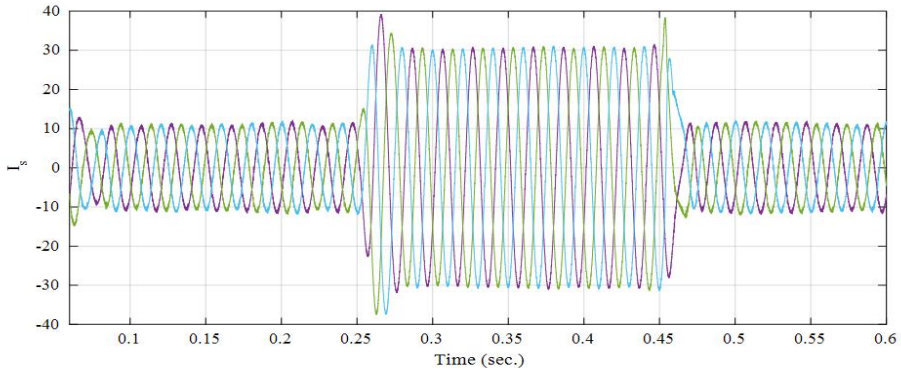

(c)

Fig. 4.5 Optimized and non-optimized response under change in linear load.
a) DC voltage response under linear load condition.
b) source/grid current under linear load condition for initial controller gains.
c) source/grid current under linear load condition for optimized controller gains.

upon the dc link voltage control for grid interfaced PV source. So, the source current is illustrated in Fig. 4.5b and c for initial controller gain and optimized gain respectively. As the optimized gain response is fast and possessing less overshoot for dc voltage control, correspondingly the source current under optimized dc voltage control reached to steady state earlier as compared to the response under initial gain. In accordance with the fast dc voltage controller response the source current also settled down swiftly. At t=0.25sec. the linear load has been increased by 100% and at t=0.45sec. it is switched to the initial load condition. The response of dc voltage control for optimized gains is possessing low overshoot and fast dynamics under disturbance caused due to load changes.

4.3.1.3 Optimized and non-optimized response for non-linear load

Generally, the real time system is having variety of loads categorized as linear and non-linear load. In this case, the grid interfaced PV system with non-linear load considered to compare the performance of controller response. The response of dc link voltage control illustrated in Fig. 4.6a for the trial and error gain (initial gain) and optimized gain obtained using FRIT-PSO. The dc voltage controller response is different under non-linear load as compared to the earlier case of linear load only. At t=0sec. the PV system is interfaced to the grid, the dc voltage controller is showing fast response with reduced overshoot for optimized gains in comparison to the response for initial gains.

The source current response is dependent upon the dc link voltage control for grid interfaced PV source. So, the source current is illustrated in Fig. 4.6b and c for initial controller gain and optimized gain respectively. As the optimized gain response is fast and possessing less overshoot for dc voltage control, correspondingly the source current under optimized dc voltage control reached to steady state earlier as compared to the response under initial gain. In accordance with the fast dc voltage controller response the source current also settled down swiftly. At t=0.25sec. non-linear load has been changed and can be observed by increase in the source current. At t=0.45sec. it is switched to the initial load condition and it can be observed as the source current decreased. The response of dc voltage control for optimized gains is possessing low overshoot-undershoot and fast dynamics under disturbance caused due to load changes. Therefore, the source current response also representing fast dynamics and settle down to steady state quickly.

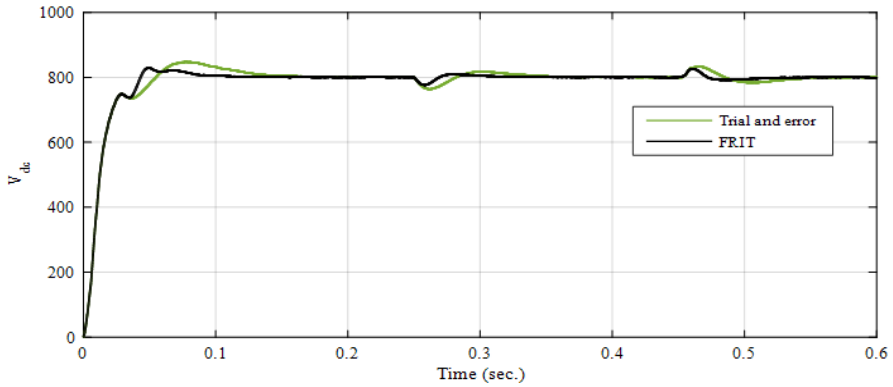

(a)

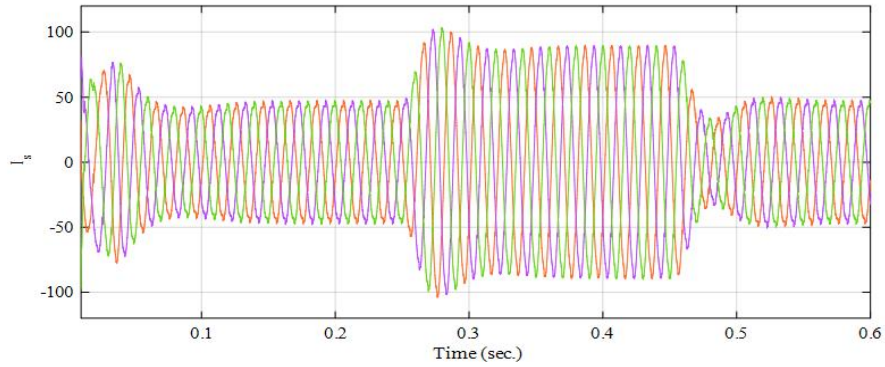

(b)

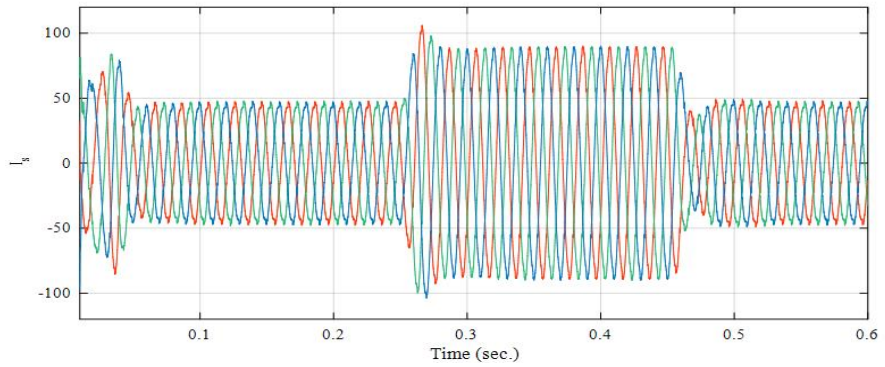

(c)

Fig. 4.6 Optimized and non-optimized response under change in non-linear load.
a) DC voltage response under non-linear load condition.
b) source/grid current under non-linear load condition for initial controller gains.
c) source/grid current under non-linear load condition for optimized controller gains.

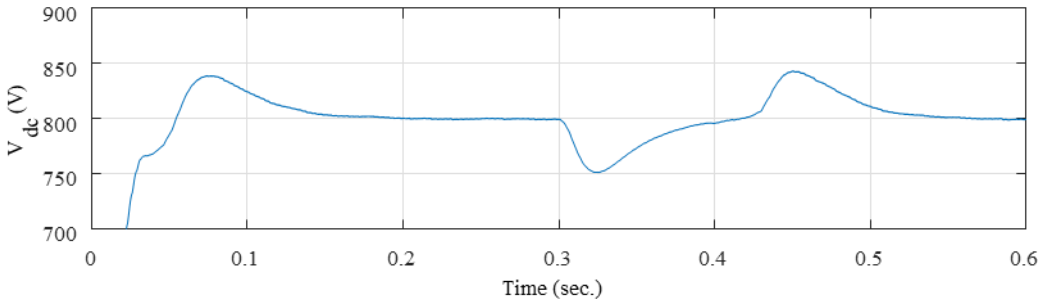

(a)

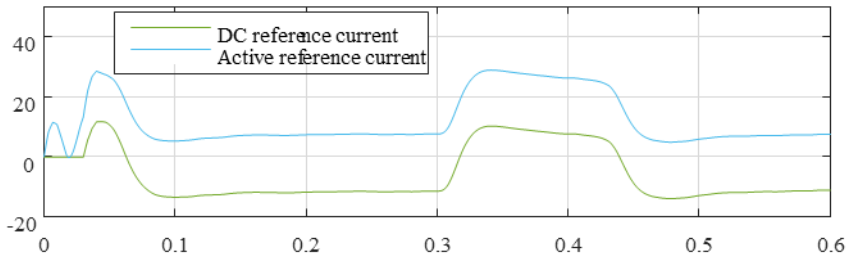

(b)

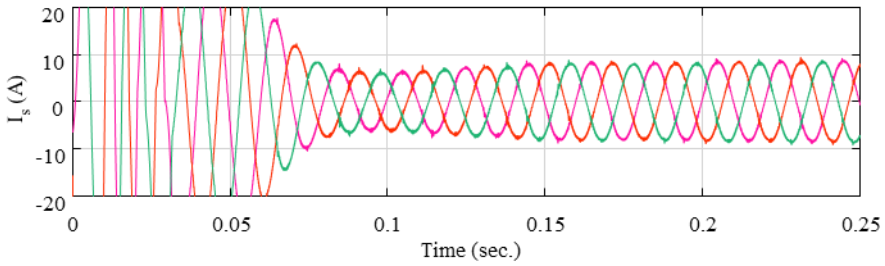

(c)

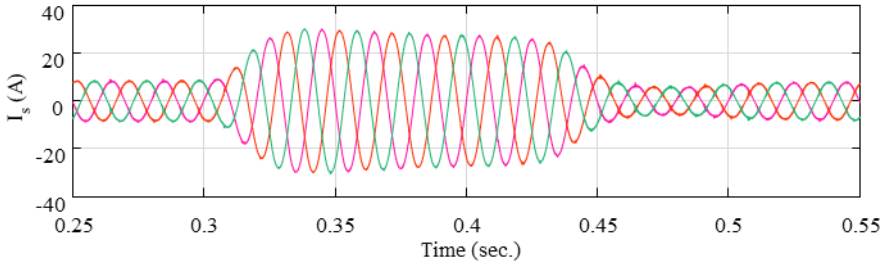

(d)

Fig. 4.7 Non-optimized response under varying ir-radiance.
a) DC voltage response for initial controller gains.
b) Reference current for initial controller gains.
c) source/grid current transient for initial controller gains while PV interfaced to grid.
d) source/grid current transient for initial controller gains.

4.3.1.4 Optimized and non-optimized response for varying ir-radiance

The PV power source has to go through the varying irradiance condition for a real time implemented system due to abrupt change in weather condition. So, it is necessary to check the robustness of the controller response for optimized gains. Also, the input and output data extracted and acquired using initial controller gains has been considered

with load change disturbance or some other disturbance condition only. Therefore, the system is tested and illustrated under changed ir-radiance condition. In this case, the controller response of grid interfaced PV system performance for initial gains illustrated in Fig. 4.7a. The dc reference current and reference current equivalent to overall active power compensation (active reference current) of the system for initial gain of the controller is illustrated in Fig. 4.7b. At t=0sec. the PV system is interfaced to the grid and the source current is illustrated in Fig. 4.7c during grid interfacing for initial gains. At t=0.3sec. ir-radiance is change from 1000W/m^2 to 0W/m^2 and at t=0.45sec switched to initial condition. The source current under the changed ir-radiance condition illustrated in Fig. 4.7d.

The dc voltage response illustrated for optimized controller gains in Fig. 4.8a subsequently dc reference current and reference current equivalent to overall active power compensation (active reference current) of the system for optimized gain of the controller illustrated in Fig 4.8b. The source current during grid interfacing of PV source and disturbance due to change in ir-radiance shown in Fig. 4.8c and 4.8d respectively. The optimized gain response is showing fast dynamic response and possessing less overshoot for dc voltage control under varying ir-radiance condition also. So, the source current reached to steady state and showing better dynamic and transient response for optimized dc voltage control as compared to the response under initial gain. The response of dc voltage control for optimized gains is possessing less overshoot and fast dynamics under disturbance caused due to change in ir-radiance and regulate the dc voltage to reference level swiftly. Consequently, the source current response also representing fast dynamics and settle down to steady state quickly. So, the better dynamic response of the controller under disturbance and transient will leads to better response for reference current generation.

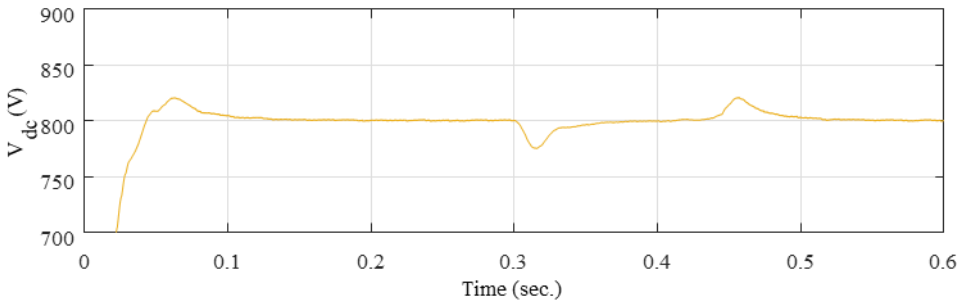

(a)

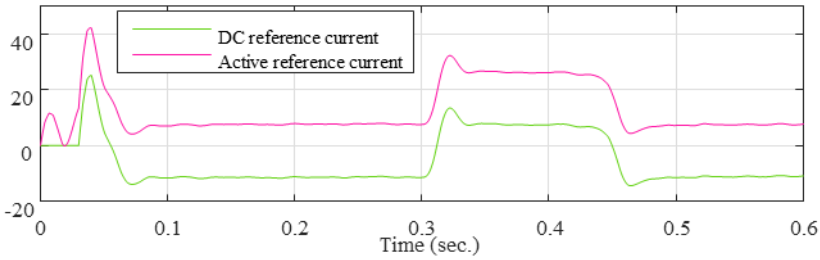

(b)

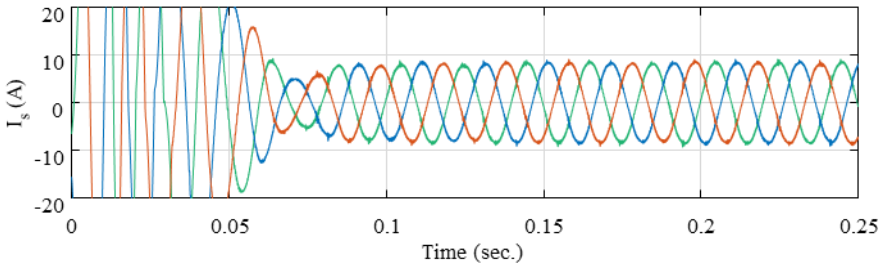

(c)

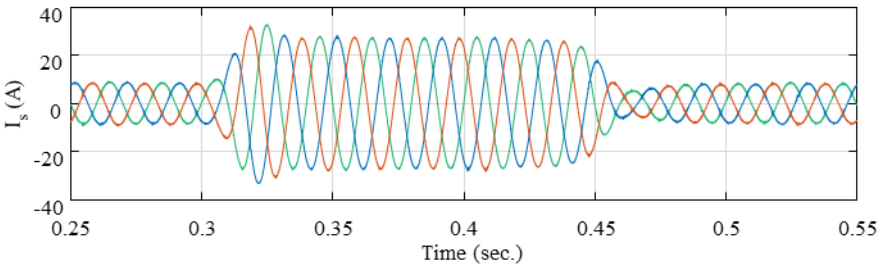

(d)

Fig. 4.8 Optimized response under varying ir-radiance.
a) DC voltage response
b) Reference current
c) source/grid current transient while PV interfaced to grid.
d) source/grid current transient under varying ir-radiance.

4.3.2 2-DOF controller (PI-P)

4.3.2.1 Optimized and non-optimized response during grid integration

For the case of 2-DOF control also the gains were obtained using trial and error method and then optimized gains have been computed using PSO-FRIT method. The optimized and non-optimized controller gains response illustrated in Fig. 4.9a. The non-optimized PI-P controller response improved in terms of overshoot but the response was still slow as for non-optimized traditional PI control. The optimized PI-P controller response shows highly improved transient response with no overshoot and fast response and settling time. The optimized response of PI-P controller settled at t=0.6 sec. and non-optimized response settled at t=0.1 sec. The controller gains for optimized and non-optimized conventional PI controller given in Table 4.1.

4.3.2.2 Comparison with conventional PI

The response of the non-optimized traditional PI and 2-DOF controller illustrated in Fig. 4.9b. The traditional PI controller showing overshoot in the response and the response is slow. The objective to design and implement 2- DOF PI controller is to minimize/reduce the overshoot in the response maintaining similar or better response time. The response illustrated in the Fig. 4.9b showing significantly improved transient response in terms minimized overshoot and maintaining good response as for the traditional PI controller. The additional proportional controller in 2-DOF control designed as feedback compensator. This feedback proportional controller helps to minimize the error of the dc voltage response and minimize the overshoot in the system response of dc voltage control. The responses of optimized traditional PI and PI-P control for dc voltage control analyzed and shown in Fig. 4.9c. The fast response obtained using optimized gains for both the controllers (PI and PI-P). However, the response of optimized 1-DOF PI is having overshoot and settled at t=0.7 sec. The optimized 2-DOF controller response is not having any overshoot and the response is even little fast as settled at t=0.6 sec.

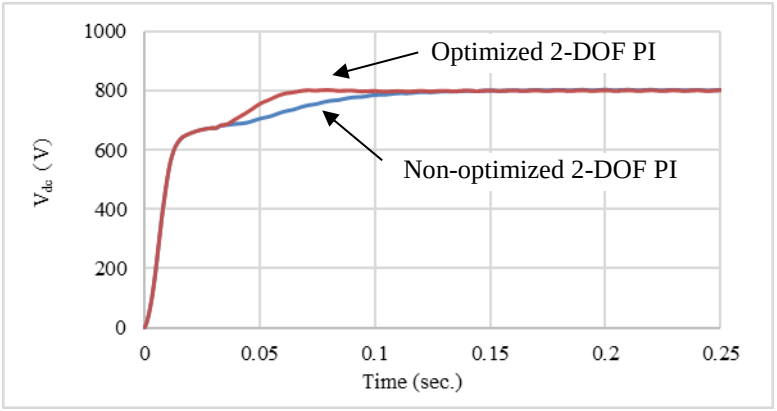

(a)

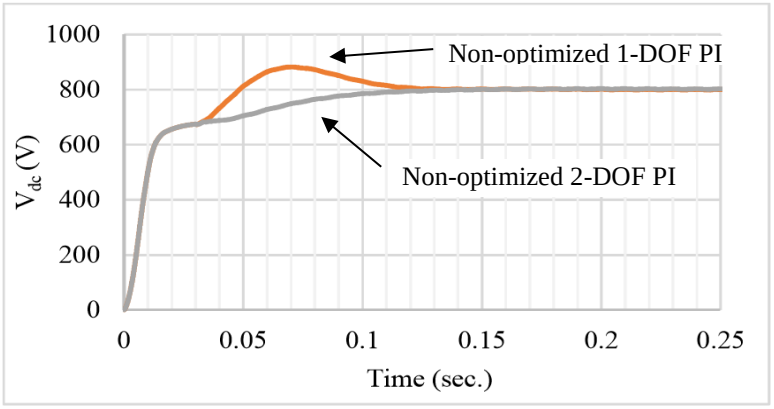

(b)

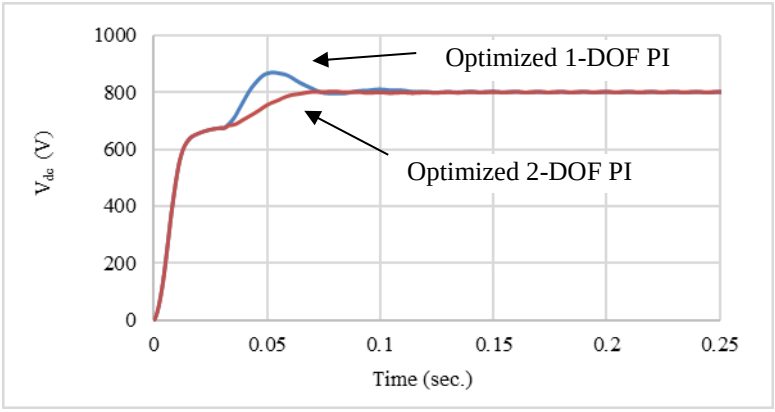

(c)

Fig. 4.9 Optimized and non-optimized response under change in linear load.
a) DC voltage response under linear load condition.
b) source/grid current under linear load condition for initial controller gains.
c) source/grid current under linear load condition for optimized controller gains.

4.3.3 Disturbance in reference dc voltage

The transient response of the controllers is analyzed under the disturbance in reference dc voltage. The reference dc voltage is changed from 800V to 840V through unit step signal. The response of non-optimized 1-DOF PI and 2-DOF PI-P is illustrated under the condition of disturbance in reference dc voltage as shown in Fig. 4.10. The response of 2-DOF controller is better in comparison to 1-DOF controller under disturbance too. The 2-DOF controller transient response is having no overshoot under disturbance occurred at t=0.25 sec and it is more likely similar to ideal response. The response of optimized 2-DOF controller illustrated under the condition of disturbance in reference dc voltage as shown in Fig. 4.10. The response of optimized 2-DOF controller is better in comparison to non-optimized controller under disturbance too. The optimized 2-DOF PI-P transient response is having no overshoot under disturbance occurred at t=0.25 sec as well as showing fast response in comparison to non-optimized 2-DOF and 1-DOF controller. The controller gains for optimized and non-optimized 2-DOF controller configuration given in Table 4.2.

4.3.4 Source current

In respect of showing transient response for regulation of dc voltage, the source current performance analyzed during transient. The source current in Fig. 4.11a and b for the 1-DOF PI and PI-P controller (non-optimized) respectively during interconnection of PV system to grid. The source current reaches to steady state at t=0.115 for the conventional 1-DOF PI control and at t= 0.08 for non-optimized PI-P control. So, the source current transient response is also improved as the dc voltage regulation response

is improved and reaches to steady state smoothly without overshoot under PI-P control. The source current for optimized 2-DOF control illustrated in Fig. 4.11c and it is showing very smooth and fast response in comparison to non-optimized 1-DOF and 2-DOF PI. The parameters of the considered grid connected PV system summarized in Table 4.3.

Table 4.1 Conventional 1-DOF PI controller gains.

1-DOF PI Trial and error	K_{p1} = 0.3, K_{int} = 8
1-DOF PI Optimized	K_{p1} = 0.78, K_{int} = 28.2 (second order reference model)
1-DOF PI Optimized	K_{p1} = 1.02, K_{int} = 25.65 (third order reference model)

Table 4.2 2-DOF controller gains.

2-DOF PI Trial and error	K_{p1} = 0.24, K_{int} = 12.5, K_{pfb} = 0.04
2-DOF PI Optimized	K_{p1} = 0.49, K_{int} = 28, K_{pfb} = 0.09

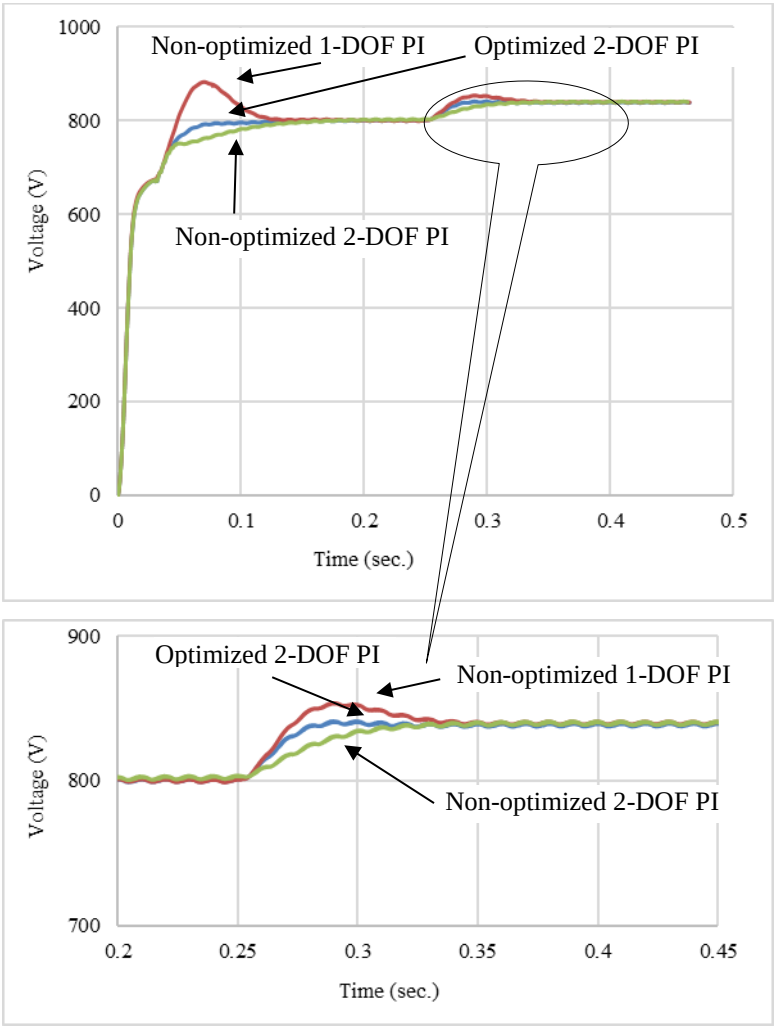

Fig.4.10 Transient response of dc voltage regulation for grid coupling to PV system and disturbance in reference dc voltage.

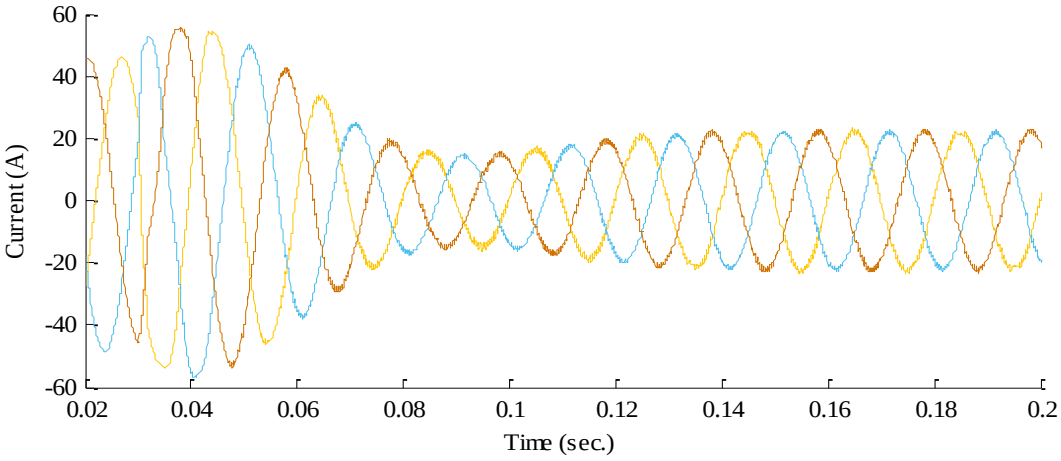

(a)

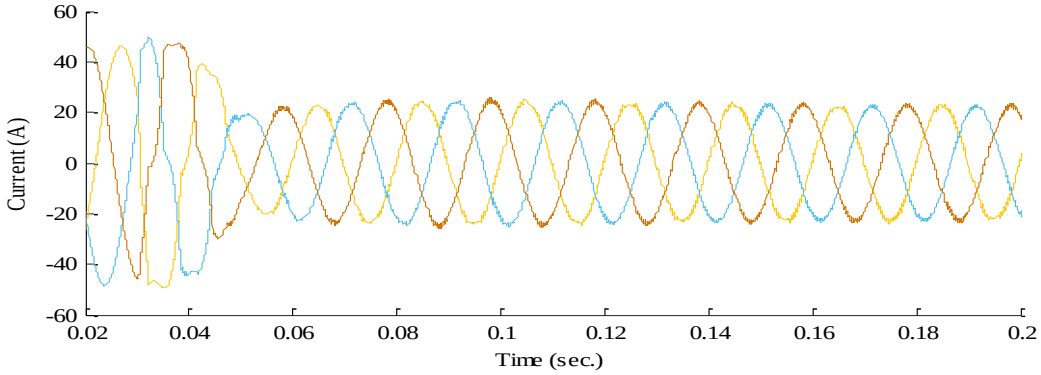

(b)

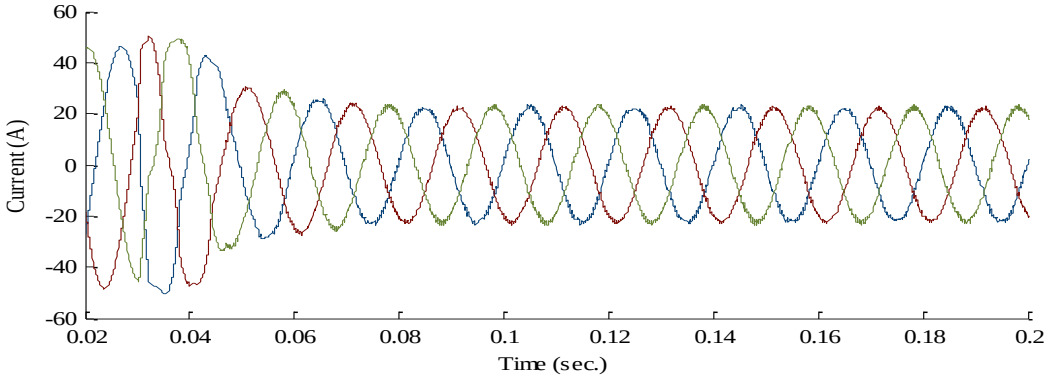

(c)

Fig. 4.11 Grid current response for
a) 1-DOF PI controller in respect to dc voltage regulation.
b) 2-DOF PI controller in respect to non-optimized dc voltage regulation.
c) 2-DOF PI controller in respect to optimized dc voltage regulation.

Table 4.3 Parameters of electrical utility grid system.

Description	**Parameter**
Line Impedance (Z_g)	R_g = 0.05Ω, L_g =1mH
Line to line grid voltage (V_{LL})	V_{LL}= 415V
LCL Filter	L_i = 1.4mH, L_g = 1.4 mH, C_f = 5 µF, R_d = 20Ω
DC link voltage (V_{dc})	V_{dc} = 800V
DC bus capacitance (C_{dc})	1500 µF
Base Impedance (Z_b)	Z_b = 17.22, C_b = 12 µF
Frequency (ω_f)	2*π*50 rad
Switching frequency (f_s)	10kHz

4.3.5 Varying Ir-radiance

The performance of the PV system usually affected due to the change in ir-radiance level. Therefore, the performance of the control investigated under the disturbance caused due to change in ir-radiance. Fig. 4.12 shows the dc voltage response for optimized and non-optimized control of 1-DOF and 2-DOF controller under the disturbance due to change in ir-radiance. One of the most critical case of change in ir-radiance considered to test the performance of the controller. The ir-radiance is changed from 1000 W/m^2 to 0W/m^2 at t = 0.25 s. and dc voltage get disturbed. The controller tries

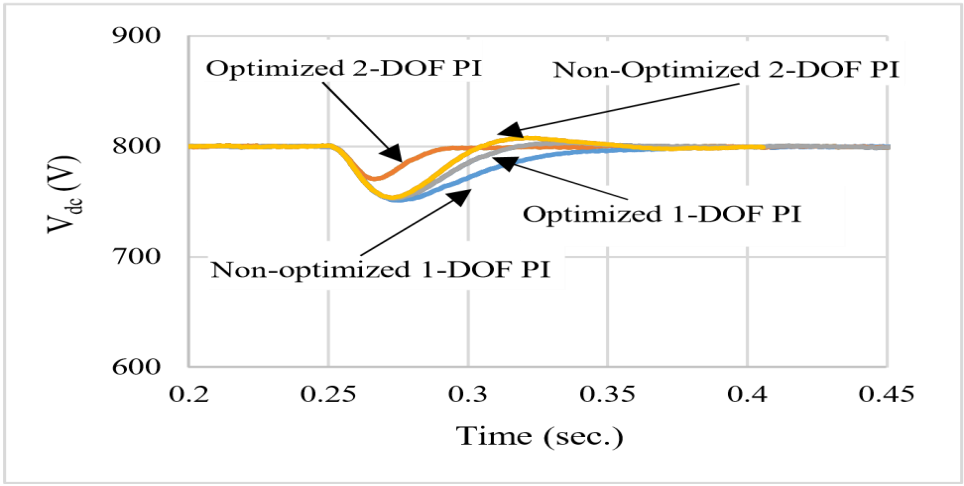

Fig. 4.12 Dc voltage controller response under disturbance due to ir-radiance.

to regulate the dc voltage to its reference level quickly. Optimized 2-DOF PI control is showing best performance with better dynamic response and having low undershoot under this condition.

4.4 Conclusion

The proposed and implemented 2-DOF PI-P controller for dc voltage control of grid connected PV system is investigated and the performance of proposed controller found satisfactory as compared to conventional control. The controller gain parameters are optimally tuned using data-driven tuning method. Data driven FRIT method programmed based upon PSO algorithm to overcome the drawback of tuning method. The optimized PI-P controller showing fast and smooth response in comparison to non-optimized PI-P and traditional PI control during grid coupling of PV system. As well as, the proposed optimally tuned controller is also effective under step change in reference dc voltage (step response) and disturbance due to varied irradiance of PV system. The grid current investigated during integration of PV system and better response achieved corresponding to significantly improved dc voltage regulation. The system performance validated considering load conditions.

CHAPTER 5

XILINX SYSTEM GENERATOR (XSG/Sys-Gen) MODELLING FOR FPGA BASED SYSTEM IMPLEMENTATION

5.1 GENERAL

The grid connected PV system is gaining high popularity due to effective and efficient utilization of PV generated power: rooftop PV application to medium and high power grid integration. The fundamental question regarding PV power generation is the low efficiency of PV panels so it is important to design and implement better electrical controls using power electronics devices to utilize the generated power efficiently and have improved power quality. The hardware implementation of electrical system requires to design and model the system on real-time simulation platform with condition similar to experimental system. There are various platforms like as Opal-RT, digital signal processing and control engineering (dSPACE) are available and familiar platform popularly utilized for hardware in loop (HIL) simulations. However, these platforms are not general purpose and having limited functionality to implement the system of power electronics converter applications. The Xilinx corporation has evolved field-programmable gate array (FPGA) consists of thousands of logic gate blocks utilized to implement circuit design in various combination. The real-time application of FPGA based control has been little complex as it requires knowledge and training of hardware description language (HDL) for example: VHDL, Verilog. In addition, the specialisation of trained and skilled researchers might be different and may require learning and be trained for newer applications. The level of complexity of the system control is different therefore to develop the system control using HDL may leads to a complex process.

The Xilinx system generator HIL used through MATLAB-Simulink and it is an easy platform to utilize the functionality of both the platforms. This platform helps to design, test and develop new hardware prototype rapidly without the knowledge of hardware description language (HDL). It also fulfils the requirement of low cost digital platform to implement HIL simulation for FPGA control. VHDL code can be generated automatically using system generator, MATLAB-Simulink combined platform, and generated code directly utilized for the real system through FPGA. It enables to develop a rapid prototype of power electronics application and control circuits using sys-gen to utilize FPGA for real time experimental system.

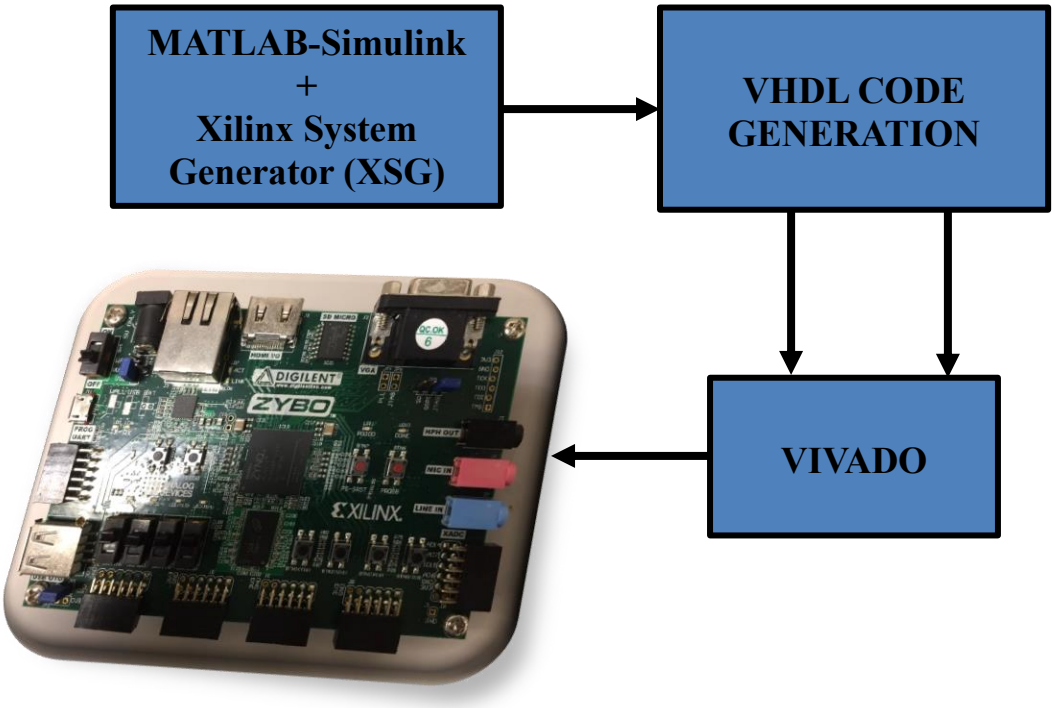

Fig. 5.1 Schematic block diagram of the HDL co-simulation and HIL circuit.

In this chapter, the fundamental components of grid connected PV system control modelled in combined platform of MATLAB-Simulink-XSG to perform real time simulation and generate HDL file and utilizing it through VIVADO for system control using Xilinx FPGA (Dgilent Zybo) board as shown in Fig. 5.1.

5.2 MODEL DESIGN

FPGA is a digital control platform therefore modelling of the system requires design of various blocks and components used in digital control system.

5.2.1 PI controller

PI controller designed based upon the Euler /trapezoidal method for the digital control application.

- Euler's forward method

$$\mathrm{x(k)} = x(k-1) + T_s u(k-1)$$

$$\frac{x(z)}{u(z)} = \frac{T_s}{z-1}$$

- Euler's backward method

$$x(k) = x(k-1) + T_s u(k)$$

$$\frac{x(z)}{u(z)} = \frac{T_s z}{z-1}$$

- Trapezoidal (Tustin) method

$$x(k) = x(k-1) + \frac{T_s}{2}[u(k) + u(k-1)]$$

$$\frac{x(z)}{u(z)} = \frac{T_s}{2}\frac{z+1}{z-1}$$

Euler's backward method commonly used for discretising continuous-time PID controller function therefore, it is chosen to model PI controller for digital control platform.

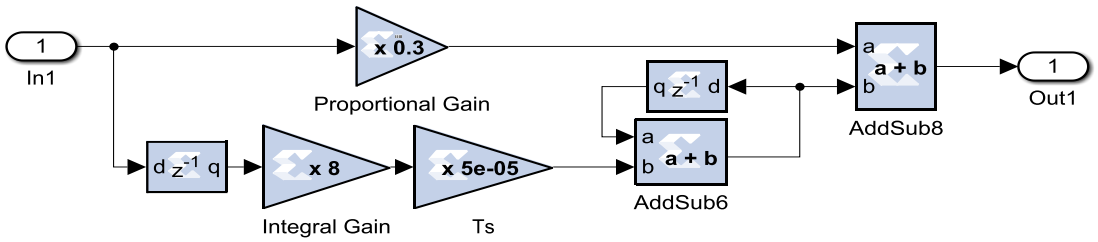

(a)

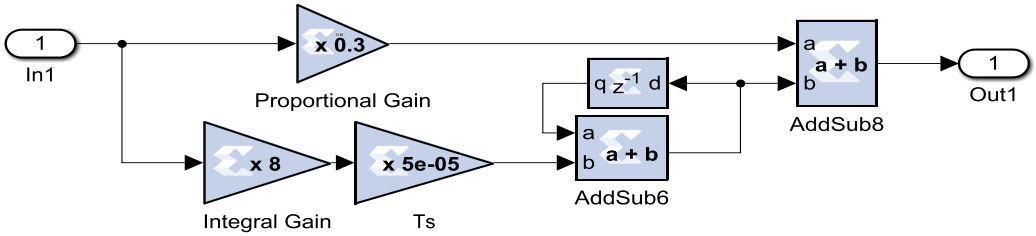

(b)

Fig. 5.2 PI controller modelling in XSG
a) Euler's forward method
b) Euler's backward method.

5.2.2 Co-ordinate Transformation

Co-ordinate transformation required by the system for implementing PLL and generation of reference current for SRF theory based control. The transformation equations already discussed in chapter3. The modeling in MATLAB-Simulink using Power System Toolbox (SimPowerSystem) have transformation blocks so just a basic understanding is enough for the purpose. The one of the key importance of

transformation come into the picture for selective compensation and especially for negative sequence compensation using SRFT. XSG is a general-purpose platform for modeling so abc→αβ→dq Fig. 5.3a and dq→αβ→abc Fig. 5.3b transformation modeled based upon mathematical equations.

5.2.3 PLL

PLL algorithm is discussed and represented using block diagram in chapter3. The purpose of PLL is to synchronize (frequency and phase) the output signal with input signal so it can be termed algorithm that generates a signal by tracking input one. PLL block is available in MATLAB-Simulink Power System Toolbox so the in-depth understanding of PLL working principle not required. The modeling of PLL is required for real time simulation in XSG and FPGA-based control.

As discussed in chapter3, measured grid voltage signal passed through co-ordinate transformation block to perform abc→αβ→dq conversion. Keeping the reference voltage (V_d^*) zero and fed to PI controller. The output of the PLL loop is an angle (θ) Fig. 5.4b. The output θ passed through the divider generator block of XSG to avoid θ becoming too large by keeping its value in between 0→2π. The co-ordinate transformation requires the sine and cosine signals generated using output θ of PLL. In XSG modelling, CORDIC sin-cos block of XSG is utilized to generate sine-cosine signals. The key point for the modelling in XSG is sine-cosine signal generation bounded by value of θ (from - π→+ π). Therefore, the value of θ adjusted according to the modelling requirement of the system, first by converting it in between 0→2π and then - π→+ π Fig. 5.4c. The sinusoidal signal generated using the output angle of the PLL is tracking the phase and frequency of the input signal Fig. 5.4d.

5.3 SYSTEM CONTROL MODELLING

System control is subdivided into three parts as: Voltage control loop and SPWM (switching signals).

5.3.1 DC voltage regulation

DC voltage regulator loop model consists of PI controller and error fed to the controller. The output of controller passed through saturation block and low pass filter (LPF). Therefore, the output of voltage control loop generated active reference current

component responsible for regulation of dc link voltage by compensating VSI losses. PI controller modeled based upon the Euler's backward method as mentioned in this chapter earlier. Saturation block modeled using the M-Code block of XSG simulation block-set and low pass discrete filter (FIR filter) designed using FDA-Tool block of XSG and then modeled using Xilinx block-set Fig. 5.5.

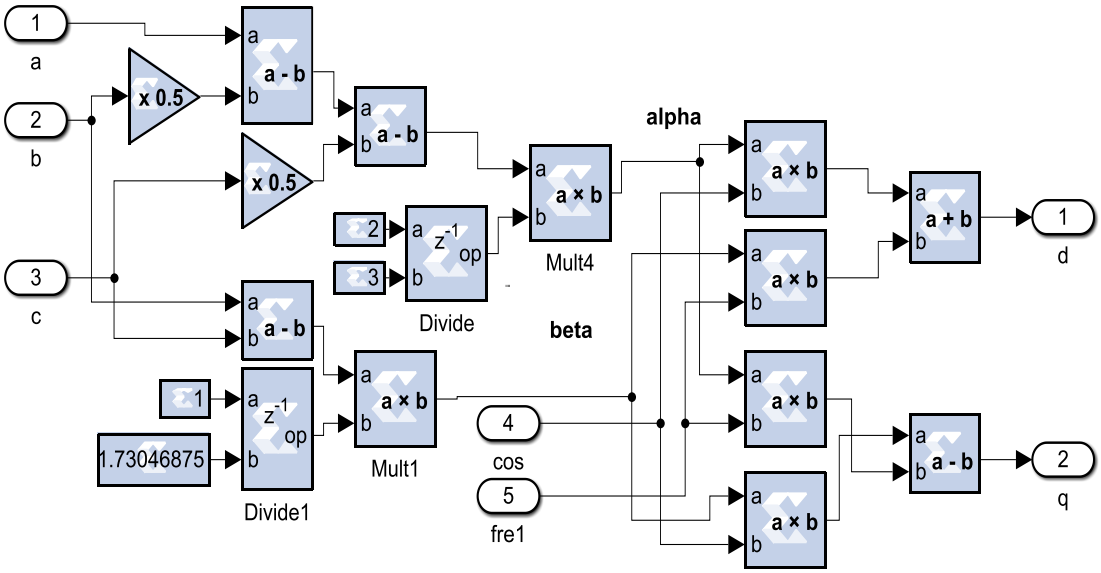

(a)

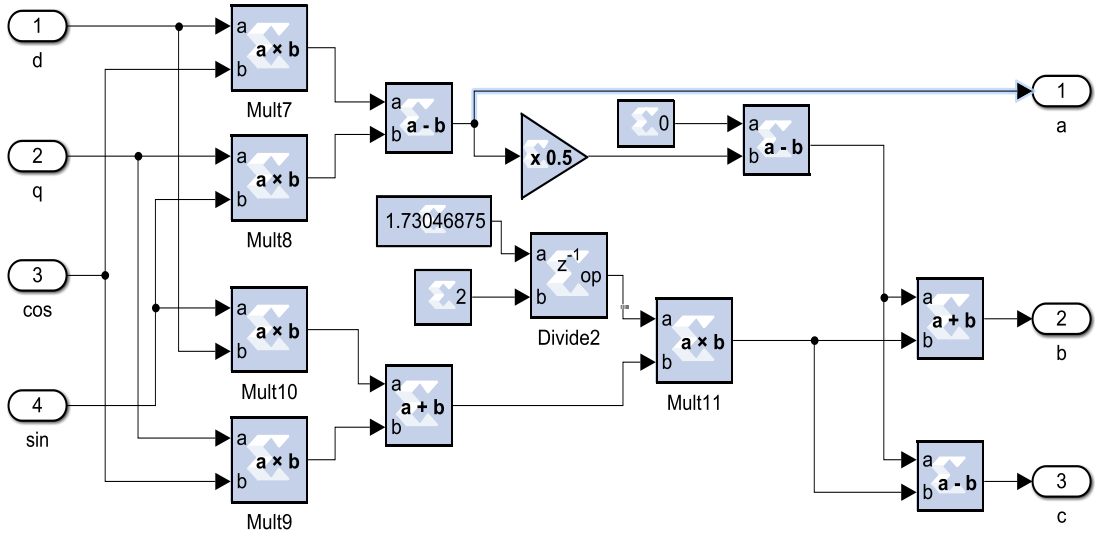

(b)

Fig. 5.3 Co-ordinate transformation model in XSG
a) abc→αβ→dq transformation
b) dq→αβ→abc transformation

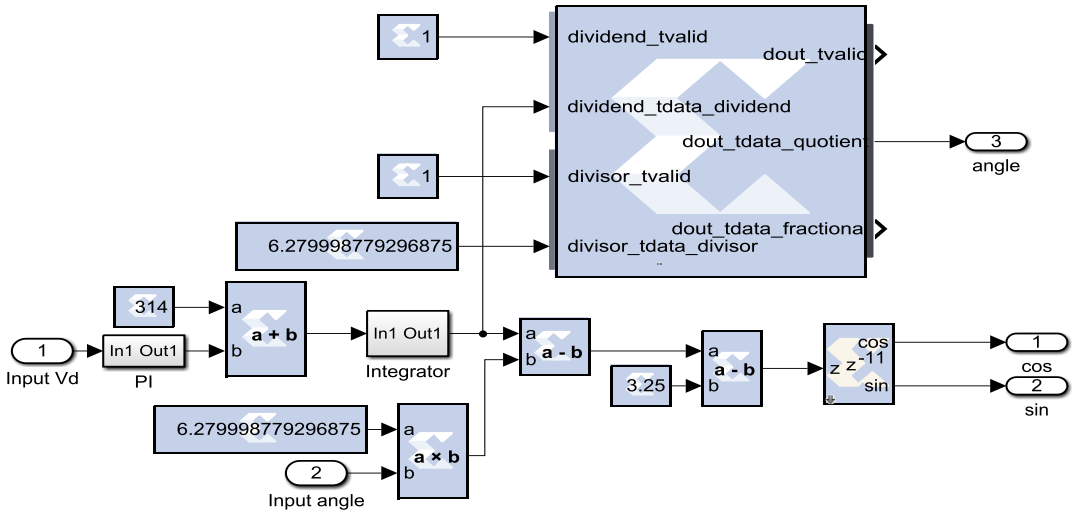

(a)

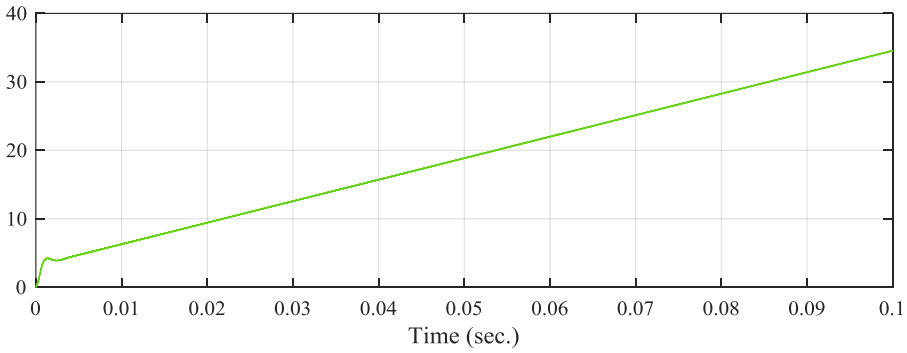

(b)

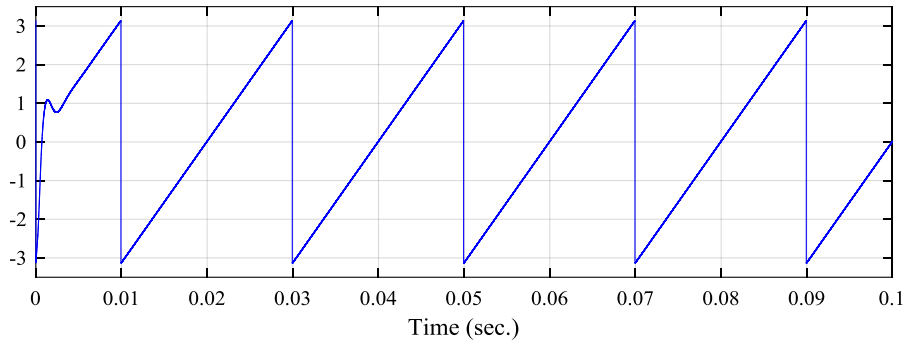

(c)

5.3.2 Generation of PWM signal

Carrier based PWM is one of the commonly used switching technique. SPWM method modeled in XSG. The carrier wave signal and modulating signal generated for open loop switching of test circuit. Only carrier wave generation requires in case of closed loop control.

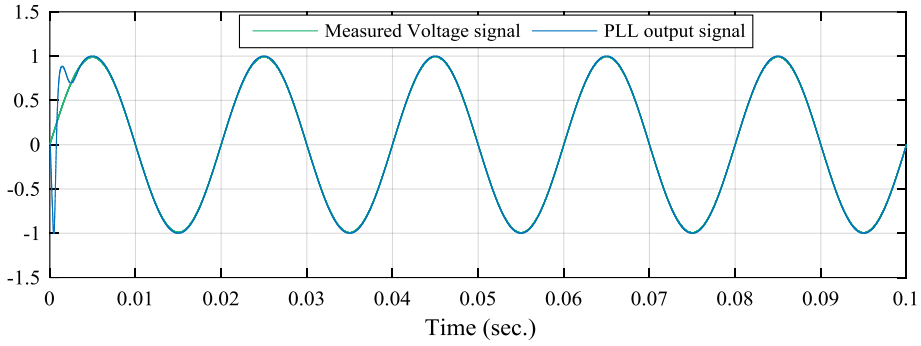

(d)

Fig. 5.4 Phase locked loop (PLL)
a) modeled in XSG using Xilinx blockset.
b) generated angle output of PLL.
c) output generated after divider generator block and shifting by pi angle.
b) generated PLL output to match phase and frequency of input signal.

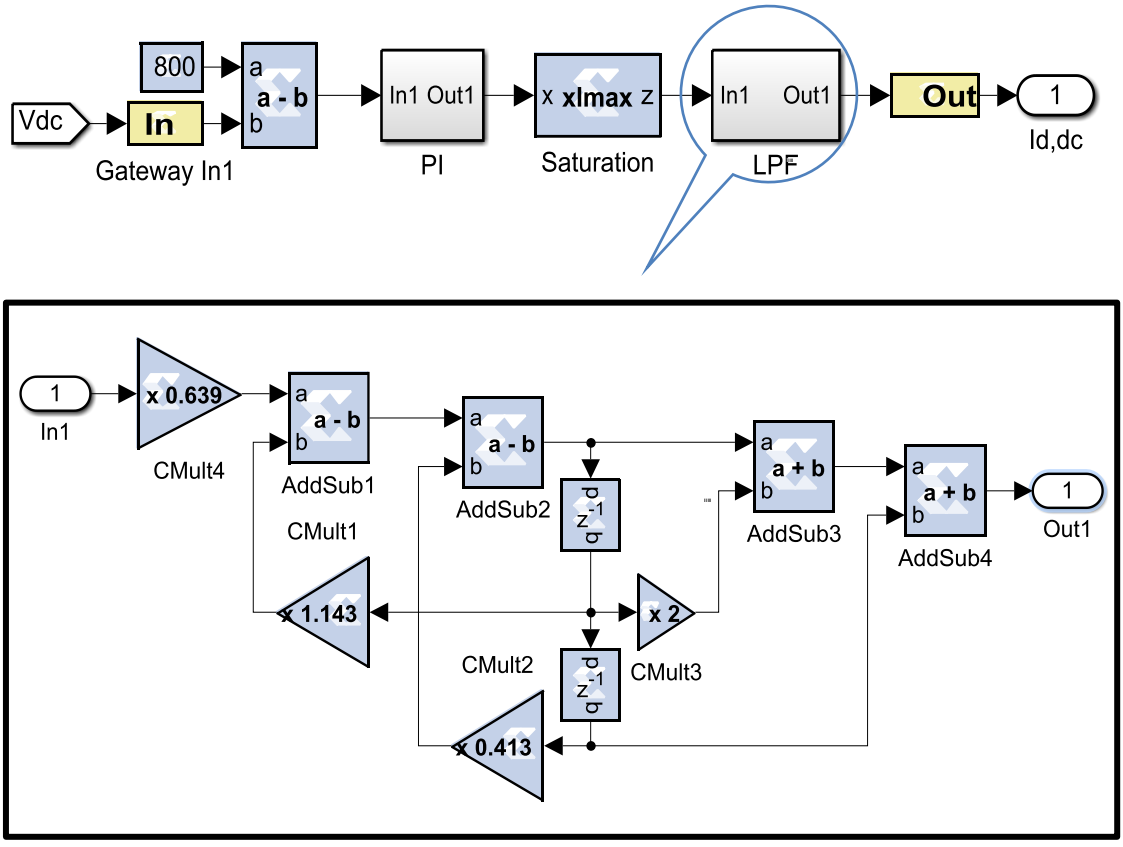

Fig. 5.5 DC voltage control loop model (with saturation block and low pass filter) in XSG.

5.3.2.1 Carrier signal generation (Triangular wave)

There are different ways to generate triangular single and the general modeling platform of XSG have various set of block that utilized in a particular way to design

new modeling method for generating waves. The triangular wave generation method in [**98**] is explained and modeled using five blocks: Up-counter, bit slice extractor, Inverter, Up-down counter and reinterpret blocks and 2kHz triangular wave has been generated.

There is a key point regarding generation of signal in XSG for simulation and FPGA implementation. The clock frequency of the FPGA board govern the time period of the signal for simulation model to achieve the desired frequency for the real-time prototype system. The triangular signal generation of 10kHz Fig. 5.6a and 1kHz Fig. 5.6b is taken as an example here as it has been utilized for experimental and simulation system of grid-connected PV system and cascaded H-bridge multilevel inverter respectively in the laboratory.

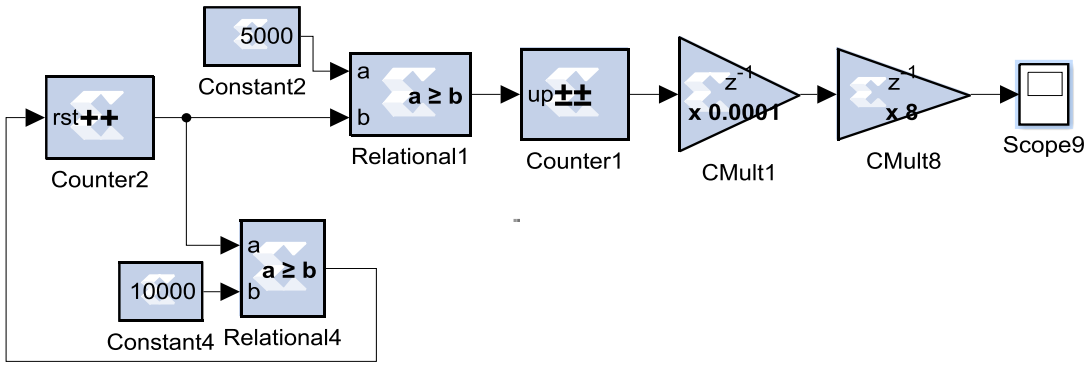

(a)

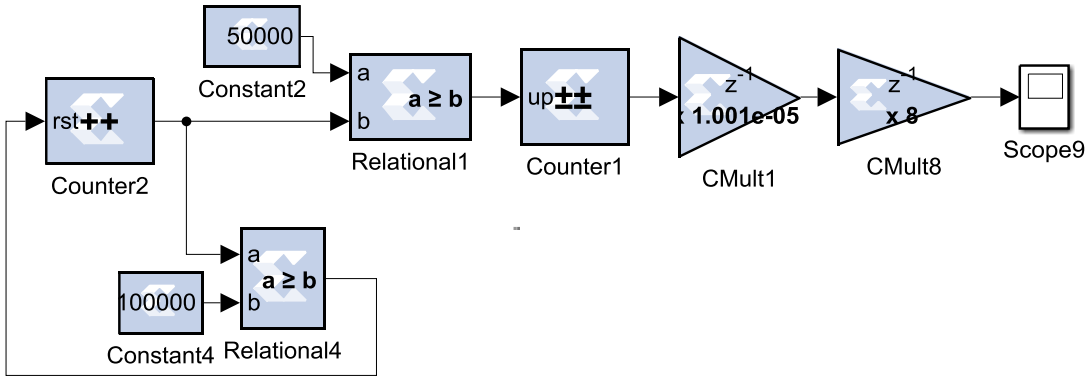

(b)

1. Counter block performing up-count operation in free running mode is reset using synchronous reset port. The rest of the counter performed by using bool output of relational operator and reset the counter after 10000 counts. The

waveform obtained from the up counter is like a ramp signal varying from 0 to 10000 and reset to 0 after reaching to 10000. The count limit of the counter chosen considering desired triangular wave period and clock frequency of the FPGA. In this case, the desired triangular wave frequency is 10kHz and clock frequency of the FPGA board is 100MHz. Therefore, the generation of 10kHz triangular wave for real-time HIL system with clock frequency 100MHz is required to generate the signal with time period of 10000 during simulation in MATLAB-Simulink and XSG integrated platform. So, the initial ramp signal generated using counter using reset after 10000 counts Fig. 5.6c.

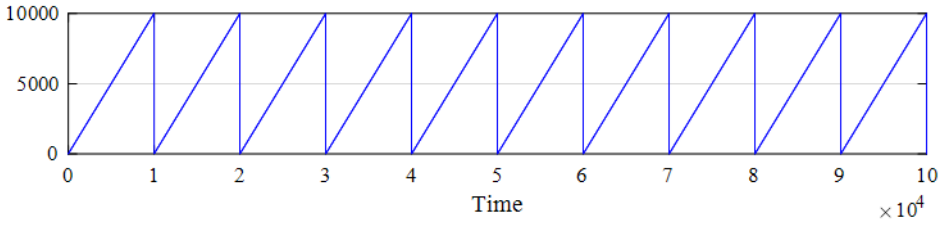

(c)

2. The output ramp signal of the reset up counter passed through the relational operator and compared with a constant block of value 5000. The comparator at this stage set the output as one or zero by comparing the input ramp signal. Therefore, the output of this stage is a binary signal Fig. 5.6d with the period of 10000.

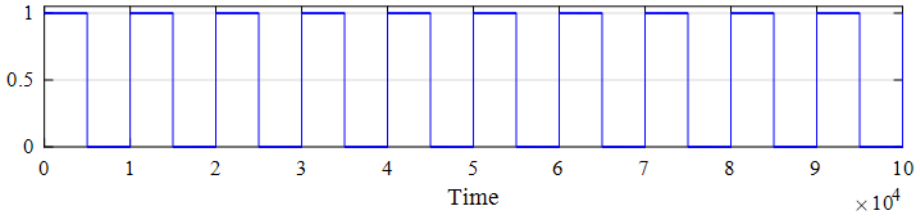

(d)

3. The binary of the earlier stage again passed through a counter performing up-down count operation. The value of binary signal decides the up and down counting sequence. If the output value of binary signal is one, then counter perform up count operation. The operation is performed using the same count operation therefore up count sequence goes till 5000. When, the binary value changes from 1 to 0, the counter start to perform down count operation. Again, by the time binary output changed to one the counter value reaches to 0 and

starting the up count when binary output become 1. The output of this stage is a triangular wave Fig. 5.6e with value from 0 to 5000 and time period of 10000.

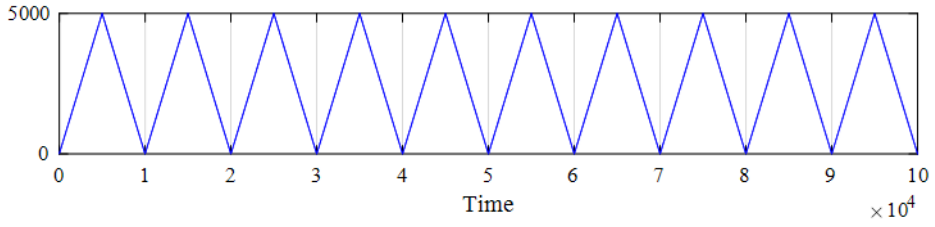

(e)

4. The multiplier block used after the up-down counter stage to generate the triangular signal output of desired value. In general, the triangular signal with maximum value one used for SPWM switching. The generated signal is unipolar and desired triangular wave output obtained for unipolar and bipolar switching by level shifting of the signal Fig. 5.6f.

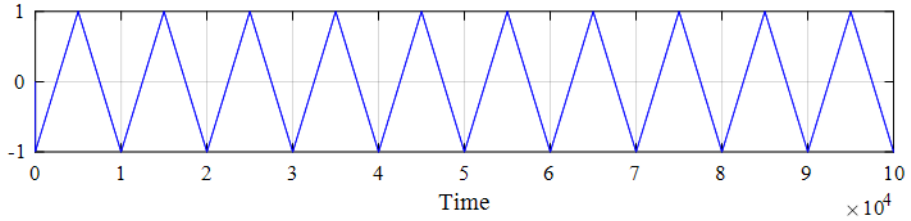

(f)

Fig. 5.6 Generation of triangular wave in XSG using Xilinx blocksets.
a) model for the generation of triangular wave of 10kHz.
b) model for the generation of triangular wave of 1kHz.
c) output of the reset counter generating ramp-like signal.
d) output generated after the relational operator block, binary signal.
e) output generated after the up-counter. triangular signal.
f) shifted output of triangular signal with magnitude in between -1 to 1.

5.3.2.2 Sine wave generation (Open loop control test circuit)

Method 1 [**89**]

1. Counter block performing up count function in limited count mode and counting from 0 to 332. The calculation of count limit is explained in referenced article.
2. ROM block is listed in Xilinx XSG blocket library having address port as an input Fig. 5.7a and used in distributed memory option with output data type chosen as fixed-point, arithmetic type-signed option.

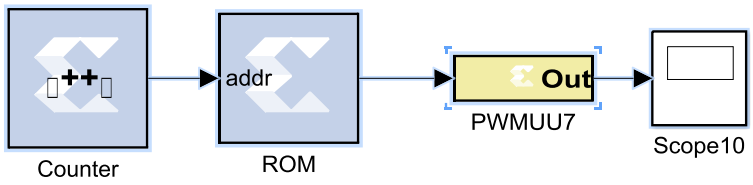

(a)

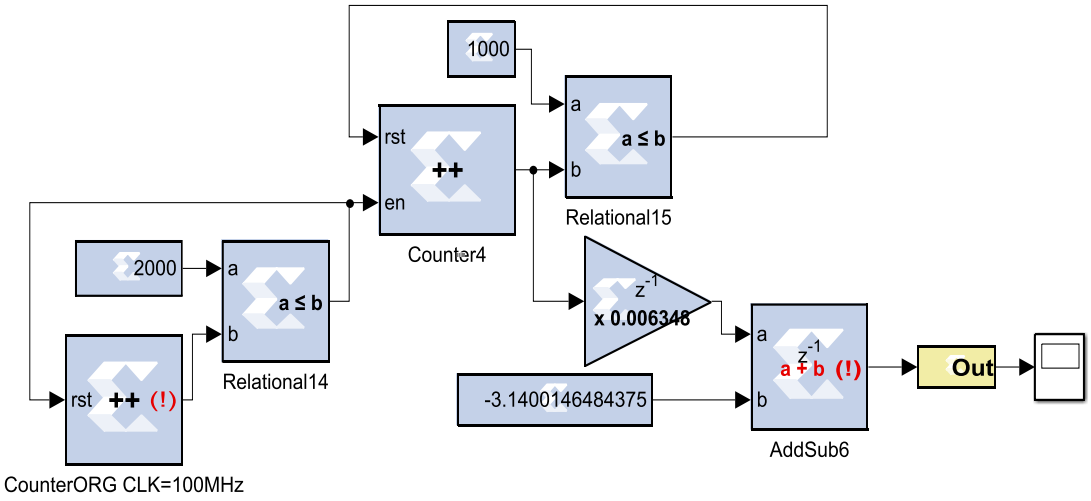

(b)

Method 2

The fundamental idea behind this method is to generate a signal similar to ramp with magnitude varying from - π→+ π. Therefore, sine and cosine signal can be generated using CORDIC SINCOS block in XSG Fig. 5.7b. The key point is generating the signal in simulation with some time period which will provide desired time period regarding the clock frequency of FPGA during real time control as mentioned for triangular signal generation.

1) A sinusoidal signal with time period of $2*10^6$ is required to be generated in XSG simulation considering the key point for generation of signal to generate a sinusoidal wave of 50 Hz in real time for FPGA having clock frequency of 100MHz. The method considered for triangular signal generation cannot be directly implemented, as the count required for generation of sinusoidal signal is very high hence, the number of bit required for the counting also become more. Therefore, the idea is similar as of generation of triangular wave and count divided in two parts.

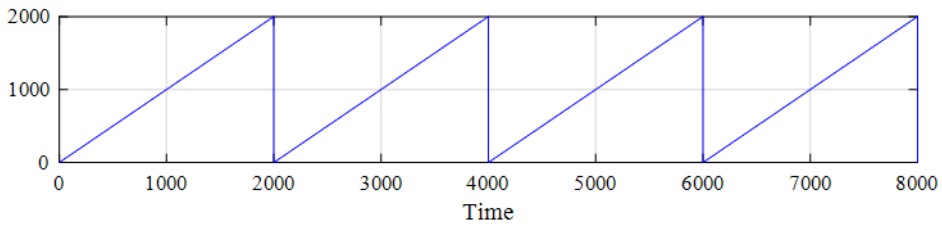

(c)

2) The count subdivided as 2000 for one counter Fig. 5.7c and 1000 for another counter for ease of implementation. The counters are working in series so overall time period for the generated signal is multiplication of the counts i.e. $2000*1000=2*10^6$ Fig. 5.7d. The desired time period of sinusoidal signal for simulation in XSG matched successfully.

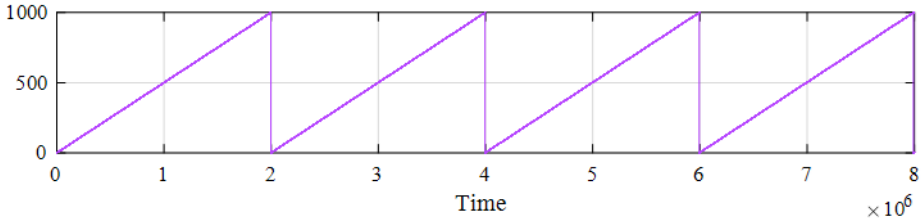

(d)

3) Counter block1 utilizing in up count mode reset by the output of the comparator1 with inputs: constant input of 2000 and output of the counter block1. The counter operates in closed loop.
4) The output of the relational comparator1 enables the counter block2. The counter block2 also works in the up-count mode reset by the output of relational comparator2 with inputs: constant input of 1000 and output of the counter block2. The output of the counter block2 resembles the ramp signal with magnitude varying from 0 to 1000 with time period of $2*10^6$ and reset to zero after each time period. After that, the signal multiplied with the value of .006348 and shifted to achieve the desired ramp signal output Fig. 5.7e with magnitude varying from $-\pi \rightarrow +\pi$. The ramp signal of magnitude $-\pi \rightarrow +\pi$ with time period of $2*10^6$ is further utilized as an input for CORDIC SINCOS block of Xilinx XSG block-set to generate sine-cosine waves Fig. 5.7f.

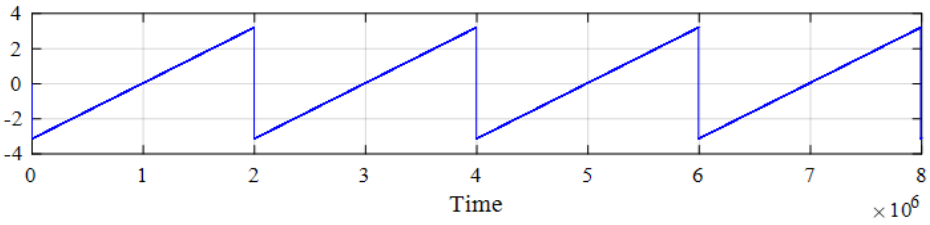

(e)

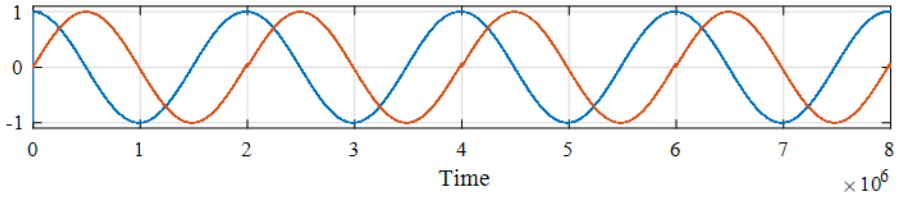

(f)

Fig. 5.7 Generation of sinusoidal wave in XSG using Xilinx blocksets.
a) model for the generation of sinusoidal wave using method1.
b) model for the generation of sinusoidal wave using method2.
c) ramp type signal output of the relational comparator with input from reset counter.
d) ramp type signal (desired time period) output of counter with reset and enable input.
e) desired ramp signal output of the angle varied from –pi to +pi.
f) generation of sine and cosine wave.

5.3.2.3 PWM Signals

The sinusoidal PWM (SPWM) signals can be generated using triangular wave (carrier signal) and comparing it with reference sinusoidal wave. The open loop system control used to test the circuit implementation at the initial stage due to ease of implementation and less complexity. The real time prototype experimental system will be further controlled in closed loop control that requires sensors to measure the control parameters. The output of the sensors is the analog signal which needs to be converted into digital signal to input it into FPGA.

The reference signal and measured signal are required in closed loop control operation. The error in between reference and measured signal is a sinusoidal modulating wave compared with the triangular wave and SPWM switching signals generated. The three phase SPWM model in Fig 5.8a and used to test the model in open loop condition also.

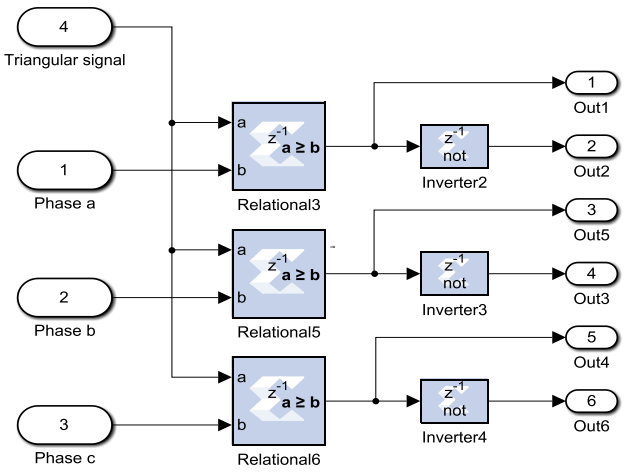
4
Triangular signal
1
Phase a
2
Phase b
3
Phase c
a
b
z-1
a ≥ b
Relational3
Relational5
Relational6
z-1
not
Inverter2
Inverter3
Inverter4
1
Out1
2
Out2
3
Out5
4
Out3
5
Out4
6
Out6

(a)

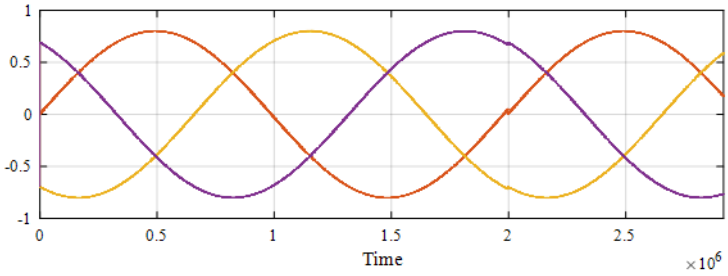
1
0.5
0
-0.5
-1
0
0.5
1
1.5
2
2.5
Time
×10^6

(b)

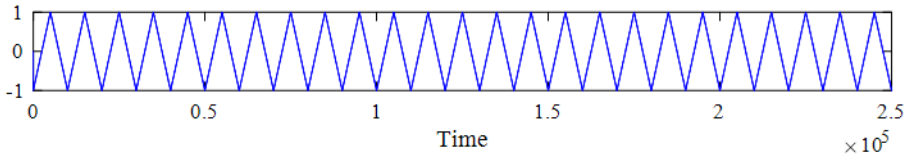
1
0
-1
0
0.5
1
1.5
2
2.5
Time
×10^5

(c)

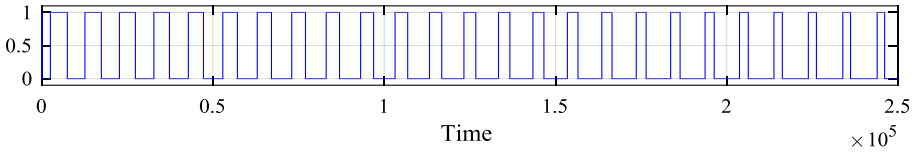
1
0.5
0
0
0.5
1
1.5
2
2.5
Time
×10^5

(d)

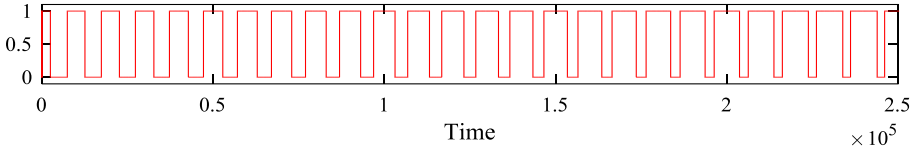
1
0.5
0
0
0.5
1
1.5
2
2.5
Time
×10^5

(e)

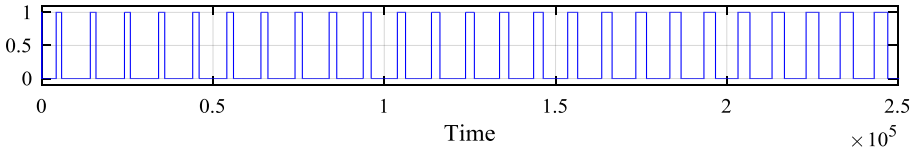
1
0.5
0
0
0.5
1
1.5
2
2.5
Time
×10^5

(f)

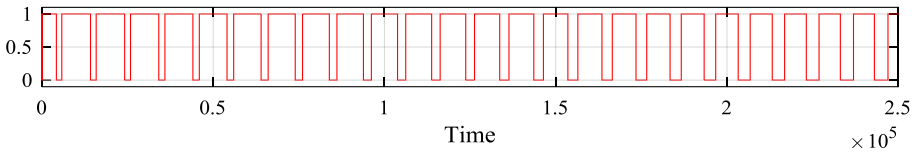

(g)

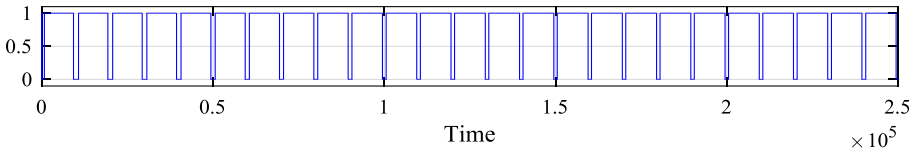

(h)

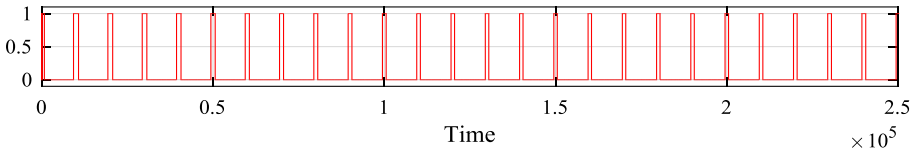

(i)

Fig. 5.8 Generation of PWM signals.
a) model for the generation of SPWM signals for an open loop system.
b) model for the generation of SPWM for a closed loop system.
c) three phase sinusoidal modulating wave with magnitude 0.8 and frequency 50 Hz for real time.
d) bipolar triangular wave with magnitude in between -1 to 1 and frequency 10kHz for real time.
e) PWM signal for phase ‘a’ upper half of leg; f) PWM signal for phase ‘a’ lower half of leg.
g) PWM signal for phase ‘b’ upper half of leg; h) PWM signal for phase ‘b’ lower half of leg.
i) PWM signal for phase ‘c’ upper half of leg; j) PWM signal for phase ‘c’ lower half of leg.

The modulating signal (sinusoid) in Fig. 5.8b and carrier signal (triangular) in Fig. 5.8c of the computed frquency is utilized to general PWM signal in Fig. 5.8d to i for three phase system to obtain the real time system with frequency 50Hz.

5.4 STEP-BY-STEP IMPLEMENTATION

The overall system can be designed and modelled by following the step-by-step approach. XSG used through SIMULINK platform of MATLAB, having its own general building blocks available in Xilinx block-set. The first step is to design and develop model of a system which will further designed and modelled using MATLAB and XSG blocks. There are some specific blocks also which enables to write the program or use HDL coder blocks in MATLAB/Simulink platform and utilized in XSG interface. The automatic code in HDL generated through system interface of XSG and MATLAB-Simulink utilizing modelled system

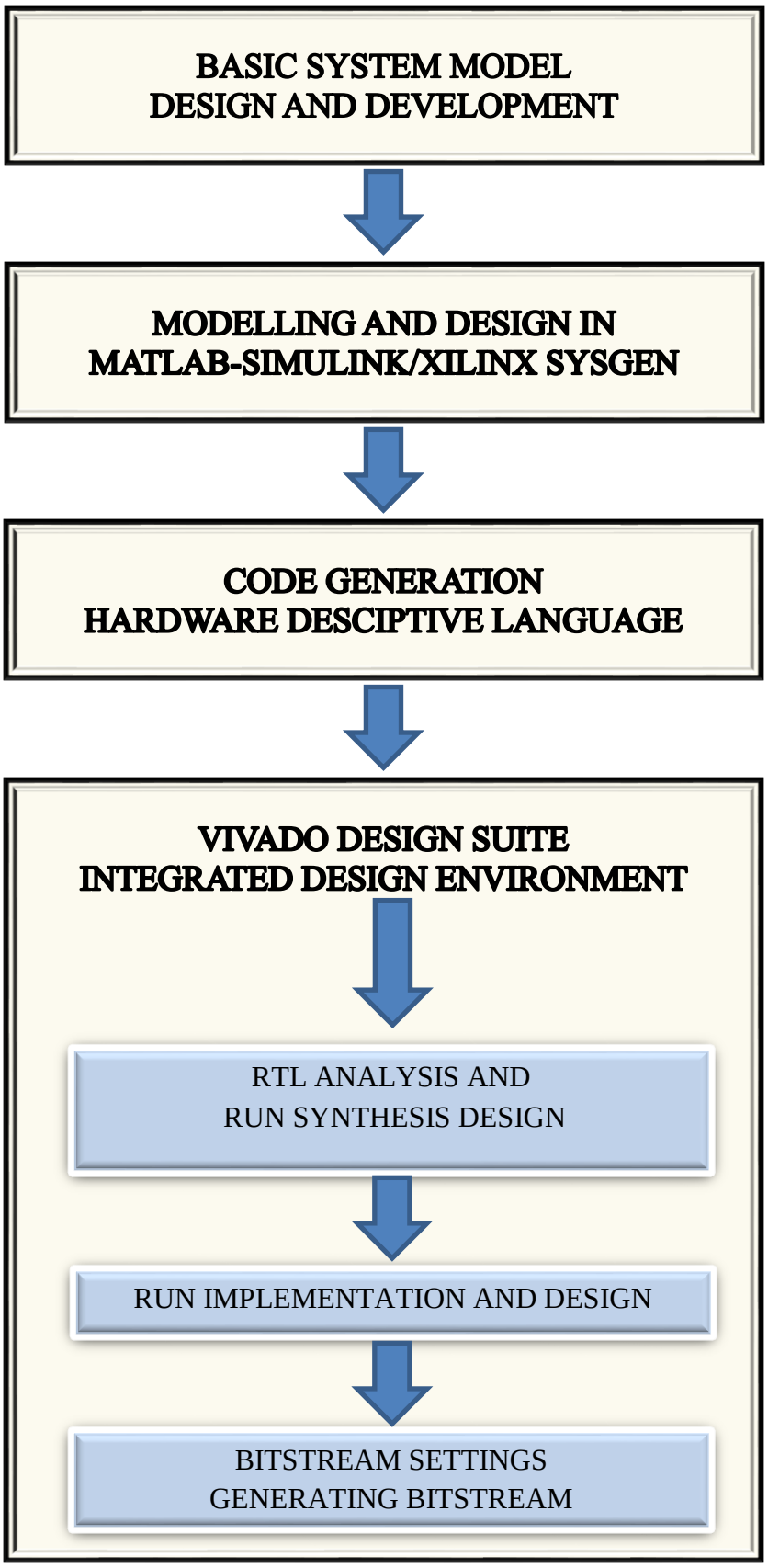

Fig. 5.9 Step by step process for code generation and writing the code in FPGA via VIVADO.

.

The automatic generated code in HDL is further utilized using VIVADO design suite software Fig. 5.9. The HIL system will be established after completing step by step process in VIVADO.

5.4 CONCLUSION

The fundamental components required for control design like as PI controller, PLL and signal generation (triangular and sinusoidal) generated in XSG. The key point regarding design of the system is the fundamental frequency of the real time system so that to adjust the system model frequency in XSG according to FPGA clock frequency. The open loop SPWM signal generation successfully generated.

CHAPTER-6

CONCLUSION

6.1 CONCLUSION

The grid integration of PV system is dominant trend for utilizing generated power. The PV power system become significant as an alternative source from kW application to power plants of MW. The PV characteristics play the vital role in tracking of maximum power generated from the system. The understanding of PV characteristic considering partial shading condition and PV system configuration developed using simulated model. In addition, the real time data obtained through the 2.88kW rooftop installed system investigated. During the partial shading, PV characteristic mainly affected by number of modules connected in series. The integration of PV system to grid concerned with the synchronization of the system, dc voltage control and generation of reference currents utilized for current control switching signals. The main problem considered out of this this for study is dc voltage control. The 2-DOF feedback type controller implemented and utilized for the dc voltage control and the better response obtained during transients (grid integration, set point response and disturbance response). The tuning of the controller is having one of the vital role in the system. Fictitious Reference Iterative Tuning (FRIT), which is one of the date driven method, utilized for optimal tuning of the controller gains of conventional controller and proposed 2-DOF controller. Particle swarm optimization (PSO) incorporated to avoid drawback of FRIT method. The grid connected PV system modeled in MATLAB/Simulink. The Xilinx system generator (XSG) platform used with MATLAB/Simulink to model the system for more practical and real time environment. The design of fundamental components required for the development, control of the system modelled in XSG, and desired results obtained.

FPGA based digitally controlled closed loop system is under consideration as a future research plan by using analog to digital (AD) and digital to analog (DA) converters. Implementation of various control strategies and switching schemes using FPGA is an important aspect for high frequency control as future aspects considering wide-band gap switching devices.

REFERENCES

[1] RNE 21 "Renewables 2016", Global status report, pp. 17,18.

[2] Nikos Hatziargyriou, Hiroshi Asano, Reza Iravani and Chris Marnay "Microgrids" , IEEE Power and Energy magazine, July-August 2007..

[3] IEA-PVPS, "Trends in Photovoltaic Applications 2015", Survey report of selected IEA countries between 1992-2014.

[4] Ministry of Renewable energy (MNRE), Government of India (GoI) "MNRE-Annual Report", 2014-15.

[5] Takuya Yamazaki, "Japan's Electricity Market Reform and Beyond", Agency for Natural Resources and Energy (ANRE), Ministry of Economy, Trade and Industry (METI), Japan, 2015.

[6] Louis du Plessis (Energy and Environment Specialist), "Japan's Solar PV Market Overview", JETRO London, November 2015

[7] Edgar Hahn, "The Japanese Solar PV Market and Industry-Business Opportunities for European Companies", EU-Japan Centre for Industrial Cooperation, November 2014.

[8] Hiroyuki Yamada, "National Survey Report of PV power Applications in Japan 2014-Photovoltaic Power Systems Programme", New Energy and Industrial Technology Development Corporation (NEDO)-IEA PVPS, 2015.

[9] IEA-PVPS, "Trends in Photovoltaic Applications 2015", Survey report of Japan.

[10] National research energy laboratory (NREL), "Solar cell efficiencies graph", October, 2016.

[11] Soeren Baekhoj Kjaer, John K. Pedersen and Frede Blaabjerg, "A review of Single-Phase Grid-Connected Inverters for Photovoltaic Modules", IEEE Transaction on Industry Applications, vol. 41, no.5, Sep. 2005.

[12] Hadi Malek,, "Control of Grid Connected Photovoltaic System using Fractional Order Operators", PhD dissertation, 2014.

[13] Ravi Nath Tripathi and Tsuyoshi Hanamoto, "Parameter Computation Using Circuit Based Approach for Two-Diode Model Based Solar PV Simulator", 28th International conference on efficiency, cost, optimization, simulation and environmental impact on energy system (ECOS), Pau, France, June 29th – July 3rd, 2015.

[14] R. Gonzalez, J. Lopez, P. Sanchis, and L. Marroyo, "Transformer less inverter for single-phase Photovoltaic system ", IEEE Transaction on Power Electronics, vol.22, no.2, March 2007.

[15] SyahrulA. Azmi, Grain P. Adam, Khaled H. Ahmed and Barry W. Williams, "Grid Interfacing of Multimegawatt Photovoltaic Inverters", IEEE Transaction on Power Electronics, vol.28, no.6, June 2013.

[16] C. Yang and K. Smedley, “Three-Phase Boost-Type Grid-Connected Inverter,” Three-phase boost-type grid-connected inverter,” IEEE Trans. Power Electron., vol. 23, no. 5, pp. 2301–2309, Sep. 2008.

[17] C. Yang and K. Smedley, “A cost-effective single-stage inverter with maximum power point tracking,” IEEE Trans. Power Electron. Power Electron., vol. 19, no. 5, pp. 1289–1294, Sep. 2004.

[18] J.M.Carrasco, L.G.Franquelo, J.T.Bialasiewicz, E.Galvan, R.C.P.Guisado, Ma.A.M.Prats, J.I.Leon and N.M.Alfonso, “ Power-Electronic Systems for the Grid Integration of Renewable Energy Sources: A Survey”, IEEE Transaction on Industrial Electronics, vol.53, no.4, August 2006.

[19] F. Blaabjerg, R. Teodorescu, Z. Chen, and M. Liserre, “Power converters and control of renewable energy systems,”. 6thInt. Conf. Power Electron., Oct. 18–22, 2004.

[20] H. Haeberlin, “Evolution of inverters for grid connected PV systems from 1989 to 2000,” in Proc. Photovoltaic Solar Energy Conf., 2001.

[21] Grid-connected Photovoltaic power system: Technical and potential problems-A review.

[22] Monfared M, Golestan S, Guerrero JM. Analysis, design and experimental verification of a synchronous reference frame voltage control for single phase inverters. IEEE Trans Industr Electron 2013;61(1):258–69.

[23] Sha D, Wu D, Liao X. Analysis of hybrid controlled three-phase grid-connected inverter with harmonics compensation in synchronous reference frame. IET Power Electron 2011;4(7):743–51.

[24] Busada CA, Blanca Bahia, Gomez Jorge S, Leon AE, Solsona JA. Current controller based on reduced order generalized integrators for distributed generation systems. IEEE Trans Industr Electron 2012;59(7):2898–909.

[25] Hwang Seon-Hwan, Liu Liming, Li Hui, Kim Jang-Mok. DC offset error compensation for synchronous reference frame PLL in single-phase gridconnected converters. IEEE Trans Power Electron 2012;27(8):3467–71.

[26] Adda R, Ray O, Mishra SK, Joshi A. Synchronous-reference-frame-based control of switched boost inverter for standalone DC nanogrid applications. IEEE Trans Power Electron 2012;28(3):1219–33.

[27] Tsengenes Georgios, Adamidis Georgios. Investigation of the behavior of a three phase grid-connected photovoltaic system to control active and reactive power. Electr Power Syst Res 2011;81:177–84. Elsevier.

[28] Herrera RS, Salmeron P. Present point of view about the instantaneous reactive power theory. IET Power Electron 2009;2(5):484–95.

[29] Singh BN, Rastgoufard P, Singh B, Chandra A, Haddad KA. Design, simulation and implementation of three pole/four pole topologies for active filters. Inst Electr Eng Proc Electr Power Appl Jul. 2004;151(4):467–76.

[30] [30] Singh BN, Singh B, Chandra A, Haddad KA. Design, digital implementation of active filters with power balance theory. Inst Electr Eng Proc Electr Power Appl Oct. 2005;152(5):1149–60.

[31] Roger A. Messenger, “Jerry Ventre “Photovoltaics system engineering”, CRC press, Second edition, 2004, ISBN 0-8493-1793-2.

[32] Ravi Nath Tripathi, Alka Singh and Tsuyoshi Hanamoto, “Design and Control of LCL interfaced grid connected solar photovoltaic (SPV) system using power balance theory”, International journal of Electrical Power and Energy Systems (Elsevier journal) 69 (2015) 264–272.

[33] Marco Liserre, Frede Blaabjerg and Steffan Hansen, “Design and Control of an LCL-Filter-Based Three-Phase Active Rectifier”, IEEE on Industry Applications, vol. 41, No. 5, 2005.

[34] Aslain Ovano Zue and Ambrish Chandra, “Simulation and Stability Analysis of a 100 kW Grid connected LCL Photovoltaic Inverter for Industry”, IEEE Power Engineering Society General Meeting, ISBN 1-4244-0493-2, Montreal, Que., 2006.

[35] Liserre Marco, Blaabjerg Frede, Hansen Steffan. Design and control of an LCLfilter-based three-phase active rectifier. IEEE Trans Ind Appl 2005;41(5).

[36] IEEE industrial electronics magazine- Evolution of ideas: control, monitoring and more, January 2016.

[37] Shweta Gautam and Rajesh Gupta, “Switching Frequency Derivation for the Cascaded Multilevel Inverter Operating in Current Control Mode using Multiband Hysteresis Modulation”, IEEE Transaction on Power Electronics, vol.29, no.2, pp. 1480-1489, 2014.

[38] Murat Kale and Engin Ozdemir, “ An adaptive hysteresis band current controller for shunt active power filter”, Electrical power system research (Elsevier), vol.73, pp. 113-119, 2005.

[39] [IEEE industrial electronics magazine- other one, October 2015.

[40] Chandra Bajracharya, Marta Molinas, Jon Are Suul and Tore M Undeland, “ Understanding of Tuning Techniques of Converter Controllers for VSC-HVDC”, Nordic Workshop on Power and Industrial Electronics (NORPIE), June, 2008.

[41] Takahiro Saeki, Kozo Ide, Yoshiyasu Takase, Hideaki Iura, Shinya Morimoto and Tsuyoshi Hanamoto, “ Robust Active Damping Method for a PWm Converter Operating with an Unknown Inductance on the Power Grid”, vol.4, no.3 pp. 277-285, 2014.

[42] Marco Liserre, Frede Blaabjerg and Antanio DellAquila, “Step-by-Step design procedure for Grid-connected Three phase PWM voltage source converter”, INT. J. Electronics, Vol. 91, No. 8, 2004.

[43] Božo Terzi´c, Goran Maji´c, Alojz Slutej, “Stability Analysis of Three-Phase PWM Converter with LCL Filter by Means of Nonlinear Model”, AUTOMATIKA 51(2010) 3, 221–232.

[44] Mituhiko Araki and Hidefumi Taguchi, “Two-Degree-of-Freedom (2-DoF) PID Controller Systems”, International Journal of Control, Automation and Systems, vol.1(4), pp.401-411, Dec. 2003.

[45] Lai Yen-Shin, Chang Ye-Then, Kuo Chun-Ting. Robust control of digital controlled buck converter based upon two-degree-of-freedom controller. IECON, Glendale, AZ; 2010.

[46] Dash P, Saikia Chandra, Sinha N. AGC of a multi-area system using firefly optimized two degree of freedom PID controller. In: Power and energy systems conference, Bangalore.

[47] Miklosovic Robert, Gao Zhiqiang. A robust two-degree-of-freedom control design technique and its practical application. In: IEEE industry application conference, Oct. 3–7.

[48] Hanif Moin, Khadikar Vinod, Xiao Weidong, Kirtley Jr James L. Two degrees of freedom active damping technique for LCL filter-based grid connected PV systems. IEEE Trans Indus Electron 2014;61:2795–803.

[49] Nemati Hosein, Bagheri Peyman. A new approach to tune the two-degree-offreedom (2DOF). In: IEEE international symposium on computer-aided control system design, Yokohama, Japan, Sep. 8–10.

[50] Wuhua Hu, Gaoxi Xiao and Wen-Jian Cai, "PID Controller Design Based on two-degrees-of-freedom Direct Syntesis", Control and Decision Conferences (CCDC), Mianyang, China, 2011.

[51] V.M. Alfaro, R. Vilanova, O. Arrieta, "Robust Tuning of Two-Degree-of- Freedom (2-DoF) PI/PID Based Cascaded Control Systems", Journal of Process Control, vol.19(10), pp.1658-1670.

[52] Ravi Nath Tripathi and Tsuyoshi Hanamoto, "2-DOF based novel controller design for dc voltage regulation of LCL interfaced three phase grid connected solar PV system", IFEEC (Conference paper), Taipei, Taiwan, Nov. 1-4, 2015.

[53] Hjalmarsson H, Gevers M, Gunnarsson S, Lequin O. Iterative feedback tuning: theory and applications. IEEE Control Syst Mag 1998;18(4):26–41.

[54] Campi MC, Lecchini A, Saversi SM. Virtual reference feedback tuning: a direct method for design of feedback controllers. Automatica 2002;38 (8):1337–46.

[55] Lecchini A, Campi MC, Saversi SM. Virtual reference feedback tuning for two degree of freedom controllers. Int J Adaptive Control Signal Process 2002;16 (5):355–71.

[56] Souma S, Kaneko O, Fujii T. A new method of controller parameter tuning based on input-output data, fictitious reference iterative tuning (frit). In: Proceedings of IFAC workshop on adaptation and learning on control and signal processing (ALCOSP).

[57] Ravi Nath Tripathi and Tsuyoshi Hanamoto, "FRIT based optimized PI tuning for dc link voltage control of grid connected solar PV system", IECON (Conference paper), Yokohama, Japan, Nov. 9-12, 2015.

[58] Kaneko Osamu, Souma Shotaro, Fuji Takao. A fictitious reference iterative tuning (frit) in the two degree of freedom scheme and its application to closed loop system identification. Trans Soc Instrum Control Eng 2006;42 (1):17–25.

[59] Masuda Shiro. A direct PID gains tuning method for dc motor control using an input-output data generated by disturbance response. In: IEEE international conference on control application (CCA), Senver, USA, Sep. 28–30.

[60] Kaneko O, Yamashina Y, Yamamoto S. Fictitious reference tuning of the feedforward controller in a two-degree-of-freedom control system. SICE J Control Measure Syst Integr 2011;4:55–62.

[61] Wakasa Y, Tanaka K, Nishimura Y. Online controller tuning via FRIT and recursive least-squares. In: IFAC conference on advance in PID control, Brescia (Italy), March 28–30.

[62] Tripathi Ravi Nath, Hanamoto Tsuyoshi. Novel controller design for dc link voltage control of grid connected PV system and optimized PI response analysis with improved transients. ISGT-Asia, Bangkok, Thailand; 2015.

[63] Gilbert M. Masters, "Renewable and efficient electric power system", John Wiley & sons, 2004, ISBN 0-471-28060-7.

[64] Kashif Ishaque, Zanial Salam and Syafaruddin, "A comprehensive MATLAB Simulink PV system with partial shading capability based on two-diode model," Solar Energy 85(2011), 2217-2227.

[65] L.Sandrolini, M.Aritioli and U. REggiani, " Numerical method for th extraction of photovoltaic module doule-diode model parameters through cluster analysis," Appl. Energy, vol. 87, no.2, pp. 452-451, 2010.

[66] Kashif Ishaque, Zanial Salam and H.Taheri, "Simple, fast and accurate teo diode model for photovoltaic modules," Solar Energy Mater. Solar cells 84(2011), 586-594.

[67] Hiren Patel and Vivek Agarwal, "A MATLAB-Based Modeling to Study the Effects of Partial Shading on PV Array Characteristics" IEEE Transactions On Energy Conversion, vol. 23, no. 1, pp.302 - 10, March 2008

[68] I.H. Altas and A.M. Sharaf, "A Photovoltaic Array Simulation Model for Matlab-Simulink GUI Environment" International Conference on Clean Power, pp. 341-345, 2007.

[69] Kun Ding, XinGao Bian, HaiHao Liu and Tao Peng, "A MATLAB-Simulink-Based PV Module and its application under conditions of Non-uniform Irradisnce," IEEE Transaction on Energy Conversion.

[70] G. Petrone, G.Spangnuolo and M. Vitelli, " Analytical model of mismatched photovoltaic fields by means of Lambert W-function," Solar Energy Mater. Solar cells. Vol.91, no. 18, pp. 1652-1657, Nov.2007.

[71] Y.Jiang, J.A.A. Qahouq and I. Batarseh, " Improved solar PV cell MATLAB simulation model and comparison," in Proc. IEEE Int. Symp. Circuits and syst. May/June 2010.

[72] M.G. Villalva, J.R. Gazoli and E. Ruppert F., "Modelling and Circuit-Based Simulation of Photovoltaic Arrays", Brazilian Journal Power Electronics, vol.14, no.1, pp. 35-45, ISSN 1414-8862, 2009.

[73] Trishan Eshram and Patrick L. Chapman, "Comparison of Photovoltaic Array Maximum Power Point Techniques", IEEE Transaction on Energy Conversion, vol.22, no.2, pp. 439-449, June 2007.

[74] Gaurav Kapil, "Fabrication & Characterization of TCO-less Cylindrical Dye-sensitized Solar Cells using Metallic Wires", PhD dissertation, 2015.

[75] Solar PV panel comparison for efficiency, material and voltage: AZOCleantech.

[76] Mary D Archer and Martin A Green, Clean Electricity From Photovoltaics ; Series on Photoconversion of solar energy –vol.4, 2nd edition, Imperial college press.

[77] Kyocera KC200GT and KD180GX high efficiency multicrystal photovoltaic module datasheet.

[78] Katiraei Farid, Iravani Reza, Hatziargyriou Nikos, Dimeas Aris. Microgrid management control and operation aspect of microgrids. IEEE Power Energy Mag 2008.

[79] Tripathi Ravi Nath, Singh Alka. Design and control of grid interconnected solar photovoltaic (SPV) system with improvement in power quality. In: Fifth international conference on power and energy systems, Kathmandu, Nepal, 28–30 October, 2013.

[80] Remus Teodorescu, Marco Liserre, Pedro Rodr´ıguez, "Grid Converters For Photovoltaic and Wind Power Systems", Wiley publications.

[81] Gerard Ledwich and Arindam Ghosh, "Custom Power Devices for Power Quality Enhancement".

[82] Farid Katiraei, Reza Iravani, Nikos Hatziargyriou and Aris Dimeas "Microgrid management Control and operation aspect of microgrids," IEEE Power & Energy Magazine, May/June 2008.

[83] S.A.Azmi, G.P.Adam, Khaled H.Ahmed, Stephen J.Finney, Barry W. Williams, "Grid Interfacing of Multimegawatts Photovoltaic Inverters," IEEE Transaction on Power Electronics, vol.28, no.6, june2013.

[84] Ravi Nath Tripathi, " Modelling and Control of Grid Connected Solar Photovoltaic (SPV) System", Master's thesis.

[85] Moin Hanif, Vinod Khadkikar, Weidong Xiao and James L. Kirtley Jr., "Two Degrees of Freedom Active Damping Technique for LCL Filter-Based Grid Connected PV Systems", IEEE Transaction on Industrial Electronics, vol.61, no.6, June2014.

[86] Ravi Nath Tripathi, "Two degrees of freedom dc voltage controller of grid interfaced PV system with optimized gains", International Journal of Electrical Power and Energy System (IJEPES)- Elsevier, vol.85 (15), pp.87-96, 2017.

[87] S. E. Evju, "Fundamentals of grid connected photovoltaic power electronic converterdesign," Ph.D. dissertation, Department of Electrical Power Engineering, Norwegian University of Science and Technology, Jan. 2007.

[88] S. Kjaer, "Design and control of an inverter for photovoltaic applications," Ph.D. dissertation, Faculty of Engineering and Science at Aalborg University, 2005.

[89] Rajasekar Selvamuthukumaran and Rajesh Gupta, “Rapid prototyping of power electronics converters for photovoltaic system application using Xilinx System Generator”, IET Power Electronics, vol.7, pp. 2269-2278, 2014.

PUBLICATIONS

- **JOURNAL:**

1. Ravi Nath Tripathi and Tsuyoshi Hanamoto, "Two degrees of freedom dc voltage controller of grid interfaced PV system with optimized gains", International journal of Electrical Power and Energy Systems (Elsevier journal) 85 (2017) 87–96.

2. Ravi Nath Tripathi, Alka Singh and Tsuyoshi Hanamoto, "Design and Control of LCL interfaced grid connected solar photovoltaic (SPV) system using power balance theory", International journal of Electrical Power and Energy Systems (Elsevier journal) 69 (2015) 264–272.

3. Ravikant Pandey, Ravi Nath Tripathi and Tsuyoshi Hanamoto, "Cascaded H-bridge multilevel inverter for renewable power generation", Journal of physics conference series (IOP science), April, 2016.

- **CONFERENCE:**

1. Ravi Nath Tripathi and Tsuyoshi Hanamoto, "FRIT based optimized PI tuning for dc link voltage control of grid connected solar PV system", IECON (Conference paper), Yokohama, Japan, Nov. 9-12, 2015.

2. Ravi Nath Tripathi and Tsuyoshi Hanamoto, "Novel controller design for dc link voltage control of grid connected PV system and optimized PI response analysis with improved transients", ISGT-Asia (Conference paper), Bangkok, Thailand, Nov. 3-6, 2015.

3. Ravi Nath Tripathi and Tsuyoshi Hanamoto, "2-DOF based novel controller design for dc voltage regulation of LCL interfaced three phase grid connected solar PV system", IFEEC (Conference paper), Taipei, Taiwan, Nov. 1-4, 2015.

4. Ravi Nath Tripathi and Tsuyoshi Hanamoto, "Parameter computation using circuit based approach for two-diode model based solar PV simulator", 28th International conference on efficiency, cost, optimization, simulation and environmental impact on energy system (ECOS), Pau, France, June 29th – July 3rd, 2015.

5. Ravi Nath Tripathi and Tsuyoshi Hanamoto, "Improvement in power quality using fryze conductance algorithm controlled grid-connected solar PV system", 4th International conference on informatics, electronics and vision (ICIEV), Kitakyushu, Japan, June, 2015.

6. Ravikant Pandey, **Ravi Nath Tripathi** and Tsuyoshi Hanamoto, "Multiband HCC for cascaded H-bridge multilevel inverter based DSTATCOM", ICIEA (Conference paper), Hefei, China, June, 2016.

7. T. Kerdphol, **Ravi Nath Tripathi**, T. Hanamoto, K. Hasan, Y. Qudaih and Yasunori Mitani, "ANN based optimized battery energy storage system and loss analysis for distributed energy storage location in PV-microgrid", ISGT-Asia (Conference paper), Bangkok, Thailand, Nov. 3-6, 2015.